GREEN BARRIER MATERIALS FROM CELLULOSE NANO FIBERS

A Dissertation
Presented to
The Academic Faculty

by

Sudhir Sharma

In Partial Fulfillment
of the Requirements for the Degree
Doctor of Philosophy in the
School of Chemical and Biomolecular Engineering

Georgia Institute of Technology
December 2015

GREEN BARRIER MATERIALS FROM CELLULOSE NANO FIBERS

Approved by:

Dr.Yulin Deng, Advisor
School of Chemical and Biomolecular Engineering
Georgia Institute of Technology

Dr. Preet Singh
School of Materials Science and Engineering
Georgia Institute of Technology

Dr. Meisha L. Shofner
School of Materials Science and Engineering
Georgia Institute of Technology

Dr. Chris Luettgen
School of Chemical and Biomolecular Engineering
Georgia Institute of Technology

Dr. Norman Marsolan
School of Chemical and Biomolecular Engineering
Georgia Institute of Technology

Date Approved: July 23, 2015

ACKNOWLEDGEMENTS

I would like to thank all my group members, friends, and family who have been incredibly supportive during the last five years as I worked on my PhD dissertation and research. I am most thankful to my research advisor, Dr. Yulin Deng, who helped me start this research project and gave me the tools for critical thinking, independent research, and help when I was lost. He assisted me throughout each step when I needed guidance and helped over the course of my research, leading me to the correct conferences, research articles, and labs, showing me how to think about critical problems and helping me to connect to the correct people to help me move forward.

I am grateful to my committee members, Dr. Meisha Shofner, Dr. Preet Singh, Dr. Chris Luettgen, and Dr. Norman Marsolan for help and support during the entire span of my research. Dr. Shofner, thank you especially for letting me use your labs! I would also like to thank Dr. Sujit Banerjee for being on my committee prior to retirement.

I would like to thank Renewable Bioproducts Institute, formerly known as the Institute of Paper Science and Technology that helped with financial support and made my research at Georgia Tech possible.

I would like to thank all the group members in the Deng group Xiaodan Zhang, Arie Mulyadi, Zhe Zhang, Wei Mu, Wei Liu, Xu Du, Junli Zhou and everyone I'm missing. Thank you all for being fantastic collaborators, friends, and researchers.

Lastly, I would also like to thank my family for all the support they have shown me in my endeavor. Completing my PhD research and dissertation would not have been possible without your support throughout the entire period.

TABLE OF CONTENTS

	Page
ACKNOWLEDGEMENTS	iv
LIST OF TABLES	vii
LIST OF FIGURES	ix
LIST OF SYMBOLS AND ABBREVIATIONS	xi
SUMMARY	xii
CHAPTERS	
CHAPTER 1 INTRODUCTION	1
1.1 Cellulose	1
1.2. Structure of Cellulose	1
1.3 Cellulose Nano Fibers	4
1.4 Barrier Materials	6
1.5 Permeability	7
CHAPTER 2 THERMALLY ENHANCED HIGH PERFORMANCE CELLULOSE NANO FIBER BARRIER MEMBRANES	10
Abstract	10
2.1. Introduction	10
2.2. Experimental Section	12
2.2.1. CNF Preparation	12
2.2.2. Membrane Preparation	12
2.2.3. Membrane Characterization	13
2.3. Results and Discusion	16
2.3.1. XRD analysis	16

2.3.2. Water Retention Value (WRV) 17

2.3.3. SEM Characterization 17

2.3.4. TGA Analysis 20

2.3.5. Mechanical 21

2.3.6. Permeability 22

2.4. Conclusions 25

CHAPTER 3 DUAL MECHANISM OF DRY STRENGTH IMPROVEMENT OF CNF FILMS BY PAE CROSSLINKING 27

Abstract 27

3.1. Introduction 28

3.2. Experimental 30

3.2.1. Materials 30

3.2.2. Fabrication of Films 30

3.2.3. Characterization 31

3.3. Results and Discussion 32

3.4. Conclusions 46

CHAPTER 4 HIGH PERFORMANCE CROSSLINKED NANO COMPOSITE CNF BARRIER FILMS 47

Abstract 47

4.1. Introduction 47

4.2. Experimental 50

4.2.1. Fabrication of Films 50

4.2.2. Materials 50

4.2.3. Characterization 51

4.3. Results and Discussion 52

4.3.1. Mechanical Properties 53

4.3.2. Pure CNF Composites 53

4.3.3. Crosslinked CNF Composites 56

4.3.4. Barrier Properties 58

4.3.5. Oxygen Permeability 58

4.3.6. Water Vapor Permeability 59

4.4. Conclusions 60

CHAPTER 5 CHARACTERIZATION OF MICRO FIBRILLATION PROCESS OF CELLULOSE AND MERCERIZED CELLULOSE PULP 62

Abstract 62

5. 1. Introduction 63

5. 2. Experimental 65

5.2.1. Materials 65

5.2.2. Pulp Mercerization 65

5.2.3. α-Cellulose Content 66

5.2.4. XRD Analysis 66

5.2.5. Disintegration, Refining, and Microgrinding with SuperMassColloider 66

5.2.6. Fabrication of Films from Pulp 67

5.2.7. Characterization of Films 67

5.3. Results and Discussion 68

5.3.1. α – Cellulose Quantification 68

5.3.2. SEM: Fiber Morphology 69

5.3.3. XRD Analysis 70

5.3.4. Physical Properties of Films 72

5.3.5. Mechanical Properties of Films 79

5.4. Conclusions 89

CHAPTER 6 CONCLUSIONS AND FUTURE WORK 91

Conclusions 91

Recommendations for Future Work 95

REFERENCES 99

LIST OF TABLES

	Page
Table 1: WRV and Contact Angle	17
Table 2: Thermal Properties	21
Table 3: Mechanical Properties	21
Table 4: Physical Properties of Films	33
Table 5: Water Interaction Properties	35
Table 6: Mechanical Properties of Composites Without Cross Linking	53
Table 7: α - Cellulose Content of Native and Mercerized Pulp	68
Table 8: Physical Properties of Films	72
Table 9: Mechanical Properties of Films	80
Table 10: Thermal Properties	88

LIST OF FIGURES

	Page
Figure 1.1: Cellulose Molecule	2
Figure 1.2: Hierarchical Structure of Cellulose	3
Figure 1.3: Inter and Intra Molecular Bonding Confirmations of Cellulose	3
Figure 1.4: Mechanism of Permeability	8
Figure 2.1: XRD Analysis	16
Figure 2.2: SEM Images of Untreated (a, b) and Films Heated at 175C(c, d)	19
Figure 2.3: TGA Analysis	20
Figure 2.4.: Permeability	22
Figure 3.1: As Obtained CNF	32
Figure 3.2: Pure CNF Films (Top), PAE Crosslinked Films (Bottom)	33
Figure 3.3: FTIR Analysis	34
Figure 3.4: Pure CNF Contact Angle (top), PAE Crosslinked CNF Contact Angle	35
Figure 3.5: TGA and DTG Analysis	37
Figure 3.6: Stress - Strain analysis (left: dry tests, right: wet tests)	38
Figure 3.7: SEM Images of Dry (a) and Wet (b) Pure CNFs Fracture Surface	40
Figure 3.8: PAE - Cellulose Cross Linking Mechanism (from Obokata et.al)	42
Figure 4.1: Starting Materials from Left (Nano Clay, Graphene Flakes, CNF)	50
Figure 4.2: Typical Stress Strain Curves for CNF + Filler Composites	53
Figure 4.3: Fracture Surface SEM (Pure CNF, CNF - G, CNF - C)	54
Figure 4.4: Typical Stress Strain Curves Cross Linked Composites	56
Figure 4.5: Fracture Surface SEM from Left (X - CNF, X- CNF -G, X - CNF - C)	56
Figure 4.6: Oxygen Permeability of CNF + Filler Materials	58

Figure 4.7: Water Vapor Permeability Values of All Composite Materials 59

Figure 5.1: Cellulose-I Fiber (left), Mercerized Cellulose Fiber (left) 69

Figure 5.2: XRD Analysis: Cellulose and Mercerized Cellulose 70

Figure 5.3: XRD Analysis of Films 71

Figure 5.4: UV Vis Spectra 74

Figure 5.5: Cellulose-I Films and Fiber SEMs (a. Disintegrated, b.PFI, c.20 Passes in SMC, d.60 Passes in SMC 76

Figure 5.6: Cellulose-II Films and Fiber SEMs (a. Disintegrated, b.PFI, c.20 Passes in SMC, d.60 Passes in SMC) 78

Figure 5.7: Typical Stress - Strain Curves 80

Figure 5.8: Cellulose-I Disintegrated Fibers, (c ,d): Cellulose-II Disintegrated Fibers 81

Figure 5.9: Cellulose-I PFI Fibers, (c ,d): Cellulose-II PFI Fibers 83

Figure 5.10: Cellulose-I 20 Passes in SMC Fibers, (c ,d): Cellulose-II 20 Passes in SMC Fibers 84

Figure 5.11: Cellulose-I 60 Passes in SMC Fibers, (c ,d): Cellulose-II 60 Passes in SMC Fibers 85

Figure 5.12: TGA / DTG Analysis 87

LIST OF SYMBOLS AND ABBREVIATIONS

CNF	Cellulose Nano Fibers
MFC	Micro Fibrillated Cellulose
OTR	Oxygen Transfer Rate
WVTR	Water Vapor Transfer Rate
OP	Oxygen Permeability
WVP	Water Vapor Permeability
XRD	X Ray Diffraction
SMC	SuperMassColloider
WRV	Water Retention Value
SRV	Solvent Retention Value
CA	Contact Angle
SEM	Scanning Electron Microscope
TGA	Thermo- Gravimetric Analysis
DTGA	Derivative Thermo- Gravimetric Analysis
PAE	Polyamide Epichlorohydrin Resin
nm	Nanometer
µm	Micrometer

SUMMARY

Cellulose is the most abundant biopolymer on the planet. It is renewable, biodegradable, and sustainable. It occurs in plants as the structurally reinforcing material and in various highly complex morphologies. Chemically, it consists of a long array of β-linked glucose units. Cellulose has been widely studied in the literature due to its excellent properties as a biopolymer, and extensive applications in various industries have resulted. The paper industry has found a wide variety of uses for cellulose in various forms such as printing, cleaning, packaging materials, and various other specialty products. In research literature, cellulose has been studied from a fundamental perspective to elucidate its chemical, physical, and crystalline structure, as well as its various polymorphs. From a chemistry perspective, cellulose also offers itself as a very flexible molecule due to an abundance of hydroxyl and carboxylate groups available as reaction sites for easy grafting of other chemicals and simple modification.

Cellulose nano fiber (CNFs) or Micro fibrillated cellulose (MFCs) are interchangeable terms used widely in the literature for the smallest structural fibers of cellulose. Broadly, CNFs range from diameters of 5 - 50 nm, and up to 1000 nm in length. CNFs occur naturally as the smallest fibril unit in a cellulose fiber. The structure of CNFs that are plant material possess a cell in the cell wall which is made from cellulose fibrils, which in turn are made of CNFs. These can be extracted by mechanically shearing the cell wall or by various chemical and enzymatic methods. CNFs have garnered huge research and industrial attention

recently due to their excellent properties as an abundant renewable, biodegradable, sustainable, and sustainable biopolymer. CNFs owe their excellent properties to a high aspect ratio, excellent inter fiber hydrogen bonding, obtainable dense packing structure, and easy structural and chemical modification. These properties lend to excellent strength, stiffness, low weight, of materials, and excellent barrier properties. Moreover, easy routes for chemical modification and grafting lend to a whole host of opportunities as well.

The one overwhelming area of CNF application, and the primary industrial use of CNF material, is barrier films. One of the main setbacks in the application of CNFs as barrier materials is their hydrophilicity and degradation of both barrier and mechanical properties in the presence of water. The focus of this dissertation is to study and enhance the barrier properties of films made from CNFs, and when possible to improve the issues caused due to hydrophilicity of CNFs. The dissertation is divided into four main studies as described below.

1. Thermally enhanced high performance cellulose nano fiber barrier membranes.

   In this study a simple oven heating was applied to CNF membranes after they had been formed by solvent evaporation. The concept of inducing hornification into CNFs was tested. Films were heated at various temperatures after forming to induce chemical and structural changes in the CNFs which would be analogous to hornification of cellulose fibers during thermal exposure or recycling. By heating the films, loss of film structure porosity, increase in crystallinity, and

increase in hydrophobicity were observed. Due to the combination of these phenomenon, a 25 fold reduction of oxygen permeability and a twofold reduction in water vapor permeability were obtained.

2. Dual mechanism of dry strength improvement of NFC films by crosslinking with PAE resin.

   In this study high grammage, robust and structurally dense CNF films with and without wet strength enhancing PAE based crosslinker Kymene™ were fabricated. To promote both hetero crosslinking between cellulose and PAE and formation of PAE networks, films with crosslinker were heated at 120°C for 3 hours. While wet strength enhancement was expected and observed, we also discovered unique, never before observed stress-strain behavior for dry crosslinked films indicating varying stress bearing mechanisms at different levels due to formation of new bonds by crosslinking. Crosslinking increased dry strength by approximately 2.5 fold as compared to pure CNF films. Wet strength enhancement was also quite significant; wet strength of crosslinked films was observed to be very close to pure dry CNF films, approximately 35MPa. Additionally, the crosslinked films showed a transition of both surface and bulk properties to hydrophobic from hydrophilic. Water contact angle increased from 50° to 110°, while the water retention value was lower by approximately 25% for the crosslinked films. Some of the increase in hydrophobic nature, as we have previously shown, can be attributed to induced hornification

during the three hour heating period for crosslinking at 120°C. Water Vapor permeability decreased as well by about 50% as a result of reduced water interaction and induced hornification.

3. Crosslinked nano composites made from CNFs and high aspect ratio nano fillers.

   High aspect ratio materials are commonly used to enhance both the barrier and mechanical properties of barrier films. A very low loading (<1%) of well dispersed, and well aligned high aspect ratio nano materials can significantly add to the performance of barrier materials. In this study, not only high aspect ratio nano filler materials, but also PAE crosslinking was studied in conjunction. The nano filler materials function as fully discrete particles enhancing the barrier and strength of the nano composite barrier, whereas the crosslinking as observed previously reduces water interaction and significantly improves the dry and wet strength of the nano composite materials. Particularly, the crosslinked nano composites showed a strength increase of up to 160% as compared to the pure CNF films. The crosslinked nano composites also showed a reduction of water vapor permeability by up to 85%, as compared to the pure NFC films.

4. Characterization of micro fibrillation of cellulose and mercerized cellulose pulp.

Detailed in this study is the fibrillation process for cellulose and mercerized cellulose pulps. Native and mercerized cellulose showed a high degree

of purity as indicated by α – cellulose content measurement and XRD analysis. Furthermore, a stark change in fiber morphology indicated aggregation of fibrils on the surface due to mercerization. Fibrillation of pulp was carried out in the following subsequent steps: disintegration, PFI refining, microgrinding by 20 passes in a SuperMassColloider, and 60 passes in SuperMassColloider. Fiber samples were collected at every stage and highly uniform films were made by ultrafiltration and hot press method. The fibers and films made from fibers were then characterized by measuring physical properties, contact angle, thermal, mechanical, and SEM analysis. The main objective was to characterize the physical properties of the films made from different degrees of fibrillation. The films obtained were of fairly close grammage at approximately 35g/m2. The target grammage was 40g/m2, and the slightly lower grammage indicated some fiber loss during the fabrication process. Additionally, it was observed that the density of the films increased with accumulative degree of fibrillation from about 180g/m3 to 455g/m3 for cellulose-I and 95g/m3 to 385g/m3 for cellulose-II. Cellulose-I films showed some contact angle initially, which increased at every stage (14° - 64°), whereas cellulose-II films did not display a contact angle until the final stage of fibrillation. The films also showed increasing strength and an evolution of tensile strength from initially displaying a tear behavior indicating poor bonding to typical micro fibrillated cellulose films behavior as the fibers became increasingly fibrillated. The ultimate tensile strength for cellulose changed from tear behavior with no defined break to 134.5MPa. On the other hand, the same change for cellulose II was a maximum of 75.1MPa from tear

behavior. Increasing fibrillation of fibrils in both cases showed a decrease in fiber size, which was well differentiated for the two types of pulps at every stage.

In summary, the barrier and mechanical properties of CNF films were studied in detail with immediate application in focus. Various simple to apply strategies were considered and developed to improve upon the existing state of CNF barrier film research. In addition, the fourth study also explored the micro fibrillation process to detail the structural and physical changes of films made from both cellulose and mercerized cellulose during different stages of the process.

CHAPTER 1

INTRODUCTION

1.1 Cellulose

With wide applications in our daily lives, cellulose is the most abundant, renewable, sustainable biopolymer in existence. It occurs in wood, hemp, cotton, algae, and is even produced by some bacteria. As Klemm et al aptly stated in their recent exhaustive review of cellulose[1],

"The polysaccharide cellulose is an almost inexhaustible polymeric raw material with fascinating structure and properties. Formed by the repeated connection of D-glucose building blocks, the highly functionalized linear stiff-chain homopolymer is characterized by its hydrophilicity, chirality, biodegradability, broad chemical modifying capacity, and its formation of versatile semicrystalline fiber morphologies."

Even before its discovery, cellulose was used by human civilization for millennia, in the form of wood used as fuel, building materials, cotton used for clothing, and even as Egyptian papyrus, the precursor to paper. Cellulose is not only an important industrial material. In many ways it has shaped human civilization. Today, cellulose is used for various applications – overwhelmingly in paper based materials as well as composite materials, drug delivery, textiles, and personal care items amongst a host of many other purposes[2-5].

1.2 Structure of Cellulose

Shown in figure (1) is the molecular structure of cellulose. It is a carbohydrate polymer, composed of units of covalently bonded β-D- gluco-pyranose units, which are linked through the equatorial hydroxyl groups of the C1 and C4 carbons atoms. This is

referred to as the β-1,4-glucan linkage of cellulose. As a result of this structure, cellulose is easy to chemically modify due to the abundance of reactive hydroxyl groups. One end of the D-glucose unit is the original C4-OH group, while the other end terminates with the C1-OH group in equilibrium with the aldehyde structure. Cellulose chains are found in nature in different chain lengths. These lengths are produced from various sources of cellulose and are referred to by their degree of polymerization (DP). Varieties of cellulose with DP values as low as 150 to as high as 20,000 have been documented[1, 4, 6-10].

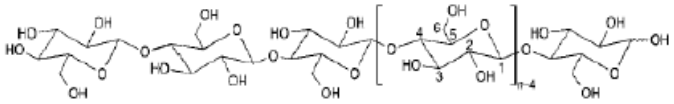

Figure 1.1: Cellulose Molecule[1]

From a morphological and structural perspective, cellulose has a hierarchical structure, with CNFs being the most basic structural unit of plant cells. Each nano fibril is composed of a string of crystalline cellulose domains known as cellulose nano crystals (CNCs) bound by amorphous parts in a string like structure. The CNFs in turn are bound together by other binding biopolymers including hemicelluloses pectin and lignin. Shown in figure (2) is a schematic of this hierarchical structure of cellulose[2, 11-15].

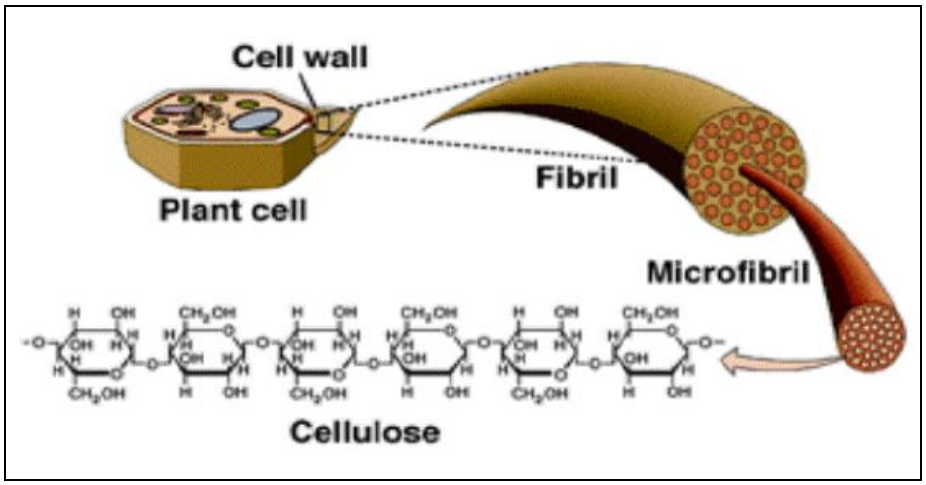

Figure 1.2: Hierarchical Structure of Cellulose

The hierarchical structure of cellulose is formed mainly by hydrogen bonding between the different hydroxyl networks. Both intermolecular and intramolecular hydrogen bonding can be observed in cellulose. Shown in figure (3) are the representative structures of both types of hydrogen bonding.

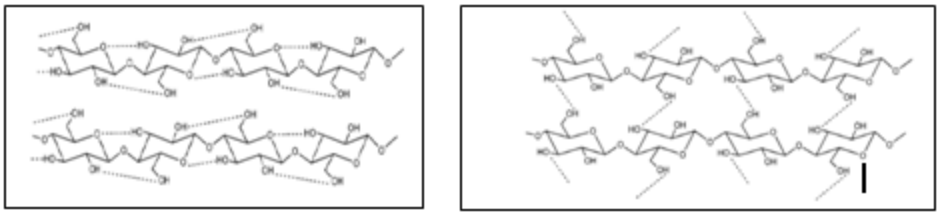

Figure 1.3: Inter and Intra Molecular Bonding Confirmations of Cellulose[1]

The morphology and physical properties of the resulting cellulose are based on the hydrogen bonding of the molecular structure. Due to the hydrogen bonding structure, the cellulose structure can vary greatly and leads to the formation of polymorphs or allomorphs depending on the source of the cellulose or the method of extraction of the cellulose. Four polymorphic forms of cellulose are recognized: Cellulose I, II, III, and IV. Conversion from native cellulose is possible to other polymorphs by chemical treatment.

1.3 Cellulose Nano Fibers

The extraction and production of CNFs from wood pulp requires extensive mechanical treatment. In some cases some chemical or enzymatic pretreatment is applied to the wood fibers to reduce the mechanical energy required for extraction of the CNFs[4, 15-21]. Depending on the degree of pretreatment, degree of mechanical treatment, and the source of the wood pulp, the characteristics of the nano fibers can significantly vary. Shown below is a table displaying some of the different CNFs documented from the exhaustive review of CNFs by Siró and Plackett[14].

Method	Raw material	Procedure	Nanofiber dimension	References
Mechanical treatment	Bleached potato pulp	Disintegration in a Waring blender; Homogenization by 15 passes through a laboratory homogenizer, operated at 500 bars and 90–95 °C	~ 5 nm in width	Dufresne et al. (2000)
	Cladodes of *Opuntia ficus-indica*			Malainine et al. (2005), Habibi et al. (2009)
	Kraft pulp	Passing 2–30 times through a refiner with a gap of 0.1 mm, subsequently passing through a high pressure homogenizer 2–30 times	ND	Nakagaito and Yano (2004)
	Kraft pulp	Passing through a refiner with a gap of 0.1 mm 30 times, subsequently passing through a high pressure homogenizer up to 30 times and finally grinder treatments up to 10 times	50–100 nm in width and several μm in length	Iwamoto et al. (2005, 2007)
	Soybean stock	Cryocrushing followed by 20 passes through a defibrillator at 500–1,000 bar	50–100 nm in width and several μm in length	Wang and Sain (2007a)
		Beating and refining in a PFI mill; 20 passes through a defibrillator at 500–1,000 Pa		Wang and Sain (2007b)
	Wheat straw	Cryocrushing followed by fibrillation using a Cramer disintegrator at 2,000 rpm; homogenization by 20 passes through a laboratory defibrillator at pressure above 300 bar.	20–120 nm in width, the majority around 30–40 nm	Alemdar and Sain (2008a, b)
	Wood pulps, Tunicin cellulose, Chitosan, Collagen	Microfibrillation by super-grinder	20–90 nm in width	Taniguchi and Okamura (1998)
	Hemp fiber, Spring flax, Bleached kraft pulp, Rutabaga	Cryocrushing followed by high shear homogenization	5–80 nm in width, the majority around 10–60 nm	Bhatnagar and Sain (2005)
	Dried sugar beet pulp chips	Disintegration by means of an Ultra-Turrax mixer at 24,000 rpm followed by homogenization by a high-pressure laboratory homogeniser at 300 bar for 10–15 passes	30–100 nm and a length of several μm	Leitner et al. (2007)
Chemical treatment[a]	Never-dried bleached sulfite/kraft pulp	TEMPO-mediated oxidation, followed by disintegration in a Waring blender	Few nm in width	Saito et al. (2006, 2007, 2009); Lasseuguette et al. (2008)
	Sugar beet pulp	Disintegration in a Waring blender; homogenization by 15 passes through a laboratory homogenizer, operated at 500 bars and 90–95 °C; TEMPO-mediated oxidation	ND	Habibi and Vignon (2008)

The first production methods for CNFs detailed by Turbak et al and Herrick et al were based on passing dilute cellulose suspensions through a mechanical homogenizer. The production of CNF solely through mechanical treatment is now accomplished through a series of steps consisting of a high degree of refining and high-pressure

homogenization. After the refining process, a common method for producing CNF is to use a disc refiner in which the fiber suspension is forced through a small gap between a rotor and stator discs. This method is highly preferred since it brings about morphological changes of the fibrils due to constant shear, resulting in better bonding potential between the resulting CNFs. Adversely, mechanical treatment may damage some of the crystalline regions.

Pure mechanical treatment however requires very high energy input, and values in the range 20,000 - 30,000 kWh/ton are commonly reported, with values as high as 70,000 kWh/ton recorded. Therefore the combination of chemical or enzymatic pretreatment is also commonly applied to reduce the energy required for the subsequent mechanical treatment. Two commonly used pretreatments are oxidation via TEMPO (2,2,6,6-tetramethylpipyridene-1-oxyl) and enzymatic pretreatment with a set of cellulases (A-, B-, C-, and D- type)[1, 2, 4, 12-14, 16, 18, 22-24].

TEMPO oxidation also introduces carboxylate and aldehyde functional groups onto the cellulose, while maintaining the morphology and the DP of the original native fibers, which produces a highly uniform diameter distribution of CNFs. However, the TEMPO based reaction uses NaBr, NaClO, and $NaClO_2$ which makes the reaction conditions quite harsh and not environmentally friendly. Enzymatic pretreatment on the other hand uses enzymes and also results in similar characteristics of CNFs obtained from the process. However, multiple steps are required: cell wall delamination, then enzymatic treatment, then a second enzyme treatment using endoglucanase, followed by another refining stage, and finally high pressure homogenization or passing through a micro fluidizer[1, 2, 4, 12-14, 16, 18, 22-24].

1.4 Barrier Materials

Barrier materials are utilized for packaging materials used on a daily basis; these include foodstuffs, dry goods, pharmaceuticals, and cosmetics amongst a host of many other products. Packaging materials serve as a barrier and protection from oxygen, water, odor, grease microbes and any other environmental factors that could infiltrate and harm or destroy a product. For the purpose of this discussion, packaging materials can be broadly classified as cellulose based packaging materials and non-cellulose based materials. The latter category contains petroleum derived polymers, plastics, glass, and metals. Some challenges exist with using pure cellulose based materials due to the limited barrier and mechanical properties of cellulose materials, as well as a susceptibility to humidity. Therefore, most paper based packing materials are coated with a layer of waxes, plastics, or aluminum. This reduces to some degree the usage of the coating material but also limits the recyclability of the paper based material[13, 24-31].

In the non-cellulose packaging material category, petrochemical derived polymers currently overwhelmingly dominate. These include low density polyethylene, high density polyethylene, and polyethylene terephthalate among a variety of other petroleum derived plastics; the unique application determines the particular types of petrochemical derived polymers that are used. Their popularity is due to their ease of processing, excellent barrier properties in most cases, and low cost. Metals and glass are also used but can have significant drawbacks, as they can be heavy, fragile, expensive, and increase the cost of transportation. In some cases, using metals is not even sustainable. Metals, though useful in some instances, are not adequate for food or pharmaceutical packaging due to their inert quality. In the case of petrochemical derivatives, the main problem

arises at the end of life disposal. Most packaging material ends up in a landfill, causing huge environmental concern. These concerns are not new and have existed for quite some time. One significant effort toward more environmentally friendly polymers has been to improve the properties of existing polymers to reduce the usage of their harmful properties[13, 24-33].

However, there is now significant impetus to develop and apply new renewable, biodegradable, and sustainable barrier materials for packaging. Not only does this have an environmental significance, but would also substantially impact the market for packaging materials, which is estimated to be about 4 billion USD annually. Since the extraction of CNFs by Turbak et al in the 1980s, CNFs have garnered a significant degree of attention for use as barrier materials. CNFs possess excellent properties – firstly they are composed of cellulose extracted from trees, which provide many environmental benefits. Due to their morphology and high surface area. Their structural perspective can be easily formed into dense films with excellent barrier and mechanical properties[13, 14].

1.5 Permeability

In the context of barrier materials, permeability is the central concept. Permeability is defined as the measure of permeate transmission through a barrier material, usually a polymer in this instance. In materials that are without defect the mechanism for permeability is composed of three steps – adsorption on the surface that is rich in permeate, diffusion through the membrane driven by a concentration gradient, followed by desorption on the other surface. Therefore, the first step is driven purely by the affinity of the permeate to the membrane material. It is well known that adsorption occurs only on the amorphous regions of the polymer and not the crystalline parts, so

there is no permeability in the crystalline parts of the polymer. The second step, diffusion, then depends on the relative shape, size, polarity, and structure of both the permeant and the membrane material[13, 29, 34-39]. Figure (4) shows the general permeability mechanism, displaying the three step process.

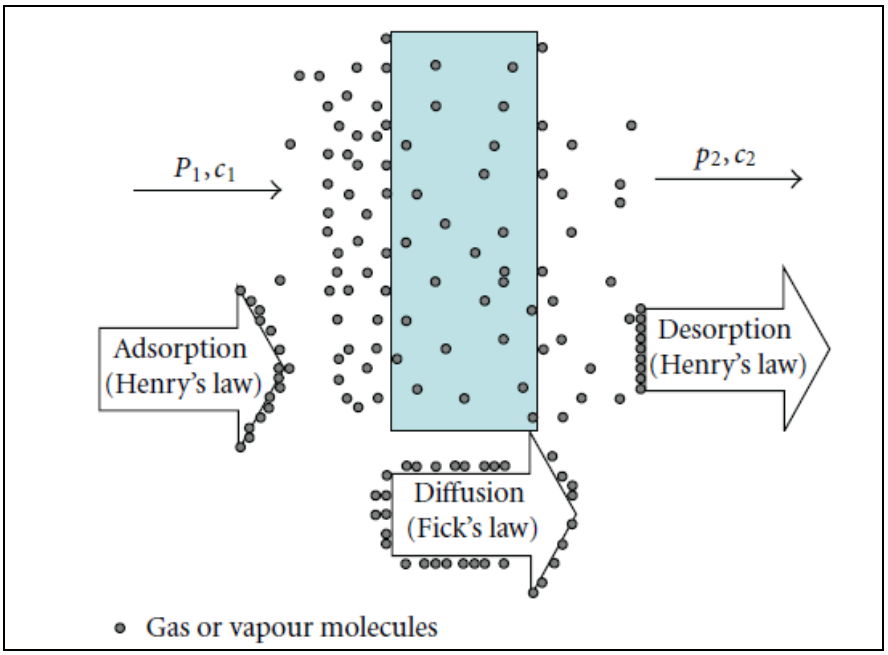

Figure 1.4: Mechanism of Permeability[32]

The expression for permeability is then derived from Fick's law and Henry's law combined. The diffusion flux is given by $J = -D.\Delta c$, where J is the flux, D is the diffusion coefficient, and Δc is the concentration gradient across the membrane. Since this is a stationary system, it can be written as $J = -D.\frac{\Delta c}{l}$, where l is the thickness of the film. Now from Henry's law the concentration gradient can be defined in terms of the vapor pressure of the permeant, Δc can be replaced by SΔp, where S is the solubility coefficient and Δp is the pressure gradient across the membrane. The two expressions

combine to create $J = -D.\frac{S\Delta p}{l}$. From this combination, we find the permeability coefficient as $P = S.D = -\left(\frac{J.l}{\Delta p}\right)$. Eventually, the permeability coefficient is just the multiplicand of the solubility and diffusion coefficients of the gas and the membrane pair. This is widely used as a standard measure for performance of barrier materials, with the units in general form written as $\frac{Volume.Length}{Area.Time.Pressure}$. The standard unit adopted by ASTM, the Barrer, named after Richard Barrer who first introduced the unit, is of the form 10^{-10}(cm^3(STP)cm)/cm.sec.(cmHg). Depending on the type of material, various units are used, these include ml.m/m^2.s.Pa, ml.µm/m^2.s.Pa, ml.µm/m^2.Day.kPa. Sometimes a slightly different scale of measure for the transfer rate is used – these have the units of the form $\frac{Volume.}{Area.Time}$. In terms of permeability literature for barrier materials used in packaging, the findings are quite inconsistent. Different groups have reported the oxygen and water permeability in varying units[13, 29, 34-39].

CHAPTER 2
THERMALLY ENHANCED HIGH PERFORMANCE CELLULOSE NANO FIBER BARRIER MEMBRANES

SUMMARY

This report covers the method of thermal treatment used to enhance barrier properties of membranes made from Cellulose Nano Fibrils (CNFs). CNF membranes of 75±5μm thickness were prepared by evaporation of water from a suspension of CNFs. This was followed by thermal treatment at different temperatures (100°C, 125°C, 150°C, and 175°C) for 3 hours and subsequent conditioning at 23°C and 50% relative humidity for 24 hours. Increasing thermal treatment temperature correlated well with enhanced barrier properties; the oxygen and water vapor permeability decreased by 25 fold and 2 fold respectively after treatment at 175°C. The reduction in permeability was attributed to an increase in crystallinity, reduction of the inter fibril space or porosity, and an increase in hydrophobicity. These effects were also demonstrated to be analogous to hornification of cellulose fibers.

2.1 INTRODUCTION

Packaging materials provide a barrier against oxygen, water, grease microbes, odor for food, pharmaceuticals, cosmetics, and other dry goods. The most commonly used barrier packaging materials are glass, metals (aluminum and tin), and petroleum based plastics. Paper based barrier packaging is also widely used; however, the paper substrate must be coated by aluminum, wax, or petroleum based plastics or polymers to enhance barrier properties that the paper substrate lacks. These materials have various

disadvantages: they are unsustainable, fragile, increase the cost of transportation, and are non-renewable[13, 33, 40-42]. Cellophane is the only cellulose based material currently used for barrier packaging. However, the production of cellophane is via a viscose route which uses reagents and produces byproducts (CS_2 and H_2S respectively) that are harmful to the environment[22, 43-45].

Membranes made from CNFs have garnered much attention as barrier materials due to their mechanical and gas barrier properties being comparable to synthetic polymeric materials currently used[13, 15, 20, 22, 35, 40, 46-49]. Moreover, they are renewable and biodegradable. Even though pure CNF films have shown good gas barrier properties under dry conditions, these barrier properties tend to degrade under humid conditions due to the hydrophilic nature of cellulose[50]. CNFs are cellulose fibrils with diameters between 10-50nm and a length up to 1000nm. CNFs show different properties than cellulose fibers in many aspects, owing to their smaller size and high aspect ratio.

In order to enhance the barrier and mechanical properties of CNF membranes, researchers have commonly used methods such as coating CNFs with polymers, grafting other polymers onto the CNFs or using a high aspect ratio filler material to obtain a composite membrane[9, 40, 51-53]. The inclusion of high aspect ratio filler materials is a widely used method that avoids chemical modification of the fibers to enhance barrier and mechanical properties[47, 54, 55]. However, this method has an inherent disadvantage in that the filler material might limit recyclability and biodegradability of the resulting composite material. The methods used to chemically modify the CNFs are at a disadvantage since chemical reagents are required for modification, which may hurt the case for the resulting composite material being a completely green material. Moreover,

these methods may inhibit the internal hydrogen bonding between fibril surface –OH groups responsible for imparting strength to the membranes.

2.2 EXPERIMENTAL SECTION

2.2.1 CNF Preparation

Elementally chlorine-free (ECF), bleached kraft pulp from softwood (loblolly pine) was obtained as a commercial sample. The pulp at 2% solids was soaked in deionized water for 24 h and then disintegrated using a lab disintegrator (TMI, Ronkonkoma, NY, USA) for 10,000 revolutions. It was then fibrillated for 12 hours using a SuperMassColloider (MKZA6-2, Masuko Sangyo Co., Ltd, Japan) at 1500 rpm. Pulp was fed continuously to the colloider consisting of two ceramic grinding discs positioned on top of each other. This was operated at contact grinding with the gap of the two discs adjusted to -100 µm. Zero gap between discs corresponds to the starting point, where the two discs just start to graze each other before loading pulp. The presence of pulp between the discs ensured that there is no direct contact between the discs even at the negative setting. The grinding process microfibrillates the cellulose fibers which start as cellulose pulp and transition to CNFs. The transformation of the fibers is shown in SEM images. The CNFs were then treated with Kathon CP/ICP II (Rohm and Haas Company, Bellefonte, PA, USA) at a dose of 10 µl/ml of fibrillated suspension in order to avoid mold growth.

2.2.2 Membrane Preparation

The CNF suspension was diluted to 1% and heated at 100°C while being vigorously stirred. Subsequently the suspension was poured on to a glass dish to air dry.

It took 2-3 days for the water to completely evaporate and form a film. Films of 75±5µm in thickness were obtained.

For permeation and water retention measurements, the films were cut into discs 50mm in diameter. The samples for tensile testing were cut into 45mmX12mm size rectangular specimens. Cut outs from the samples were also used for SEM, XRD, and TGA analysis. The samples were then heated in an oven at different temperatures (100°C, 125°C, 150°C, and 175°C) for 3 hours each, leaving an unheated set of samples as the reference sample. After the thermal exposure, all samples were allowed to cool to room temperature and stored in a humidity controlled room at 23°C and 50% relative humidity for 24 hours before any measurements were made.

2.2.3 Membrane Characterization

Oxygen Permeability was measured with a constant pressure difference device. The device consists of a membrane holding cell of diameter 47mm (Milipore XX 45 047 00) connected to an oxygen tank, pressure gauges, and a digital flow meter with a least count of 0.01ml/min to measure flow rate. Flow measurements were made at various operating pressures. Oxygen Permeability was calculated as below,

$$OP = \frac{flow.T}{A.\Delta P}\left(\frac{cc.\mu m}{day.m^2.kPa}\right) \quad (1)$$

Here, the flow was measured by the flow meter in ml/min, T was the thickness of the film (µm), A the area of the film (m^2), and ΔP the pressure drop (in kPa) across the film. Measurements were made in triplicate.

Water vapor permeability was measured using a modified version of the ASTM E-96-95 method. Films were glued using quick drying epoxy onto 15ml, 1.52cm diameter centrifuge tubes (3/4 full with water). These tubes were then double sealed using Teflon

tape and electrical tape. The tubes were weighed and placed in vertical orientation in a vacuum oven. After eight hours, the tubes were weighed again. The Water Vapor Permeation was measured as below,

$$WVP = \frac{\Delta m.T}{\Delta t.A.\Delta P}\left(\frac{g.\mu m}{day.m^2.kPa}\right) \quad (2)$$

Here, Δm is the weight loss of water from the centrifuge tube, and Δt is the time of experiment in seconds. A and ΔP are area (m^2) and pressure drop (kPa), respectively. In this case, the vapor pressure of water outside the film (downstream, in the oven) is assumed to be zero, while inside the centrifuge tube (upstream) the saturation pressure of water is at 40°C. Measurements were made in triplicate.

Water retention value was measured as the increase in weight of the membranes when in contact with water in fully flooded conditions. A 50mm circular sample was placed into a beaker containing 150ml of water. The sample was kept fully submerged in the beaker for 30 minutes. After 30 minutes, the excess water was squeezed out by placing the sample between two sheets of blotting paper that were pressed with a Cobb test rolling pin. The difference between the squeezed final wet weight and the initial dry weight of the samples was used to calculate the Water Retention Value. The measurements for each sample were made in triplicate.

Contact angle of water on the membranes was measured using a First Ten Angstrom contact angle measurement device and FTA32 software. 5µm droplets of water were carefully placed on the sample surface using a Hamilton precision syringe. Five measurements were made for each sample.

X ray Diffraction (XRD) analysis was carried out using a PANalytical X Ray diffractometer using a Cu-Kα source (λ = 0.154nm) with a 2θ range from 10 - 26° with a scanning step of 0.033°.

The average width of crystallites in the 002 lattice planes were evaluated as

$$L_{002} = \frac{K\lambda}{\beta_\theta . cos\theta} \quad (3)$$

Where K is the Scherrer Constant (0.9), λ is the wavelength of the diffractometer (0.154nm), β is the width of the crystalline peak at half height, and θ is half of the 2θ value at maximum intensity for the crystalline peak.

Thermogravimetric Analysis (TGA) was done using a Perkin Elmer Pyris 2600 TGA instrument. The original heat treated and conditioned samples were heated from 30°C to 500°C at a rate of 10°C/min. All measurements were made under 20ml/min nitrogen flow.

SEM images were taken using a LEO 1530, Carl Ziess instrument. Cross section samples were prepared and were coated with gold using a Quorum 150 R ES instrument before imaging. The images were taken at 3kV - 5kV accelerating voltage as necessary.

Mechanical testing of the material was carried out with an Instron Bluehill 2 instrument. The films were tested with a 10KN load cell and were stretched at a rate of 50mm/min.

2.3 RESULTS AND DISCUSSION

2.3.1 XRD Analysis

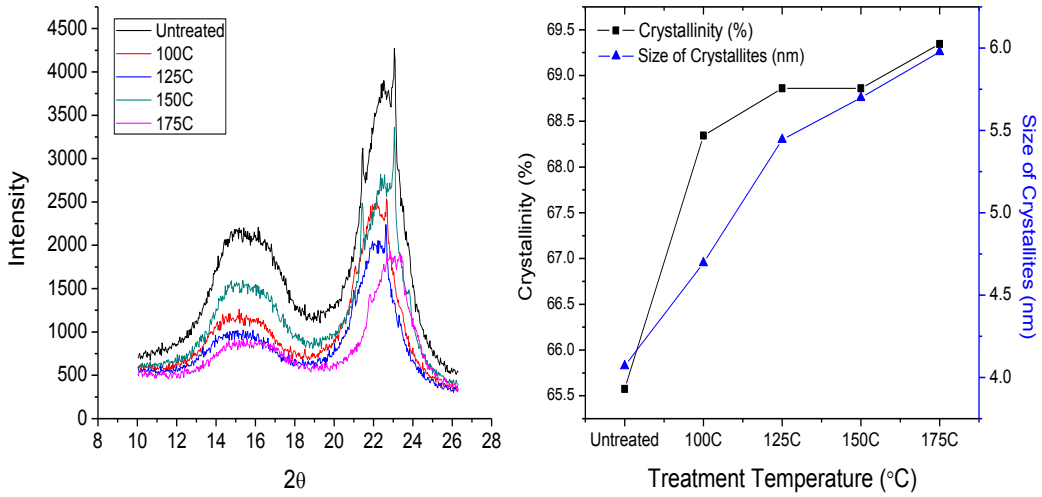

Figure 2.1: XRD Analysis

XRD analysis showed that the crystalline structure of the membranes was altered significantly with increasing treatment temperature. The XRD spectrum (Figure 1) showed a reduction in the intensity of the amorphous region, whereas the crystalline peaks became broader with increasing treatment temperature. The crystallinity increased from 65% to almost 70% after treatment at 175°C. The size of crystallites in the 002 lattice plane calculated from the widths at half maximum of the crystalline peak heights also showed increase with growing temperature[56, 57]. The crystallites amplified in size from 4nm to 6nm after treatment at 175°C. The increase in crystallinity and the size of the crystallites is caused by two mechanisms, co – crystallization of crystalline regions in the CNFs and some degradation of the amorphous regions during thermal exposure[56-58].

2.3.2 Water Retention Value (WRV)

Table 1: WRV and Contact Angle

Sample	Untreated	100°C	125°C	150°C	175°C
WRV (g/m^2)	126.8±6.3	113.4±5.2	97.2±5.4	76.3±3.8	53.6±2.7
Contact Angle (°)	61.2±3.1	62.7±3.1	81.6±4.1	89.3±4.4	95.2±4.7

With a growing treatment temperature, the contact angle increased while the water retention value decreased. The water retention value decreased by almost 57%, while the contact angle increased from 64° to 95° in the samples treated at 175°C as compared to untreated samples. As shown in table 1, both bulk (WRV) and surface hydrophobicity (Contact Angle) gradually grew with an increase in treatment temperature. Decreasing water retention value correlates directly with reduced porosity between fibrils[8, 56, 57, 59]; whereas, a shrinking more wrinkled surface causes increased contact angle due to an increase in surface roughness[60]. Furthermore, the observation of reduction in porosity and the increase in hydrophobicity inferred from these measurements also point toward an increased degree of internal hydrogen bonding of the fibril surface –OH groups[8, 59].

2.3.3 SEM Characterization

The change in fibril morphology analogous to hornification of cellulose fibers is evident in the SEM images of both the surface and the cross section of the CNF membranes. In the SEM images of the untreated samples (Figure 2(a) and 2(b)) an open, porous structure can be observed. Whereas, in the SEM images (Figure 2(c) and 2(d)) of samples treated at 175°C, the loss of the inter fibril porous space is observed in both the surface and cross section. In the untreated samples, the fibrillated structure of the individual fibrils can still be observed, whereas in the treated samples, the fibrils are

matted down and packed much more densely. This change in fibril morphology can be explained by the removal of water from the inter fibril space causing the fibrils to shrink and hydrogen bond with each other via surface –OH groups[3, 7, 56, 59, 61].

The SEM images corroborate the two observations of increase in crystallinity and hydrophobicity. Since the three important mechanisms of hornification – reduction of porosity, increase in hydrophobicity, and increase in crystallinity – were observed concomitantly in the CNF membranes upon thermal exposure, it can be safely asserted that thermal exposure results in the same effects for membrane made from CNFs as the mechanism for hornification of cellulose fibers.

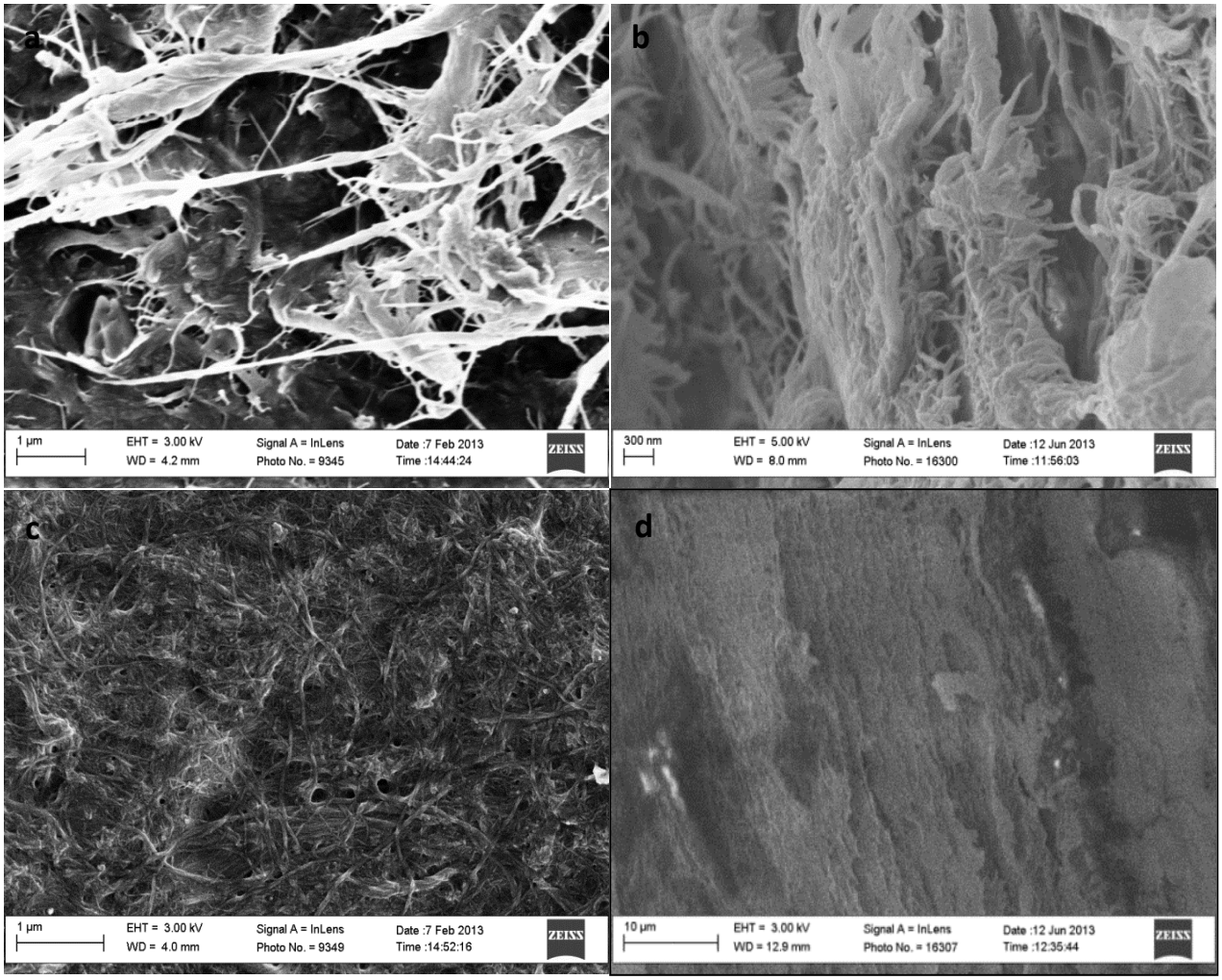

Figure 2.2: SEM images of untreated (a, b) and films heated at 175C(c, d)

2.3.4 TGA Analysis

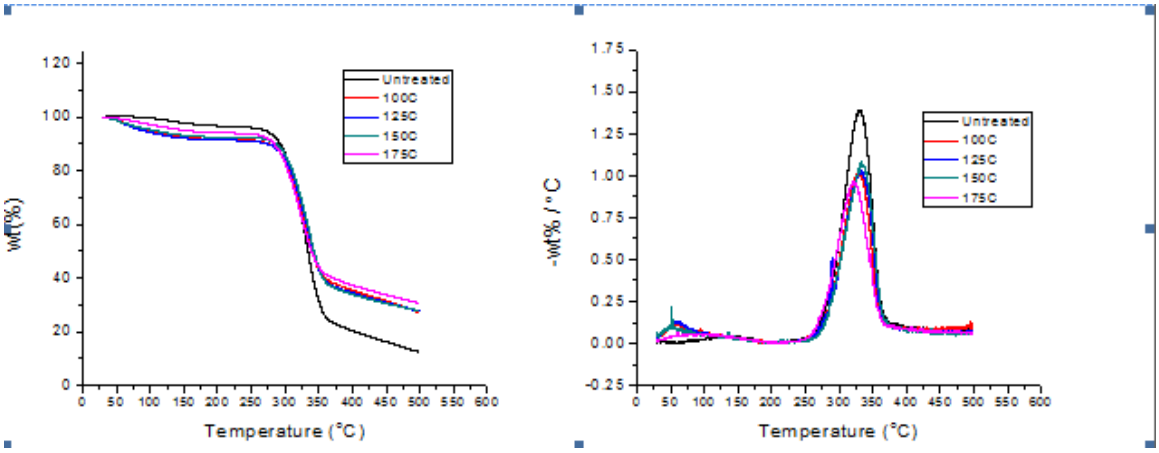

Figure 2.3: TGA Analysis

The TGA curves (Figure 3) show that the characteristic shape of the curves has not changed but the onset and magnitude of weight loss before degradation has reduced significantly. It must be noted that these measurements were made after the membranes had been conditioned for 24 hours at 50% relative humidity. Therefore, this points to the reduced hygroscopic property of the membranes, which also agrees with reduction in water retention value. It can also be observed from the derivative TGA curves that the temperature at which maximum rate of degradation is observed has somewhat decreased for the thermally treated membranes, which could mean there is some degradation of the membrane during the thermal treatment.

Table 2: Thermal Properties

Sample	Untreated	100°C	125°C	150°C	175°C
Max Weight Loss %	71.8	55.09	52.55	51.57	49
Onset Temperature (°C)	288.5	280	271	260	245

Table 2 shows that the change in thermal properties is gradual with an increase in treatment temperature. This is important because the equilibrium water adsorbed acts as a plasticizing agent keeping the membrane soft and elastic. This adsorbed water also acts as a medium for gas permeation through the membrane.

2.3.5 Mechanical

Table 3: Mechanical Properties

Sample	Untreated	100°C	125°C	150°C	175°C
Modulus (GPa)	1.14±0.06	1.2±0.06	1.1±0.05	0.9±0.04	0.77±0.04

The membranes showed decline in strength with increasing treatment temperature (Table 3). The reduction in strength is due to the decomposition of the amorphous cellulose polymer networks and the increase in the crystalline nature of the material, which causes it to be increasingly brittle[8, 56]. Additionally, it is thought that water acts as a plasticizing agent enhancing the tensile property of the material. With removal of the water held in the pores of the membranes, the plasticizing effect is reduced and the membranes show loss of strength and increased brittleness.

2.3.6 Permeability

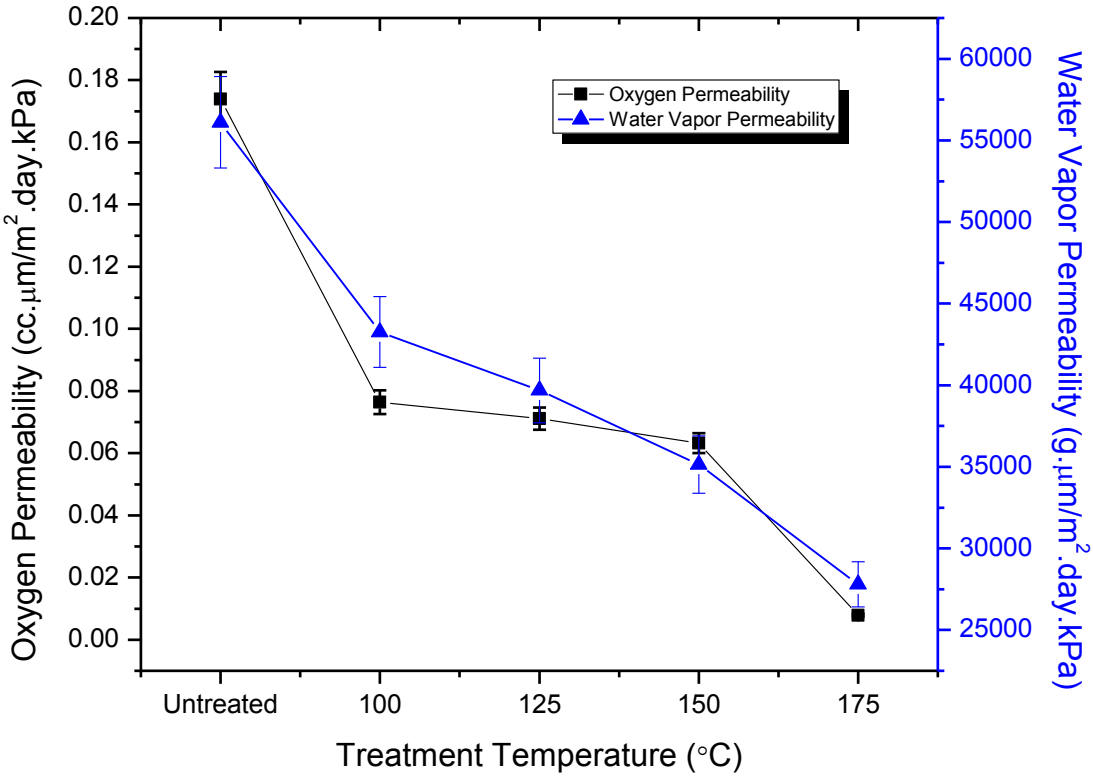

Figure 2.4: Permeability

Oxygen and water vapor permeability decreased significantly with increasing treatment temperature, as shown in figure (4). In the best case, oxygen permeability declined by almost 25 fold while the water vapor permeability declined to half of the untreated membrane value. The reduction in oxygen and water vapor permeability is due to three factors. The first two as hypothesized are common reasons, primarily the significant reduction in porosity of the material hinders diffusion and the increase in crystallinity hinders the solubility of the gas and water vapor in the material[22, 27, 50]. The third reason for reduction in water vapor permeability is the increase in hydrophobicity of

the material. While the untreated membrane adsorbs water quickly in the presence of a water vapor stream, the thermally treated membranes show a much lower degree of water adsorption. This effect arises from the internal hydrogen bonding of the free –OH groups causing increased hydrophobicity rather than just an increase in crystallinity. While this clearly would reduce the water vapor permeability, it also has a significant effect on the oxygen permeability of the membrane.

Since water also acts as a permeation medium for gases, the reduction of water retention helps in reducing overall permeability of the membrane. This effect is demonstrated well where gas is permeated under humid streams and the gas barrier deteriorates. However, in this case, it can be easily contended that due to the limited ability of thermally treated CNF membranes to adsorb water, the deterioration of gas barrier properties under humid conditions can be avoided. A similar effect has been noted by Ostberg et al.[35] who used a hot press method to form CNF membranes. Since the membranes formed were quite dense and had some thermal exposure during the drying process they showed reduced degradation of barrier under humid conditions when compared to CNF films from other studies that were prepared from methods not involving any thermal exposure.

The effects of thermal exposure demonstrated here are in agreement with past studies demonstrating the effects of thermal exposure on cellulose fibers. Previous studies have demonstrated that the loss of porosity occurs due to the removal of water from between the pores of the cellulose fibers which causes the fibers to shrink. Researchers have used solute exclusion, low temperature nitrogen adsorption, 1H and 2H NMR relaxation to determine the changes in pore structure during the drying process[3, 7, 56, 59, 61].

In all studies it was demonstrated that increasing thermal exposure caused reduction in porosity. The concomitant increase in crystallinity has also been studied by various methods including XRD analysis, 1H, 2H, Carbon 13 NMR, and FTIR methods[8, 56-58]. In most cases it was shown that the crystallinity increased due to the co - crystallization of the crystalline regions. Some authors have also contended that the increase in crystallinity is due to amorphous regions being converted to crystalline during the drying process.

The hornified fibers not only become less porous and more crystalline but also increasingly hydrophobic during the drying process. The increase in hydrophobicity is indicated by an increase in water contact angle and reduction of water retention value. The reduction of fiber water retention value is mainly attributed to the formation of irreversible hydrogen bonds between free – OH groups on the cellulose fibrils. This hydrogen bonding is also related to the changes in morphology, and the fibrils are observed to shrink and suffer a loss in porosity upon drying. We also noted that the surface became increasingly wrinkled and had increased surface roughness, which could be the cause of increased contact angle. This is an agreement with past studies relating surface roughness to hydrophobicity and contact angle. Studies have demonstrated time and temperature play an important role in the degree of hornification achieved. Here, the drying of the membranes at different temperatures would have caused different drying rates, and at higher drying temperatures a more significant degree of porosity loss and a reduction in water retention values are observed as a consequence.

2.4 CONCLUSIONS

In this study the effects of thermal exposure on CNF membranes analogous to hornification to improve barrier properties were demonstrated. The effects were observed on a bulk level in the membranes and also on a fibril level. This method avoids the usage of any filler materials or chemical reagents. The XRD analysis determined that both size of crystallites and the crystallinity of the material grew with increasing treatment temperature. Water retention value decreased significantly while surface contact angle increased from hydrophilic to hydrophobic, pointing towards an intensification of surface roughness, fiber shrinkage, internal hydrogen bonding between the fibrils, and a loss of porosity. SEM images concurred with the XRD and water retention measurements in making evident that the fibrils underwent shrinking and a loss of inter fibril porosity. Finally, both oxygen permeability and water vapor permeability decreased significantly upon thermal treatment due to mechanisms analogous to hornification of cellulose fibers. The reduction was ascribed to hindered diffusion due to a more dense structure and reduced gas solubility due to increased crystallinity. The significant decrease in water vapor permeability was also thought to be due to the significant increase in hydrophobicity of the membranes. Even though a loss of mechanical strength of the materials was observed due to an increase in crystallinity and brittleness, the enhancement of barrier properties is significant.

Hereby, we have demonstrated that controlled thermal exposure can serve as a good method for enhancing the barrier properties of CNF membranes without using external chemical agents, which maintains the native cellulose material as a green,

recyclable, and biodegradable material. The study also paves the path for further tuning of CNF membrane properties via controlled thermal exposure.

CHAPTER 3

DUAL MECHANISM OF DRY STRENGTH IMPROVEMENT OF CNF FILMS BY PAE CROSSLINKING

ABSTRACT

In this study we prepared high grammage, robust, and structurally dense CNF (Cellulose nano fibrils) films with and without wet strength crosslinker Kymene™ (PAE, a polyamide-epichlorohydrin resin). Both self- crosslink of PAE network and hetero crosslink between cellulose and PAE were formed at elevated temperature. Besides expected wet strength improvement, we also discovered unique stress-strain behavior for dry crosslinked films, which has never been before. This stress-strain behavior indicates varying stress bearing mechanisms at different levels of crosslinker addition due to formation of new bonds by crosslinking. Crosslinking increased dry strength by approximately 2.5 fold compared to pure CNF films. Wet strength enhancement was also quite significant; wet strength of crosslinked films was observed to be very close to pure dry CNF films, approximately 35MPa. Additionally, the crosslinked films showed a transition of both surface and bulk properties from hydrophobic to hydrophilic. Water contact angle increased from 50° to 110°, while the water retention value for the crosslinked films decreased by approximately 25%. Moreover, water vapor permeability also decreased by two fold. As previously shown, some of the increase in hydrophobic nature can be attributed to induced hornification during the 3 hour heating period for crosslinking at 120°C. Possible mechanisms for the changes in behavior are discussed in detail.

3.1. Introduction

Polymer films are in great demand for various packaging applications. However, most pose significant environmental concern due to production from petroleum derived sources and end of life challenges when they are deposited directly in landfills. Barriers made from micro fibrillated cellulose or cellulose nano fibrils (CNF) have garnered significant attention due to their excellent biodegradability, renewability, barrier, and mechanical properties. CNFs possess these excellent properties due to their high aspect ratio, strong inter, and intra molecular hydrogen bonding between fibrils, and a dense packing structure obtainable for films[14, 31, 62].

Even though films made from cellulose nano fibrils possess these excellent properties, their mechanical and barrier properties will degrade in humid environments due to high affinity to water. The hydrophilic nature of cellulose therefore limits their applicability for packaging applications. Because of this, it is imperative to develop solutions that can stop or limit the degradation of mechanical and barrier properties of CNF membranes in humid environments[10, 14, 31, 62, 63].

Crosslinking using Polyamide- epicholorohydrin(PAE) resins is common in the paper manufacturing industry to increase wet strength of specialty products such as tissue paper, paper towels, liquid packaging base papers and other products which may come in contact with water. PAE crosslinkers are commercially available as PAE/water solutions. The increase in wet strength due to PAE crosslinking of cellulose has been extensively studied and is well understood. The mechanisms of wet strength enhancement have been attributed to covalent ester bond formation between carboxyl groups of cellulose and

azetidinium groups of PAE. A secondary mechanism of self-crosslinking of PAE groups to form a water insoluble network also occurs during the curing process[64-67].

Previously our group has demonstrated excellent properties of PAE crosslinked CNF aerogels in wet environments[12]. Additionally, no studies have been done on the mechanical performance of crosslinked CNF films. Some studies have shown that CNFs are better at adsorbing PAE due to a higher accessibility of anionic carboxyl sites; however, most studies have relied on carboxymethylation of cellulose to increase the concentration of carboxyl sites[12, 64-68].

Even though PAE crosslinkers enhance wet strength, there is a trade off with biodegradability and recyclability. If too much PAE crosslinker is used, the fibers are rendered non-biodegradable and non-recyclable due to a high degree of crosslinking[64]. Thus, it is imperative to use as small an amount of PAE as possible. Here we propose the crosslinking of mechanically produced CNFs with a very low concentration of PAE crosslinker Kymene™ (1% by fiber weight), so as to not significantly affect the biodegradability of the films. We propose taking advantage of a longer curing period to promote not only hetero crosslinking between carboxyl sites and PAE azetidinium groups, but also the formation of PAE networks[12, 66, 67]. Additionally, we expect the longer curing period to induce some hornification in the films, as we have shown previously, to change the film surface and bulk behavior from hydrophilic to hydrophobic[69]. Even though it is not explored in this study, we expect that usage of a very low amount of crosslinker would have a limited effect on the biodegradability of the CNFs. In this study we will mainly explore the function of mechanical strength enhancement and water interaction as a result of crosslinking of CNF films.

3.2. Experimental

3.2.1. Materials

Cellulosic nanofibers were obtained from the University of Maine as approximately 3% solids slurry in water. Commercially available crosslinker Kymene™ was obtained from Ashland Inc. (Covington, KY, USA) as a 12.5% solid suspension.

3.2.2.Fabrication of Films

The CNF slurry was first diluted to 1% and a weighed amount was vigorously stirred for 30 minutes. Crosslinked films were prepared by adding 1wt% Kymene™ with respect to dry fiber weight to the slurry while stirring. Subsequently, films were fabricated via an ultrafiltration process followed by hot press drying and conditioning. Millipore polyvinylidene difluoride (PVDF) membranes of 142mm in diameter and a pore size of 0.22µm were used for the ultrafiltration process. A grammage of approximately 300g/m^2 was targeted to obtain thick, dense, and robust films. The slurries were dewatered until no more water could be removed. The dewatered mat was placed between smooth metal caul plates and four sheets of blotter paper and compressed at a load of 60psi to remove any excess water after dewatering. After pressing, films were dried in a flatbed dryer under approximately 50 - 60 psi load and 50°C for 24 hours.

Following the drying process, the films with crosslinker were heated in an oven at 120°C for 3 hours to complete the crosslinking procedure. Subsequently all films were conditioned at 23°C, and 50%RH for 24 hours. Multiple films were made for each type of pulp.

3.2.3. Characterization

The films were characterized by physical dimensions, water retention, contact angle, thermal properties, stress-strainanalysis, FTIR, and SEM imaging of surface and cross section of fracture surface.

First, films were cut into discs of 42mm in diameter and weighed. Three discs were cut and for every disc, five measurements of thickness were made with a Mitutoyo micrometer to ascertain film thickness and grammage. Water retention was measured by soaking the film discs in water for 30 minutes and measuring the difference in weight to determine adsorbed water.

Contact angle was measured with a First Ten Angstrom goniometer, and FTA32 software was used to perform image analysis. FTIR spectra for the films were collected by the direct film method. A Bruker Vector 80v was used for the FTIR analysis.

For mechanical testing, a standard ASTM dogbone D-1708 was used and 3 samples for each type of film were tested in an Instron Bluehill II machine for measuring the mechanical strength of films. Mechanical testing was performed for dry and wet samples. In the case of the wet strength test, the samples were soaked in deionized water for 30 minutes prior to testing, and excess water was removed by blotters according to TAPPI Test Methods. Morphology of the films was analyzed by SEM (LEO 1530 SEM, Carl Zeiss) at 3 -15kV. The samples were mounted SEM stages and gold sputtered (Quorum 150ES) for 60 seconds. Thermal analysis was performed in a Perkin Elmer TGA from 25°C – 500°C at a rate of 10°C/min.

3.3. Results and Discussion

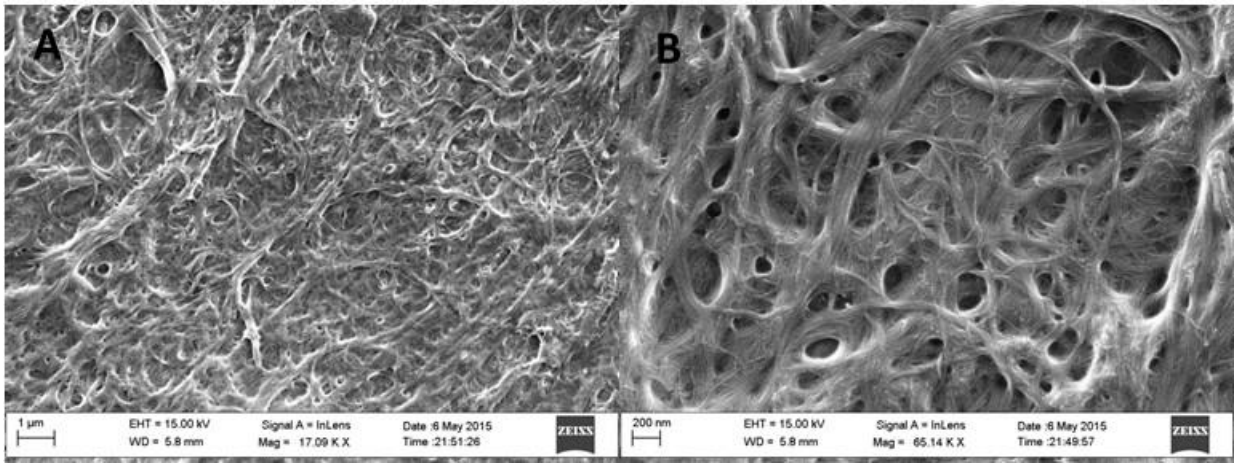

Figure 3.1: As Obtained CNF

To prepare the films commercially, CNFs obtained as 3% slurry in water was used. In the SEM micrographs of the obtained material (figure **1**), fibrils of diameters in the 10 - 100 nano meter range and bundles of CNFs can be observed. It was important to produce films with physical uniformity to compare the pure and crosslinked films consistently. The slurry was diluted to 1% with and without PAE crosslinker and films were fabricated via an ultrafiltration, compression and hot press method. Highly uniform films with physical characteristics shown in table (**1**) were obtained. The similarity in thickness and grammage also indicates comparable apparent density of the films. After drying, films containing PAE were heated at 120°C for 3 hours to complete the PAE crosslinking, and subsequently all films were conditioned. SEM images of the surface of the films are shown in figure (**2**). While both films were of high grammage close to the intended target and were visually uniform, the surface structure of the pure CNF films shows a lot of surface roughness, and a large number of free fibrils on the surface. Whereas the crosslinked film's surface shows a significant amount of smoothing and

densification. This is expected since the crosslinking forms extra bonds within the CNF film, and there is also significant loss of porosity and densification observed in the film structure due to thermal exposure[57, 60, 69].

Table 4: Physical Properties of Films

Sample	Pure CNF	Crosslinked CNF
Thickness (µm)	289.1±15.4	291.7±14.3
Grammage (g/m^2)	94.5±4.8	95.5±4.4

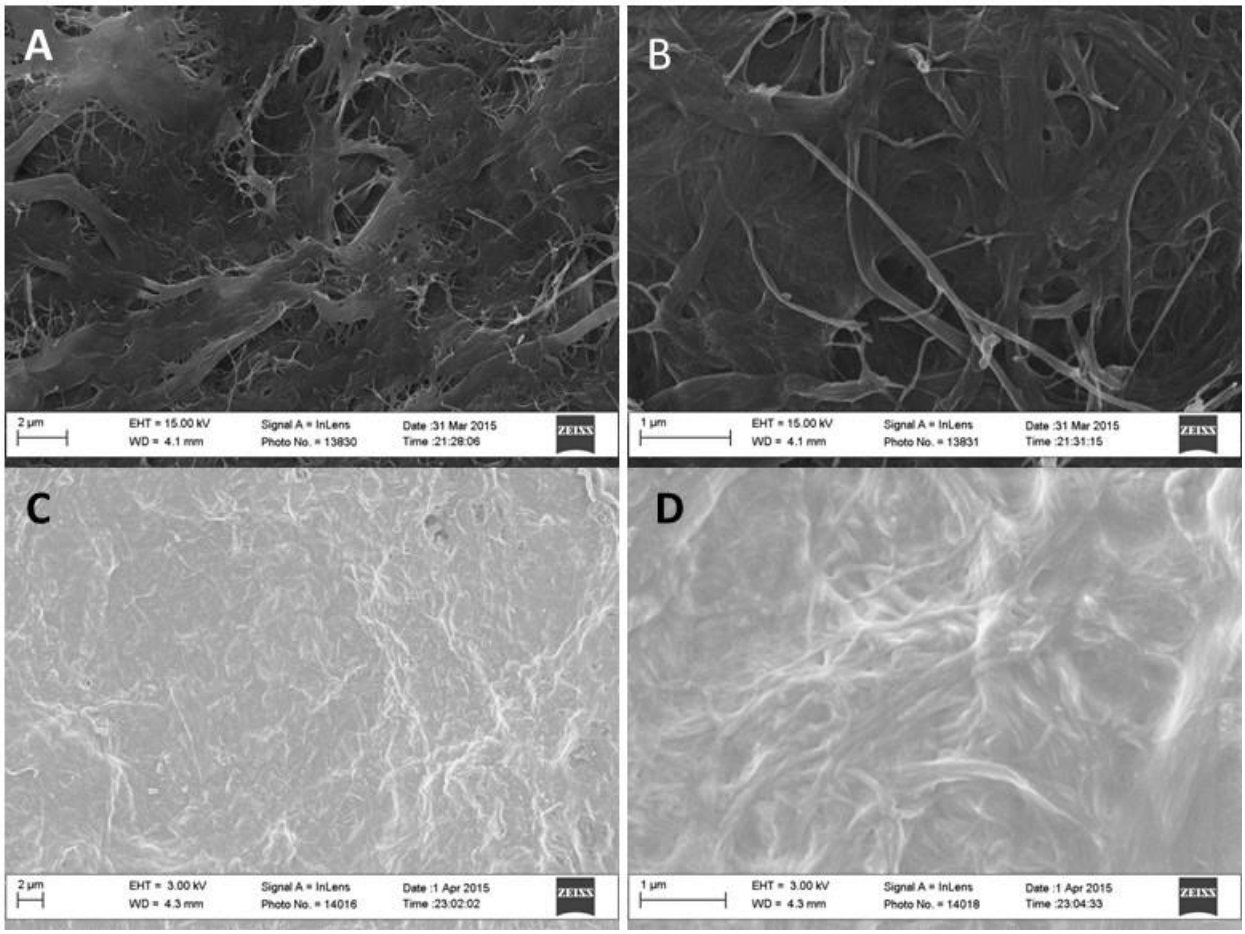

Figure 3.2: Pure CNF Films (Top), PAE Crosslinked Films (Bottom)

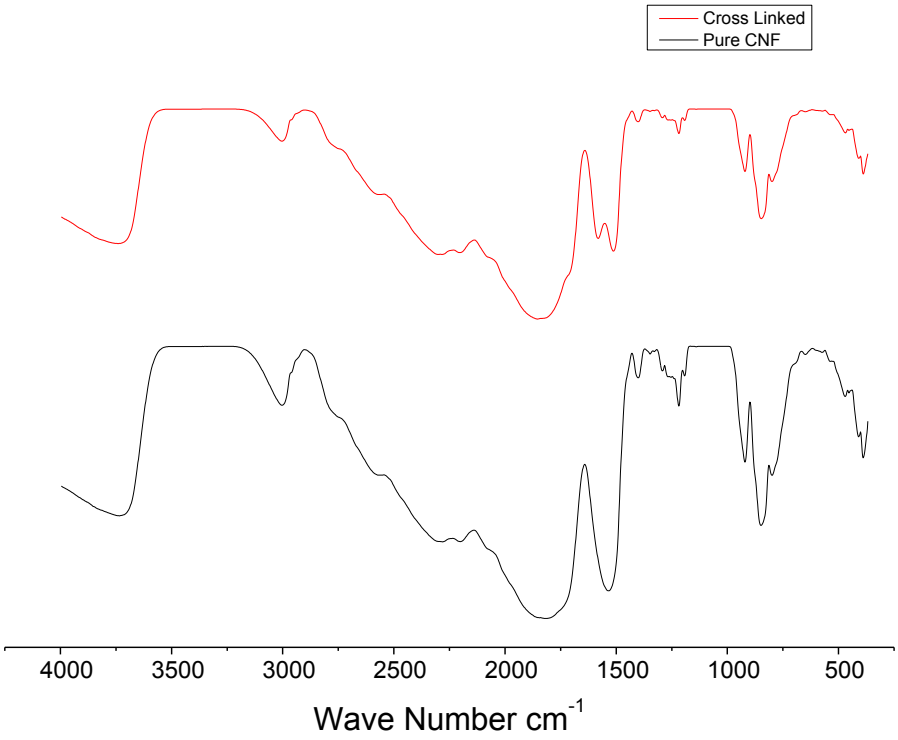

Figure 3.3: FTIR Analysis

FTIR analysis shown in figure (**3**) was performed to confirm the crosslinking between MCF films and PAE. The primary difference to note between the two is the presence of a new peak in the 1550 cm^{-1} region. This peak is attributed to the amide II (-NH) groups of PAE crosslinker, and confirms the presence of PAE in the crosslinked films. The presence of a shoulder in the crosslinked film spectrum at 1728 cm^{-1} confirms the crosslinking between PAE and cellulose. This is attributed to the stretching of C=O ester bonds formed between the PAE azetidinium groups and cellulose carboxyl groups. Additionally, 1260 cm^{-1} area of the crosslinked film spectrum also shows a reduction of the valley, thought to be due to the formation of additional C-O ester bonds between PAE and cellulose[12, 68].

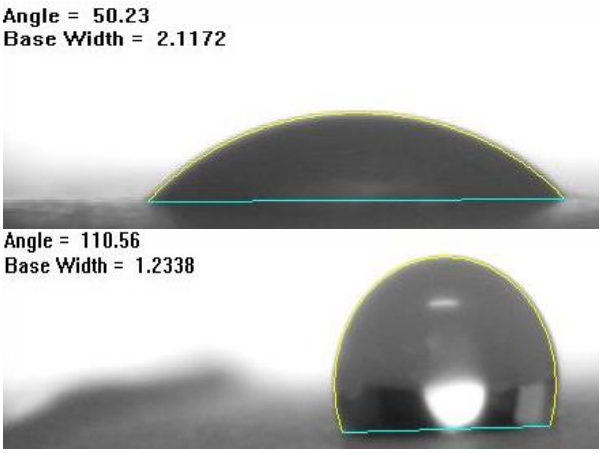

Figure 3.4: Pure CNF Contact Angle (top), PAE Crosslinked CNF Contact Angle (bottom)

Table 5: Water Interaction Properties

Sample	Pure CNF	Crosslinked CNF
Contact Angle (°)	50.2±0.6	110.5±0.7
Water Retention Value (g/m^2)	77.4±3.9	52.1±2.6
Water Retention Value (g water/g dry film)	0.81±0.04	0.59±0.03

After confirming the crosslinking from FTIR, the interaction with water was of primary interest. Previously in the literature, severe degradation of mechanical and barrier properties in humid conditions has been extensively studied[50]. Due to PAE crosslinking, it is expected that degradation of CNF film properties should be significantly reduced due to adsorption of water. Since crosslinking is carried out by heating at 120°C for 3 hours, there should also be some hornification of the films which

would limit interaction with water[64-66, 69, 70]. To observe the surface and bulk interaction, contact angle and water retention values were measured. Figure (**4**) shows the typical observations of water droplets on the surface of the films after 5 minutes of placing the droplets. Figure (**2**) shows the measured contact angle and water retention values.

Pure CNF films showed hydrophilic characteristics typical of cellulose, whereas crosslinked films showed a transition to hydrophobic in both surface and bulk properties. The contact angle transitioned from 50° for pure CNF films to 110°C for crosslinked films which is indicative of a hydrophobic surface, while the water retention decreased by approximately 25% after crosslinking. The crosslinking of PAE / CNF films is accomplished by heating the films at 120°C for 3 hours; this is also responsible for inducing some hornification into the films, as we have shown previously. Typically hornification due to thermal exposure causes the cellulose hydroxyl groups to irreversibly hydrogen bond with each other, reducing sites for interaction with water[8, 60, 71]. Additionally, due to this inter fibril hydroxyl hydrogen bonding the fibrils are pulled closer together causing the loss of porosity in the films, thereby reducing the pore space for water to be absorbed[8, 60, 61]. Both the loss of hydroxyls and porosity concurrently aids in the significant increase in water contact angle. PAE crosslinking further helps in this process of bringing the fibrils closer together because it covalently bonds with the carboxyl groups of the cellulose during the cross liking process, creating bonds between the fibrils that did not previously exist or would occur as a consequence of thermal exposure[66-68].

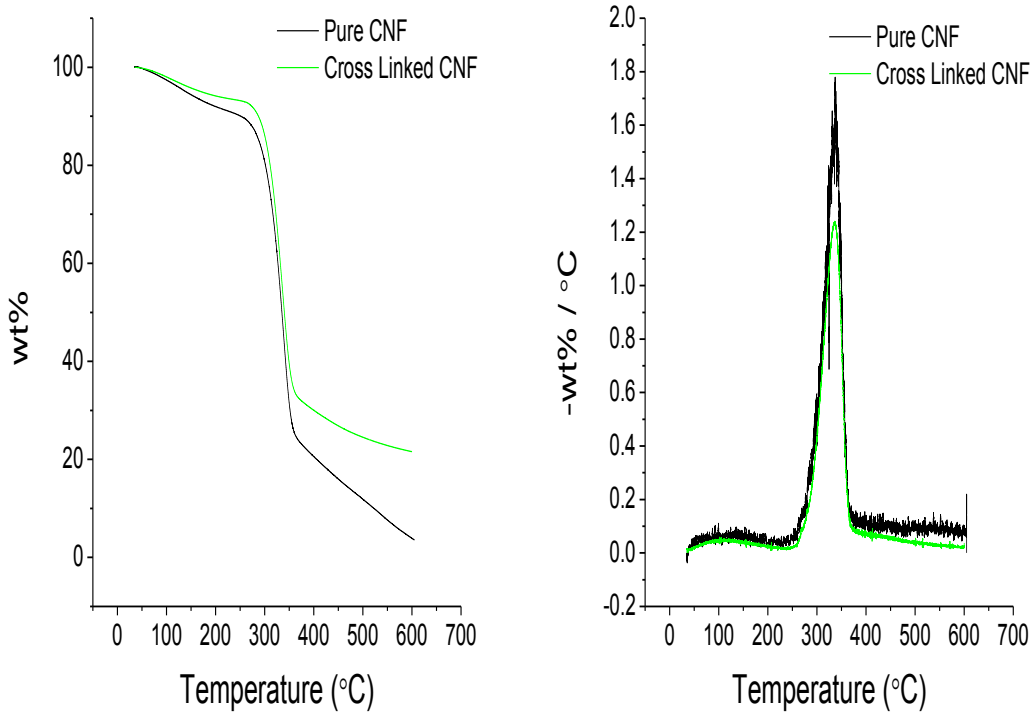

Figure 3.5: TGA and DTG Analysis

The thermal analysis curves for pure CNF film and the crosslinked films in figure (**5**) show clear differences between the thermal stability of the two materials. The crosslinked films displayed a delayed onset, lower maximum rate of degradation, and reduction in weight loss before the maximum degradation temperature is reached. During the conditioning process carried out at 50% RH for 24 hours before analysis, the films are expected to absorb an equilibrium amount of water at those conditions, and thermal analysis can help indicate the differences between amounts of water adsorbed by the two different materials. The crosslinked films show significantly less weight loss overall, indicating that the amount of absorbed water is much lower. The crosslinked films, as observed from the water retention value, are expected to show less water retention due to inter hydroxyl hydrogen bonding, loss of porosity, and crosslinking[8, 60, 69, 71].

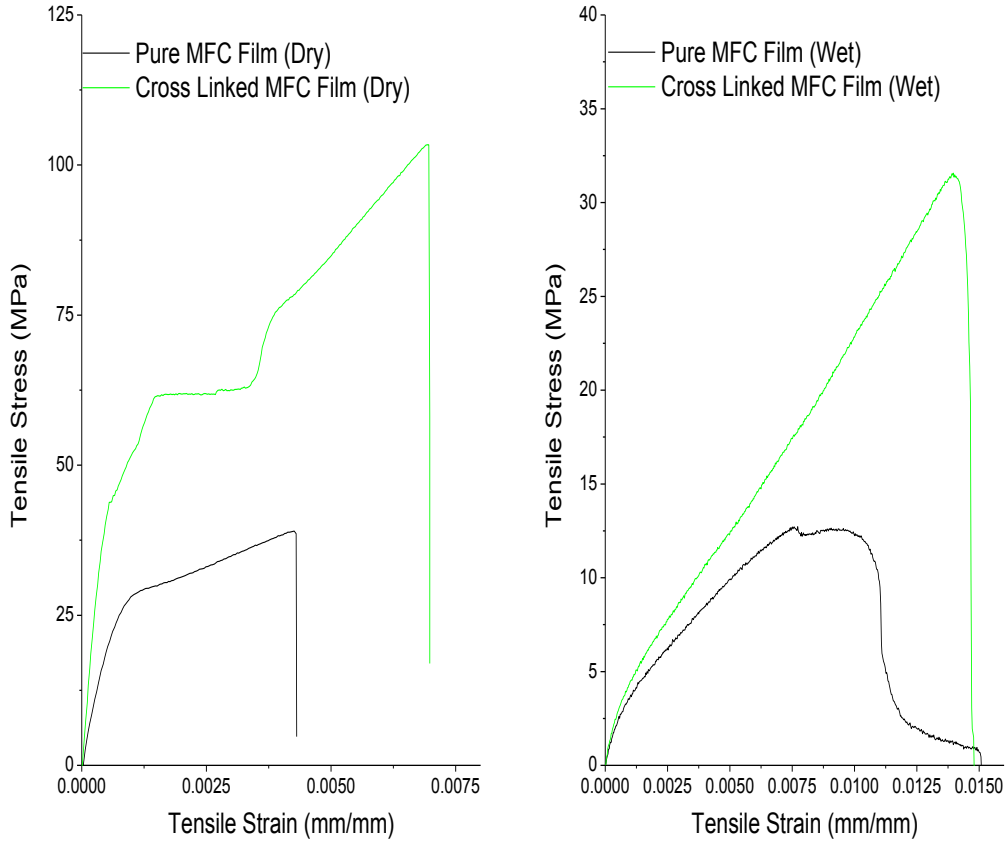

Figure 3.6: Stress - Strain Analysis (left: dry tests, right: wet tests)

Shown in figure (**6**) are typical tensile stress-strain / extension curves obtained for dry and wet, pure and crosslinked CNF films. The dry tests refer to the samples which were tested after the conditioning, whereas the wet samples refer to samples that were soaked in water for 30 minutes prior to mechanical testing. For SEM analysis the wet samples had to be dried beforehand at ambient conditions. Shown in figures (**7(a, b)**) are the fracture surface SEM micrographs of the dry and wet, pure CNF films respectively after mechanical testing and drying in the case of wet test samples. Shown in figures (**9(a,**

b)) are the fracture surface SEM micrographs of the dry and wet, pure CNF films respectively after mechanical testing and drying in the case of wet test samples. The pure dry CNF films displayed typical behavior characteristic of CNF films, whereas the wet CNF films displayed a "*tear*ing" behavior. The dry crosslinked CNF films showed a very distinct, and to our knowledge never before observed for CNF films stress- strain behavior: multiple knees, plastic deformation, and multiple strain hardening regions. On the other hand wet crosslinked CNF films showed a singular elastic region before break, atypical from the expected tear behavior for pure CNF films.

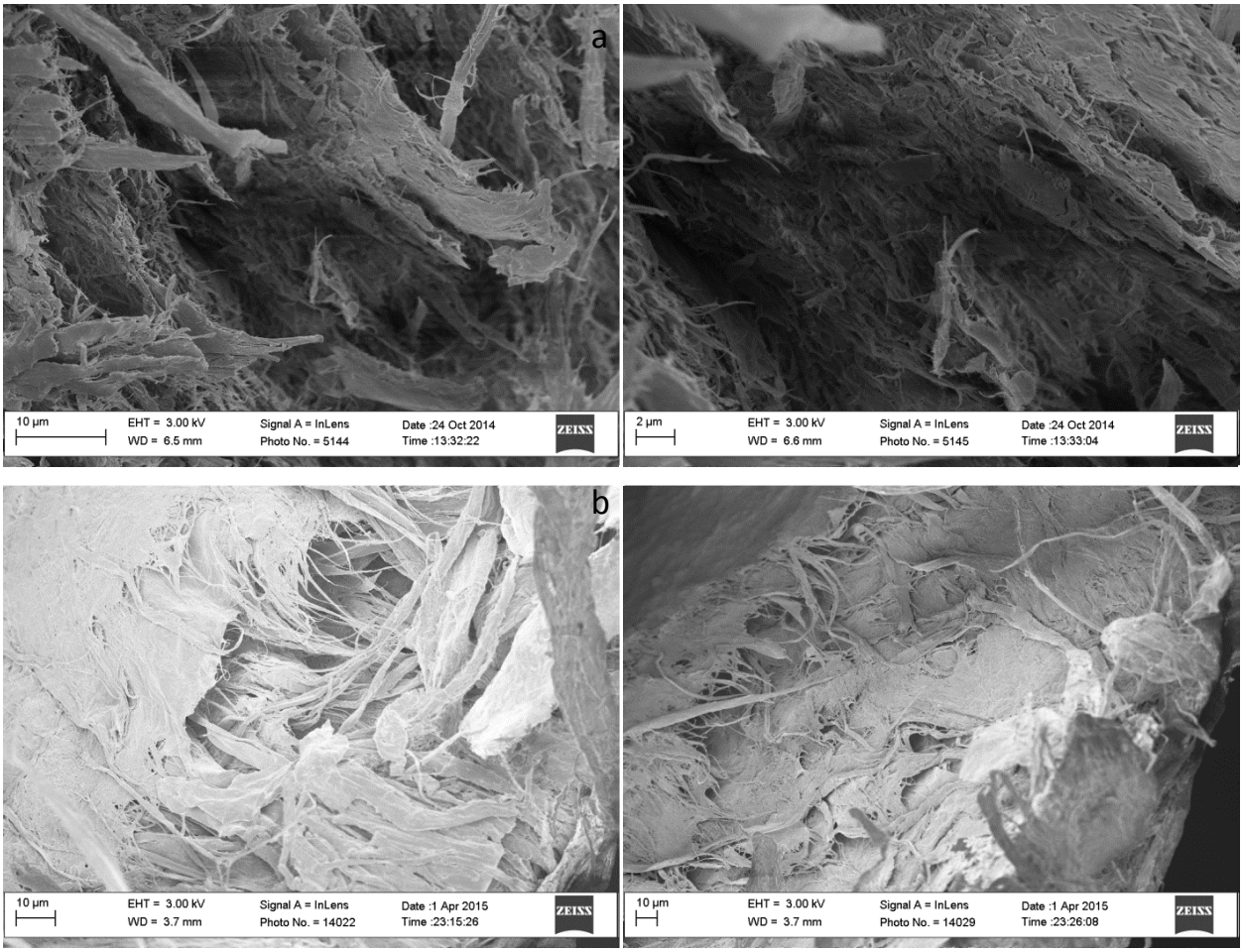

Figure 3.7: SEM images of dry (a) and wet (b) pure CNFs fracture surface

The dry pure CNF films show a linear behavior up to approximately 25MPa of tensile stress. After this pseudo-elastic region, there is a knee in the curve which is thought to occur due to some fibril-fibril de-bonding. The knee is followed by a linear strain hardening region to approximately 40 MPa, where failure occurs. In the strain hardening region, there is significant reinforcement effect due to straightening and reorientation of nano fibrils and inter fibril slippage. This reinforcement behavior is caused due to the alignment of nano fibrils in direction of the applied strain. Failure of the film occurs by failure of fibrils and breakage of bonds between them[13, 15, 20, 72-75]. This is also observed in the SEM micrographs of the fracture surface of the pure CNF films

(figure (**7a**)), where broken individual fibrils and bundles of aggregated broken fibrils are visible. Some ordering of the fibrils in the direction of the applied strain, which was caused during the strain hardening period, is also visible. This behavior is typical of CNF films and has been well documented in the literature[13, 15, 72-75].

The wet CNF films do not show a linear behavior in their stress-strain behavior. This is expected because CNF films absorb a significant amount of water and swell. Adsorption of water causes the inter fibril bonding to be disrupted and lose strength. Therefore, instead of the films displaying typical CNF stress-strain behavior, they display a *tearing* behavior, where weakened bonds are easily being broken and the water swelled fibrils are simply pulling apart from each other. With a loss of stress and increasing strain, the fibrils start coming apart in an elastic region and some necking is observed. Subsequently, with increasing strain the film completely tears apart. This is also clearly observed in the SEM images (figure (**7b**)) of the fracture surface of the wet films. Instead of the broken fibrils observed in dry CNF, these fibrils are clearly pulled apart and broken.

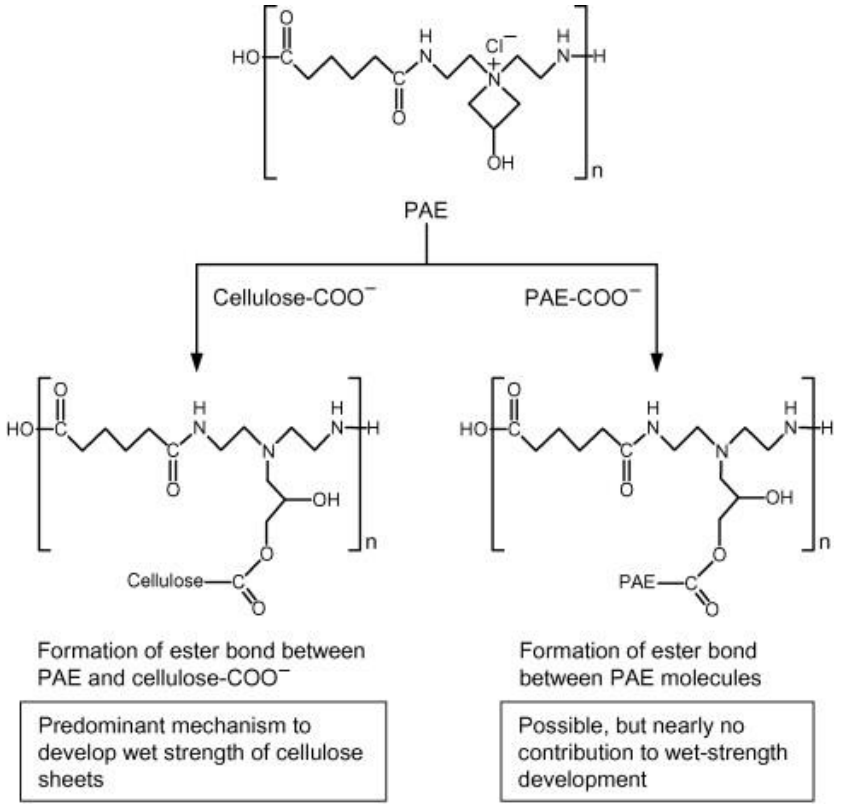

Figure 3.8: PAE - Cellulose Crosslinking Mechanism (from Obokata et.al)[66]

After being wetted, crosslinked films did not display a tearing behavior in the mechanical analysis like the pure CNF films did since they are protected by the PAE crosslinking and show failure at a stress level, just slightly less than dry pure CNF films. Obokata et al, our group, and various research groups have studied this mechanism in detail, and the mechanism shown in figure (8) has been proposed by Obokata et al[66]. The mechanism of interaction of PAE and cellulose has been described as dual, consisting of a reinforcing and protection mechanism. The reinforcement mechanism is the reaction between carboxyl functional groups of the cellulose and azetidinium groups of the PAE. The protection mechanism on the other hand is due to inhibition of inter fiber detachment in water caused by formation of water – insoluble PAE networks. Previously other authors have

characterized PAE crosslinked carboxymethylated native cellulose sheets with FTIR analysis and showed that ester bond formation between azetidinium groups of PAE and carboxyl groups of the cellulose was the main factor for wet strength development[66, 67, 76]. Ahola et al[65] studied the adsorption of PAE on cellulose nanofibrils and used that as a wet strength additive for paper. They were able to show that when both PAE and cellulose nanofibrils were adsorbed onto native cellulose fibers a significant increase in wet strength could be observed.

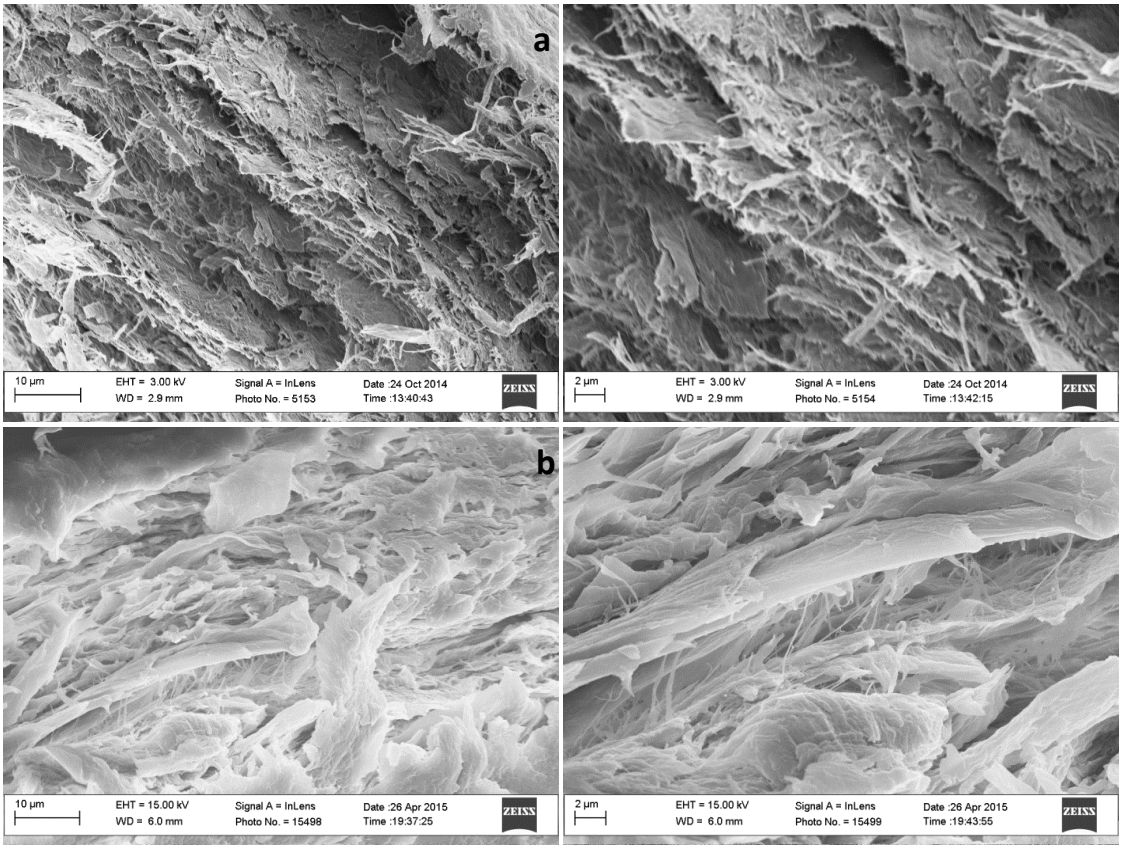

Figure 3.8: SEM images of dry (a) and wet (b) crosslinked CNFs fracture surface

The SEM images of the wet tested crosslinked film fracture surface (Figure 9(**b**)) show a very different structure than the pure wet tested CNF films. The wet tested crosslinked films do not show a tear behavior due to the protection mechanism whereas the pure CNF films do. The difference between the stress-strain behavior of the wet pure and crosslinked CNF films shows clearly that in the case of crosslinked films the stress bearing mechanism is different, and that most of the stress is borne by the new bonds created due to crosslinking since no tearing behavior is observed[64-68].

The dry crosslinked samples on the other hand showed a complex, never before observed stress-strain behavior for CNF films, with multiple distinct regions implying different load bearing mechanisms at different stress levels. The curve can be observed as two distinct phases, one before the plastic deformation region with constant stress observed at approximately 67.5MPa and one after.

The region before the plastic deformation is very similar in behavior to pure CNF films initially, albeit with a much higher slope. It begins in a pseudo-elastic region followed by a knee and a strain hardening region, but the result is a plastic deformation region, rather than failure. After the plastic deformation region, there is another knee leading into a secondary strain hardening region after which failure occurs. The SEM micrographs of the fracture surface (Figure 7(**a**)) show not only broken fibrils and bundles of fibrils but also highly ordered sheet like structures. The broken fibrils indicate that the eventual mechanism of film failure is breakage of fibrils and breakage of inter fibril bonds just as observed for pure CNF films. Therefore, we can reasonably assume

that the stress-strain behavior after the plastic deformation is due to load bearing by the cellulose fibrils and inter hydroxyl hydrogen bonds as in pure CNF films. During the plastic deformation region there is no increase in film stress. We postulate this is due to the breaking of the PAE networks that are formed during the crosslinking process, and that none of the CNF bonds are broken in this region. The highly ordered sheet like fibril structures observed in the fracture surface SEM images (Figure 7(**a**)) indicate that the reorientation of the fibers in the strain hardening region is much more prolonged than pure CNF films. It is possible that fibril reorientation also occurs during the plastic deformation and not just in the strain hardening regions.

The stress-strain behavior prior to plastic deformation indicates that there is a different load bearing mechanism in that region than for pure CNF films. This can only be attributed to the additional bonds formed due to crosslinking, since the pure CNF films do not show this behavior. It can be assumed that the initial pseudo elastic behavior is due to PAE-carboxyl bonds, followed by the knee which is representative of inter fibril de-bonding. This is followed by some strain hardening for a very short strain range because PAE networks take over the load bearing right after de- bonding. The plastic deformation seems to be occurring due to breakage of bonds of the PAE networks, because during this region there is virtually no increase observed in the stress of the films. Additionally, the highly ordered sheets observed seem to occur from "*sliding*" of ordered fibril networks over each other without load bearing. Moreover, the strain hardening region observed for the crosslinked films after plastic deformation is larger in range than the pure CNF films, providing increased opportunity for the ordering of fibril

networks. Eventually, breakage seems to occur due to the typical breakage of fibril bonds.

3.4. Conclusions

PAE resin based wet strength enhancing agents are commonly used in the paper industry. Previously significant study has elucidated the mechanism of PAE crosslinking with cellulose by heat curing the resin. Other studies have also shown significantly better retention of PAE resins in NCF materials as compared to native cellulose fibers. Previously our group has shown significant improvement of CNF based aerogels for application by crosslinking with PAE. Here we investigated the properties of CNF films crosslinked with PAE based crosslinker Kymene™. We observed that the CNF film surface transitions from hydrophilic to hydrophobic after the crosslinking process, displaying a contact angle increase from 50° to 110°. Additionally, the water retention value also displayed about a 25% decrease implying an increase in bulk hydrophobicity of the material. As was expected, the wet strength of the crosslinked material showed significant enhancement. The pure CNF film showed a simple *tear* behavior as expected to be displayed by wet and swollen CNFs; while on the other hand the crosslinked films showed a single elastic region, ending in an eventual failure at a similar stress level as dry CNF film. Most importantly we demonstrated never before observed complex stress-strain behavior and an increase in strength of the dry crosslinked CNF films which was comprised of multiple different phase behaviors indicating stress bearing by different mechanisms in the crosslinked material at different stress levels.

CHAPTER 4
HIGH PERFORMANCE CROSSLINKED NANO COMPOSITE CNF BARRIER FILMS

Abstract

Composite films of CNF and nano filler materials were studied in the context of mechanical and barrier properties. The filler materials used were high aspect ratio nano clay and graphene flakes. Additionally the composite films were also wet strength crosslinking agent Kymene™, a PAE resin. First the effects of making a composite material were analyzed without crosslinking. Stress-strain analysis showed that incorporation of 1% clay and graphene flakes significantly modified the stress-strain behavior of CNF films. An increase in the ultimate tensile strength is also observed, 55%, and 96% for clay and graphene respectively. The crosslinked composites showed a more complex behavior as compared to the crosslinked CNF films. The crosslinked films showed delayed transition to the next phase, whereas they also showed a marked increase in ultimate tensile strength over the crosslinked CNF films. The oxygen and water vapor permeability of the composite films without crosslinker showed that the filler materials were extremely effective in improving the barrier properties. There was a reduction of 47%, and 65% of oxygen permeability and 60% and 67% for the clay and graphene composites without crosslinker. Whereas when the films were crosslinked, a reduction of 50% of the water vapor permeability in the films was demonstrated. The crosslinked composite films showed a further improvement, with an 85% reduction in the water vapor permeability for the crosslinked graphene composite films.

4.1. Introduction

Polymer films are in great demand for various packaging applications. However, most pose significant environmental concern due to production from petroleum derived

sources and end of life challenges when they are deposited directly in landfills. Barriers made from micro fibrillated cellulose or cellulose nano fibrils (MFC / CNF) have garnered significant attention due to their excellent biodegradability, renewability, barrier, and mechanical properties. CNFs possess these excellent properties due to their high aspect ratio, strong inter and intra molecular hydrogen bonding between fibrils, and dense packing structure obtainable for films[14, 31, 62]. Even though films made from cellulose nano fibrils possess these excellent properties, their mechanical and barrier properties start to degrade in humid environments due to high affinity to water. In consequence, the hydrophilic nature of cellulose limits its applicability for packaging applications. Therefore it is imperative to develop solutions that can stop or limit the degradation of mechanical and barrier properties of CNF membranes in humid environments[10, 14, 31, 62, 63].

The barrier and mechanical properties of barrier membranes can be enhanced significantly by a common method of including a high aspect ratio filler material with a very low loading. High aspect ratio materials help to enhance the barrier properties by increasing the tortuosity of the films, while the mechanical properties of the resulting composite are also enhanced due to the filer material acting as fully discrete functional particles within the polymer matrix. Various authors have done significant studies on this method. Cussler et al studied the diffusion mechanisms of permeates through barrier membranes in exhaustive detail, and developed various models to estimate the properties of such membranes. Malho et al studied the direct exfoliation of graphene crumpled sheets in to a CNF matrix to obtain high strength composites. Additionally, this method has no significant impact on the processing and handling of the matrix polymer. In this

context, the study of clay-polymer composites is quite common. However, clays may be hydrophilic and might not be compatible with hydrophobic polymers. They also pose some additional problems in the context of exfoliation and aggregation. Therefore, the application of polymer-clay composites has been limited in nature. The more recent literature points to the usage of graphene flakes which can be functionalized to be compatible with a wide variety of polymers, and can be obtained from inexpensive graphite powder.

Crosslinking using Polyamide-epicholorohydrin(PAE) resins is common in the paper manufacturing industry to increase wet strength of specialty products such as tissue paper, paper towels, liquid packaging base papers, and other products which may come in contact with water. PAE crosslinkers are commercially available as PAE/water solutions. The increase in wet strength due to PAE crosslinking of cellulose has been studied extensively, and is well understood. The mechanisms of wet strength enhancement have been attributed to covalent ester bond formation between carboxyl groups of cellulose and azetidinium groups of PAE. There is also the secondary mechanism of self-crosslinking of PAE groups to form a water insoluble network during the curing process[64-67].

In this study the application of CNF composites with high aspect ratio clay and graphene flakes were both taken into account. However, to alleviate the concern with hydrophilicity of the underlying CNF matrix and degradation in humid conditions, the composite materials are also crosslinked with PAE crosslinker as a follow up from the last study.

4.2. Experimental

4.2.1. Materials

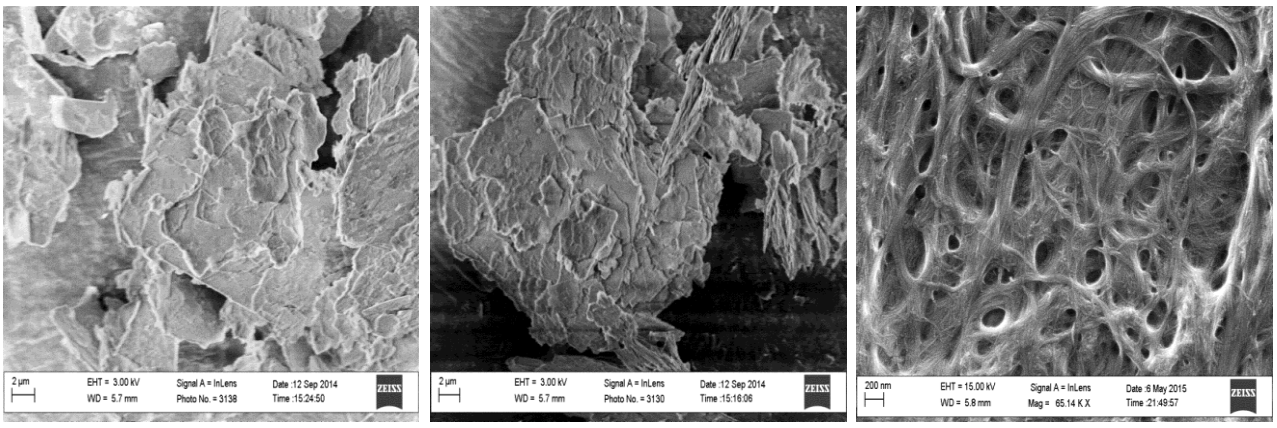

Figure 4.1: Starting materials from left (Nano Clay, Graphene Flakes, CNF)

CNFs were obtained from the University of Maine as an approximately 3% solids slurry in water. Commercially available crosslinker Kymene™ was obtained from Ashland Inc. (Covington, KY, USA) as a 12.5% solid suspension. High aspect ratio clay was obtained as a sample from IMERYS (Atlanta, GA). The clay was reported to have an aspect ratio of 250 - 1000. Graphene flakes were purchased from Sigma Aldrich, and were reported to have an aspect ratio of 500 - 2000. Shown in figure (1) are the starting materials.

4.2.2.Fabrication of Films

The CNF slurry was first diluted to 1% and a weighed amount was vigorously stirred for 30 minutes. Composite films were prepared by adding 1% filler material by dry fiber weight to the slurry. Crosslinked films were prepared by adding 1wt% Kymene™ with respect to dry fiber weight to the slurry while stirring. Subsequently, films were fabricated via an ultrafiltration process followed by hot press drying and conditioning. Millipore polyvinylidene difluoride (PVDF) membranes of diameter

142mm and a pore size of 0.22µm were used for the ultrafiltration process. A grammage of approximately 300g/m^2 was targeted to obtain thick, dense, and robust films. The slurries were dewatered until no more water could be removed. The dewatered mat was placed between smooth metal caul plates and four sheets of blotter paper and compressed at a load of 60psi to remove any excess water after dewatering. After pressing, films were dried in a flatbed dryer under approximately 50 – 60 psi load and 50°C for 24 hours. After drying, the films with crosslinker were heated in an oven at 120°C for 3 hours to complete the crosslinking process. Subsequently all films were conditioned at 23°C, and 50%RH for 24 hours. Multiple films were made for each type of pulp. The CNF + filler films are referred to as: Pure CNF, CNF-C, and CNF-G for pure CNF, clay, and graphene composite respectively. Whereas, the crosslinked films are referred to as: X-CNF, X-CNF-C, X-CNF-G, for crosslinked CNF, crosslinked clay, and crosslinked graphene composites.

4.2.2. Characterization

First, films were cut into discs of 42mm diameter and weighed. Three discs were cut and for every disc, five measurements of thickness were made with a Mitutoyo micrometer to ascertain film thickness and grammage. Water retention was measured by soaking the film discs in water for 30 minutes and measuring the difference in weight to determine adsorbed water.

For mechanical testing, a standard ASTM dogbone D-1708 was used and 3 samples for each type of film were tested in an Instron Bluehill II machine for measuring the mechanical strength of films. Mechanical testing was performed for dry and wet samples. In the case of the wet strength test, the samples were soaked in deionized water

for 30 minutes prior to testing, and excess water was removed by blotters according to TAPPI Test Methods. Morphology of the films was analyzed by SEM (LEO 1530 SEM, Carl Zeiss) at 3 -15kV. The samples were mounted SEM stages and gold sputtered (Quorum 150ES) for 60 seconds. Thermal analysis was performed in a Perkin Elmer TGA from 25°C – 500°C at a rate of 10°C/min.

Oxygen permeability was measured using a constant volume permeability device, at 23°C, at an upstream pressure of 14.7psig, and the downstream constant volume was $66cm^3$.

Water Vapor Transmission Rate (WVTR) was estimated by a modified ASTM E96 disc-cup method; the films were sealed on top of 15ml centrifuge tubes which were three quarters full with water. The tubes were then weighed and subsequently placed in a vacuum oven at 37°C.

4.3. Results and Discussion

In the previous study with CNF crosslinking it was shown that crosslinking not only helps with wet strength and dry strength of the material, it also helps in significantly reducing the interaction with water. Both the water retention value and water vapor permeability were reduced by approximately 25%. This is significant given the hydrophilic nature of cellulose. Moreover, in the first study where hornification was induced in the films via heating, a significant decrease in the mechanical properties of the films was observed. In this instance, the case was reversed by crosslinking the films. The mechanical properties were significantly improved and an increase in the ultimate tensile strength of the dry material by 2.5 fold was observed. In terms of wet strength, the wet to dry strength ratio of ultimate tensile strength was observed to be greater than 90%.

Furthermore, the benefits of hornification in the context of loss of porosity proved a reduced interaction with water and a reduced water vapor permeability.

In this case, by the addition of a high aspect ratio nano filler material, the benefits of both strategies could be realized.

4.3.1.Mechanical Properties

4.3.2. Pure CNF Composites

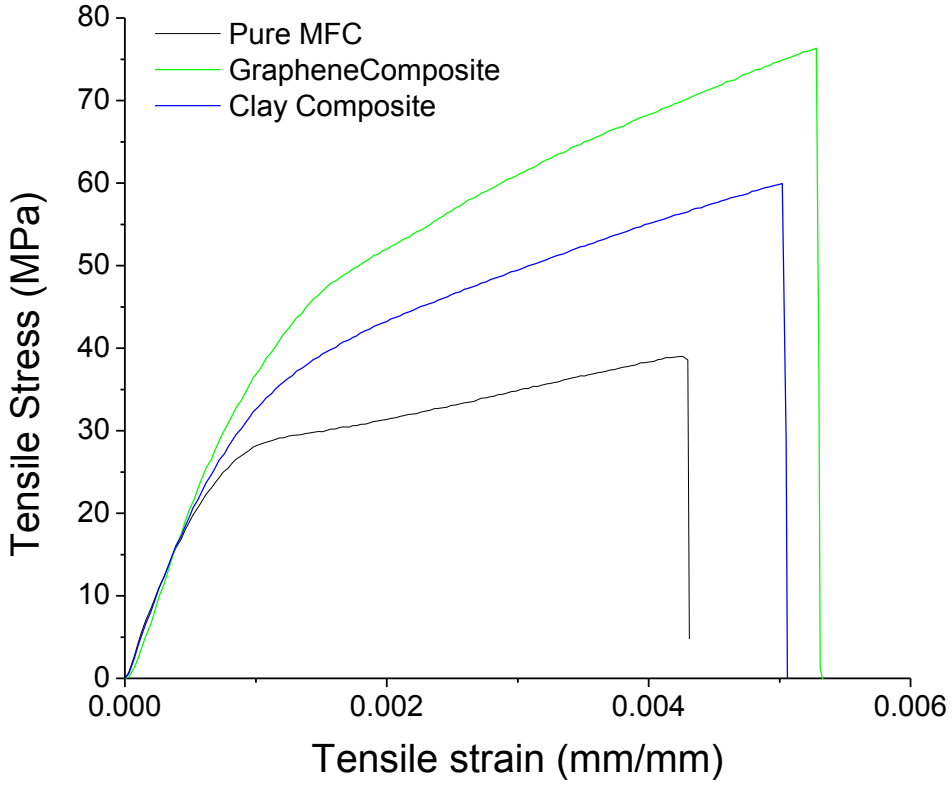

Figure 4.2: Typical Stress Strain Curves for CNF +1% Filler Composites

Table 6: Mechanical Properties of Composites Without Crosslinking

Sample	Pure CNF	CNF - C	CNF - G
Knee / De-bonding Region (MPa)	25	40	50
Strain at Break (mm/mm)	0.0043	0.0052	0.0054
Ultimate Tensile Strength	38	57.5	77.2

Typical stress strain curves obtained for CNF and nano filler composites are shown in figure (2). Table 1 shows the mechanical properties of the materials as a mean of three observations. The CNF composites with nano filler showed significantly different properties than the pure CNF material. The knee observed in the transition from the pseudo-elastic region to the strain hardening region is delayed and is less sharp. Additionally the strain hardening region is significantly larger when compared to the pure CNF films. The dry pure CNF films show a linear behavior up to approximately 25MPa of tensile stress. After this pseudo-elastic region, there is a knee in the curve which is thought to occur due to some fibril- fibril de-bonding. The knee is followed by a linear strain hardening region to approximately 40 MPa, where failure occurs. In the strain hardening region, there is a significant reinforcement effect due to straightening and reorientation of nano fibrils, and inter fibril slippage. This reinforcement behavior is caused due to the alignment of nano fibrils in direction of the applied strain. Failure of the film occurs by failure of fibrils and breakage of bonds between them.

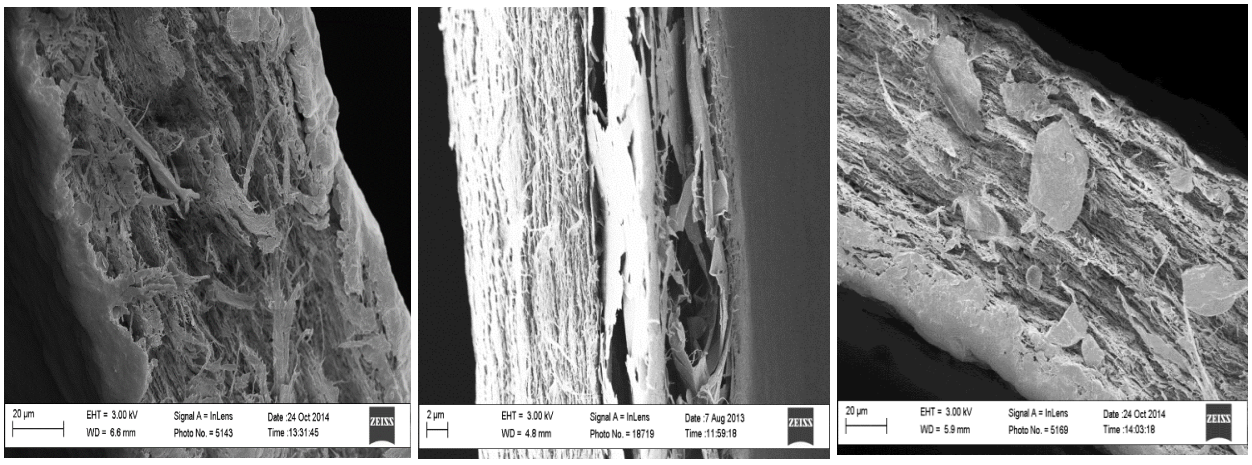

Figure 4.3: Fracture Surface SEM (Pure CNF, CNF - G, CNF - C)

In the case of the composite materials, curves show different shapes. The knee is shifted to a much higher value, and the transition from the pseudo-elastic region to the strain hardening region is somewhat smoother. Additionally, the strain hardening region is extended, while failure occurs at much higher values. These observations are not unique and have been extensively documented in the literature. Malho et al suggest interactions between the filler materials and the CNFs by hydrogen bonding. They also suggested the covering of the graphene with layers of CNFs, and the existence of stabilized π-interactions. Wu et al studied in detail clay-CNF composites and also found that effective dispersion of clay within the CNF matrix improved the mechanical properties by a reinforcing the effect of the flaky clay material.

The SEM images of the cross section of the pure CNF, CNFC, and CNFG composites are shown in figure (3(a, b, c)). The cross section of the pure CNF clearly shows broken fibrils and bundles of broken fibrils supporting the breakage of bonds and fibrils mechanism of failure for pure CNF films. Whereas figure 3 (b, c) show not only the breakage of fibrils but also the filler materials being pulled out from the matrix. This clearly indicates that the slippage of filler material also occurs during the application of stress on the composite, and we postulate that this is what causes the strain hardening region to be extended as the fillers also participate in the reorientation behavior during strain hardening.

4.3.3. Crosslinked CNF Composites

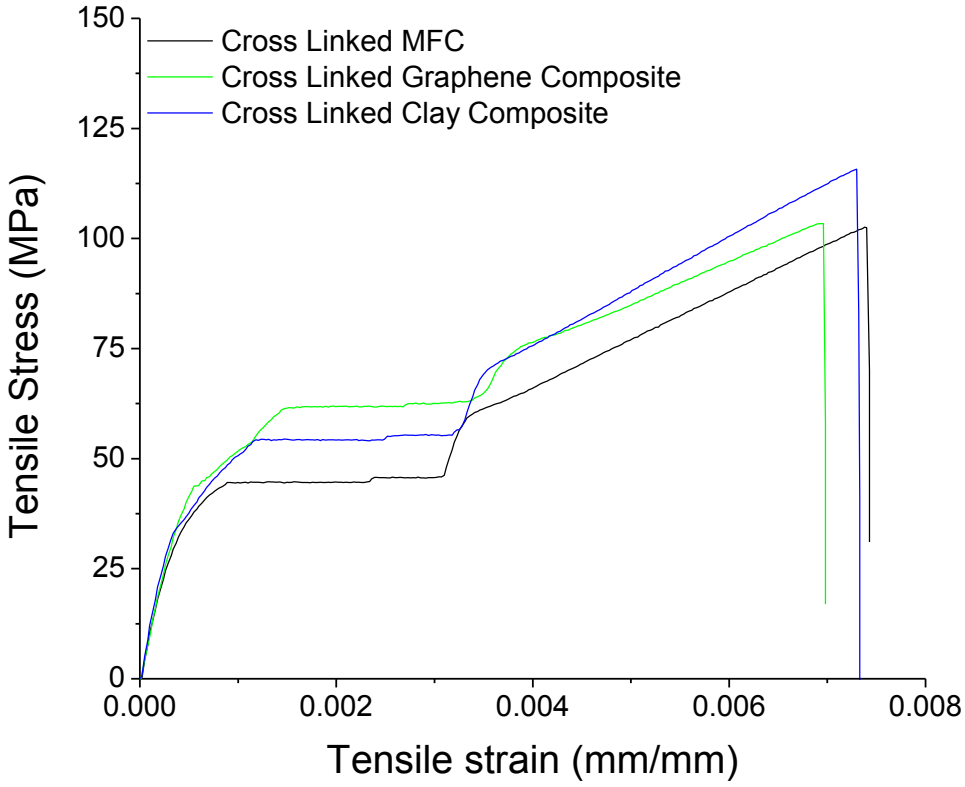

Figure 4.4: Typical Stress Strain Curves Crosslinked Composites

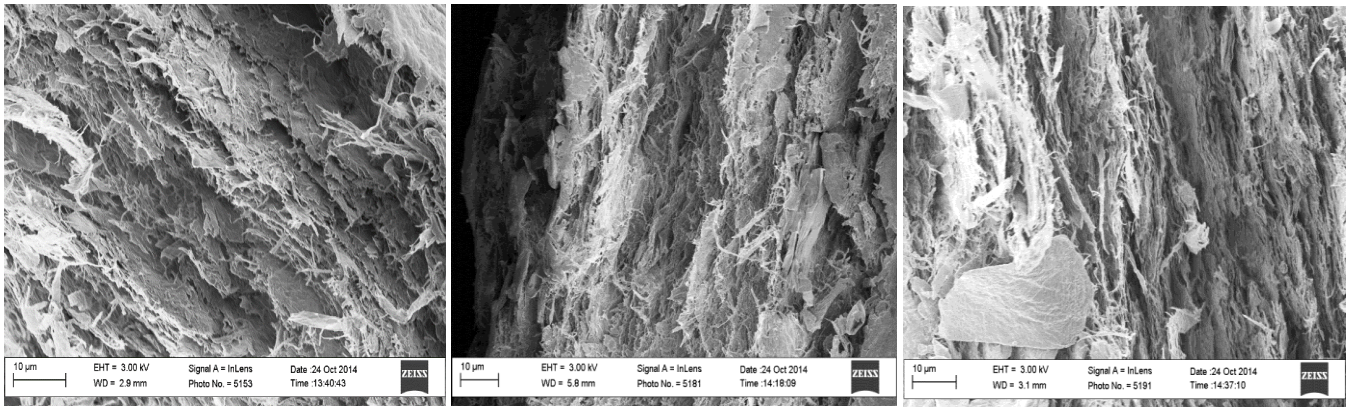

Figure 4.5: Fracture surface SEM from left (X - CNF, X- CNF -G, X - CNF - C)

Figure 4 shows typical stress-strain curves obtained for the crosslinked composites. Figure 5 (a, b, c) show the fracture surface of the tested crosslinked

composite films. The crosslinked CNF composites show properties that were clearly a combination of the crosslinked CNFs shown previously and also the pure CNF composites shown just above. The crosslinked CNF films show a clear dual mechanism of mechanical stress bearing. Particularly, the PAE crosslinking has a dual mechanism of bond formation. One is of crosslinking between PAE and the carboxyl groups of the CNFs, whereas the other mechanism is of formation of PAE networks within the matrix. The combination of the two mechanisms produces the dual mechanism proposed. In the case of the composites, the characteristic behaviors due to presence of the filler materials are also observed. The transition of both knee regions is delayed, as was the case in the pure CNF composites. The stress levels at which the plastic deformation region is reached is also elevated in the case of the composite materials. Finally, the stress at break for both composites is higher when compared to the pure CNF composites.

4.3.4. Barrier Properties

4.3.5. Oxygen Permeability

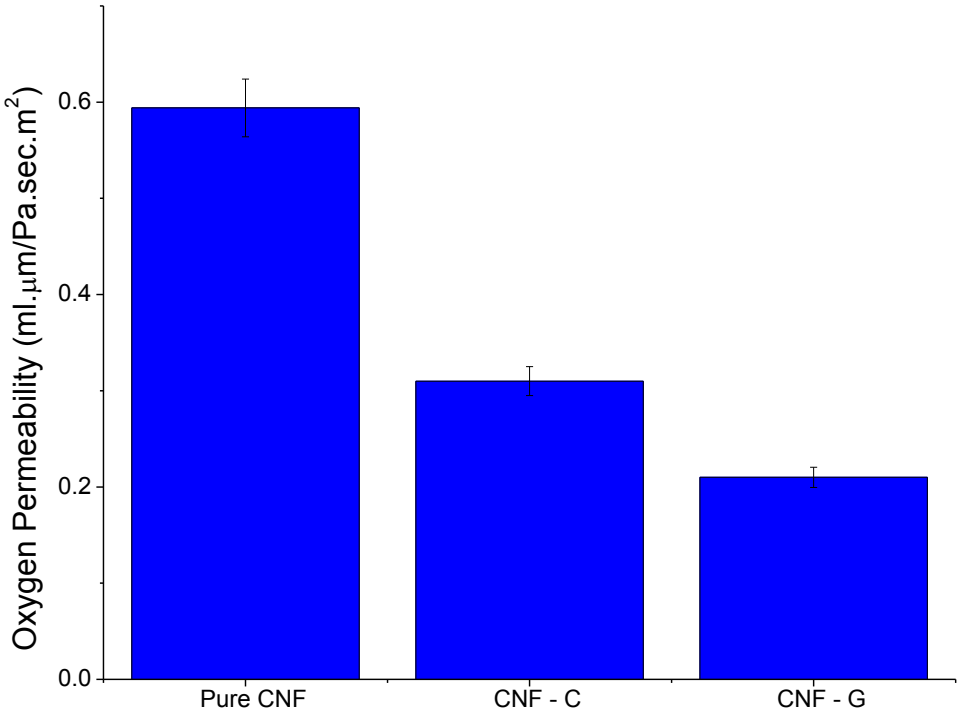

Figure 4.6: Oxygen Permeability of CNF +1% filler materials

Shown in figure (6) are the oxygen permeability values for the pure CNF composites. Oxygen permeability for only pure CNF materials was measured since it was to only ascertain the effect of compositing with the nano filler materials, and the main aim was to reduce the water vapor permeability of the composite barrier materials formed. The oxygen permeability of the materials decreased significantly. The oxygen permeability of the clay composite decreased by 47%, whereas the graphene composite permeability decreased by almost 65% by a 1% loading of the composite material. This

reduction and the SEM images of the cross section of the films clearly demonstrate the effectiveness of the high aspect ratio material as an effective tool for improving barrier properties of barrier films.

4.3.6. Water Vapor Permeability

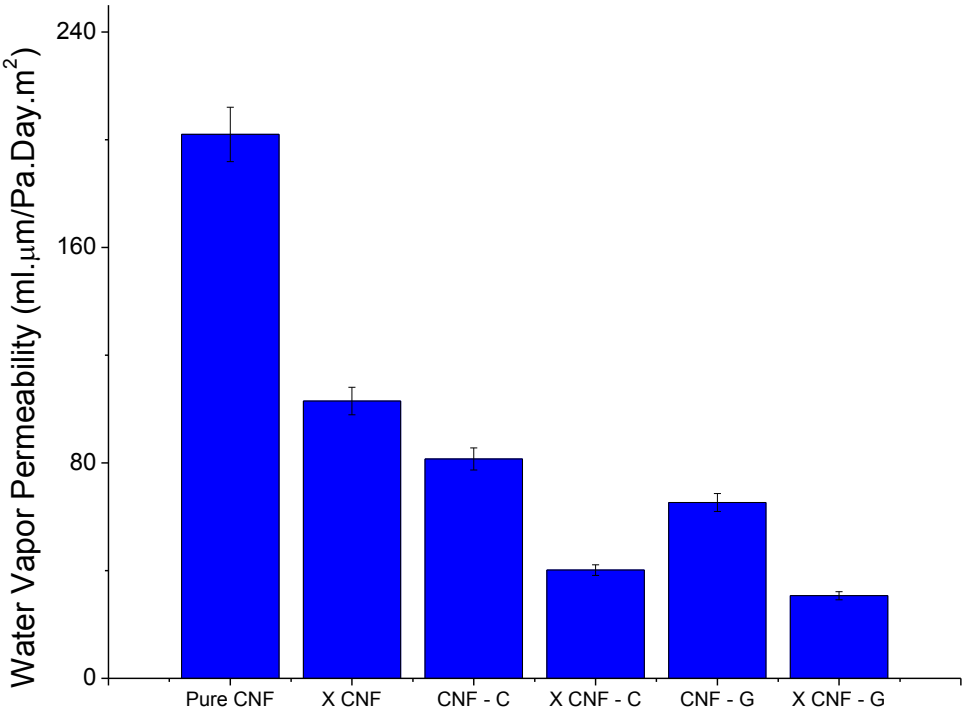

Figure 4.7: Water Vapor Permeability Values of All Composite Materials

Shown in figure (7) are the water vapor permeability values for all the pure and crosslinked samples. Just an addition of 1% of filler material showed a reduction in water permeability by 60% for clay and 68% for graphene. In the case of crosslinking, the reduction over pure CNF was just under 50%. When compared to pure CNF, the crosslinked composites showed a reduction of 80% for clay and 85% for graphene. The

improvement in the graphene films is slightly higher than the clay films, which is expected due to the higher aspect ratio of the graphene films as compared to the clay. Additionally, the clay is slightly more hydrophilic as compared to the graphene, therefore it might aid in adsorbing some water. The reduction in water vapor permeability due to crosslinking is somewhat expected due to both the reduction in water interaction and absorption due to crosslinking and the fact that some effects of hornification are induced in the films as well. This would attribute to not only the reduction of absorption of water but also the diffusion through the films.

After the crosslinking of the composite films, the effects become much more pronounced. In this case, diffusion is hindered by the presence of the filler material. The crosslinker aids in the reduction of water absorption, while the effects of formation of extra bonds and some hornification in the films aids in reduction of permeability as well. These improvements in water barrier are highly significant since the fabrication process for the films required little modification. Additionally, the addition of the minute amounts of crosslinker and filler material has little effect on the renewability or the biodegradability of the material while offering huge improvement over pure CNF materials.

4.4. Conclusions

The mechanical and barrier properties of crosslinked CNF, crosslinked CNF-clay, and crosslinked CNF-Graphene films were studied. Both the clay and graphene flakes were in the form of a high aspect ratio nano flakes. The main objective of the study was to exploit the improvement of barrier and mechanical properties by making composites with the high aspect ratio. Improvement of barriers was achieved due to an increase of the

tortuosity of the resulting films, whereas mechanical properties were improved due to the reinforcing mechanism of the high aspect ratio materials. The composite films showed improvement in the ultimate tensile strength of as much as 96% - 38MPa for pure CNF compared to 75MPa for CNF- graphene composites. The oxygen permeability and water vapor permeability for the same composite reduced by 65% and 67%. Further improvement was observed by crosslinking the same composites with wet strength enhancing PAE resin crosslinker Kymene™. The ultimate tensile strength of the crosslinked composites increased by over 150%, whereas water vapor permeability reduction of up to 85% was observed in the crosslinked graphene composites when compared to pure CNF films.

CHAPTER 5

CHARACTERIZATION OF MICRO FIBRILLATION PROCESS OF CELLULOSE AND MERCERIZED CELLULOSE PULP

Abstract

Here we detail the fibrillation process for cellulose and mercerized cellulose pulps. Native and mercerized cellulose showed high degree of purity as indicated by α – cellulose content measurement and XRD analysis. Furthermore, stark change in fiber morphology indicated aggregation of fibrils on the surface due to mercerization. Fibrillation of pulp was carried out in the following subsequent steps: disintegration, PFI refining, microgrinding by 20 passes in SuperMassColloider, and 60 passes in SuperMassColloider. Fiber samples were collected at every stage and highly uniform films were made by ultrafiltration and hot press method. The fibers and films made from fibers were then characterized by measuring physical properties, contact angle, thermal, mechanical, and SEM analysis. The main objective was to characterize the physical properties of the films made from different degrees of fibrillation. The films obtained were of fairly close grammage of approximately 35g/m^2. The target grammage was 40g/m^2, and the slightly lower grammage indicated some fiber loss during the fabrication process. Additionally, it was observed that the density of the films amplified with increasing degree of fibrillation from about 180g/m^3 to 455g/m^3 for cellulose-I and 95g/m^3 to 385g/m^3 for cellulose-II. Cellulose-I films showed some contact angle initially, which increased at every stage (14° - 64°), whereas cellulose-II films did not display a contact angle until the final stage of fibrillation. The films also showed increasing

strength and an evolution of tensile strength from initially displaying a tear behavior indicating poor bonding to typical micro fibrillated cellulose films behavior as the fibers became increasingly fibrillated. The ultimate tensile strength for cellulose changed from tear behavior with no defined break to 134.5MPa.Compairitivly, the same change for cellulose-II was a maximum of 75.1MPa from tear behavior. Increasing fibrillation of fibrils in both cases showed a decrease in fiber size, well differentiated for the two types of pulps at every stage.

Keywords: Cellulose, micro fibrillated cellulose, nano cellulose, microgrinding, mercerization

5.1 Introduction

Cellulose is the most abundant, renewable bio polymer on earth, naturally occurring in a variety of sources [14, 49]. Recently the production and potential application of micro fibrillated cellulose fibers have garnered much attention due to their excellent mechanical properties, biodegradability, and renewability. In the scientific literature, there are reports of various applications of micro fibrillated cellulose based materials including composites, barrier materials, tissue scaffolds, cell growth media, electronic materials, solar cells, and super capacitors [13, 35, 46, 70, 77-80]. Nanofibers from native cellulose-I have been made using a variety of chemical, mechanical, and enzymatic treatment methods. These include high pressure mechanical homogenization, TEMPO ((2,2,6,6-Tetramethylpiperidin-1-yl)oxyl) oxidation, and enzymatic hydrolysis amongst a host of other methods [15, 18, 19, 46].

Four polymorphs of crystalline cellulose-I, II, III, and IV are known, and out of these, cellulose-I and II are the most widely studied. Cellulose-I is identified as native

cellulose, and is found abundantly in nature. Cellulose-I can be converted easily to cellulose-II via the mercerization or regeneration processes [10]. An interest in cellulose-II fibers exists because they have a monoclinic structure which is a thermodynamically more stable structure. While the intra sheet bonding structure is essentially the same as cellulose-I, there is also the possibility of formation of additional inter-sheet hydrogen bonds providing the structure with extra stability. In the regeneration process, native cellulose fibers are solubilized in a solvent and then re-precipitated in water as cellulose-II. Yet, this disrupts the fibrous and crystalline structure of the cellulose, bringing about poor mechanical properties of the resulting cellulose-II fibers [23, 81]. Mercerization entails swelling the native fibers in a concentrated NaOH solution and then washing off the excess solution after conversion into cellulose-II. Since the fibers are not solubilized, the crystal and fibrous structure of the cellulose remains intact. Thus, mercerization is preferred over regeneration [1, 10, 82, 83].

Various authors have previously studied in depth the crystalline, structural, and chemical changes of cellulose fibers upon mercerization in which there is a loss of hemicelluloses, a reduction in degree of polymerization, and change in the crystal structure of the resulting cellulose due to rearrangement of the crystalline parts. Due to these chemical and structural changes, the resulting physical properties of pulp and films made from the pulp should show significant differences in behavior[23, 81, 83-88]. Moreover, due to the seemingly different fiber structure and easy conversion into cellulose-II, it would be conducive to study the characteristics of cellulose-II nanofibers as well. Fibrillated cellulose-I fibers have been subjected to mercerization and characterization before. However, cellulose-II nanofibers obtained from mercerization of cellulose-I

nanofibers resulted in irregular aggregation and an undispersed suspension [23, 81, 83, 89]. These aggregates cannot be re-dispersed effectively again to the nano fibril suspension, as is the case for cellulose-I.

Given these previously observed issues and the relatively small body of literature on cellulose-II nanofibers, it is imperative to understand the physical process of fibrillation of cellulose-II fibers to form nanofibers. This characterization would help in understanding and elucidating the physical, chemical, and morphological evolution of properties of cellulose-II fibers as they undergo fibrillation to nanofibers, and help to design strategies to optimally produce cellulose-II nanofibers for potential applications. In particular, we would elucidate the structure property relationships for films made from fibrils at different stages of fibrillation for both cellulose I and II. For this study, commercially available bleached softwood pulp was used as starting material. Cellulose-II fiber pulp was prepared from the raw material via mercerization of cellulose-I native cellulose pulp. Subsequently cellulose-I pulp was also subjected to the same processes for characterization to elucidate the differences in evolution of physical properties of the two materials.

5.2 Experimental

5.2.1 Materials

Commercially available, elementally chlorine free, bleached loblolly pine (softwood) pulp was used as a starting material.

5.2.2 Pulp Mercerization

The pulp was soaked in deionized water for 24 hours to form slurry with 2% consistency. After 24 hours of soaking the pulp was mercerized by soaking, adding in an

excess of 20% NaOH solution to the slurry. After 24 hours, the slurry was washed with a 1% acetic acid solution to remove any excess NaOH, and subsequently washed with deionized water and adjusted to a consistency of ~2% for further processing.

5.2.3α-Cellulose Content

α - Cellulose content of both types of cellulose was quantified by dissolution in 17.5% NaOH solution. The method as described by Wang et al[23] was used. Particularly, 1 gram of the dried sample was soaked in 17.5% NaOH solution at 20°C for 45 minutes. After this period, the sample was filtered through a filter glass and subsequently washed thoroughly with distilled water until neutral pH was achieved. Finally, the samples were dried at 105°C for 12 hours. The remaining sample was the α-cellulose content of the sample. The measurement was repeated 5 times for each type of cellulose.

5.2.4 XRD Analysis

X ray Diffraction (XRD) analysis was carried out using a PANalytical X Ray diffractometer using a Cu-Kα source (λ = 0.154nm) with a 2θ range of 5 - 30° with a scanning speed of 1°/minute.

5.2.5 Disintegration, Refining, and Microgrinding with SuperMassColloider

The fibrillation process for both celluloses of pulps was carried out in stages, and samples were collected at every stage to fabricate films and characterize. First the pulps were disintegrated using a standard lab disintegrator (TMI, Rokonkoma, NY, USA) for 15,000 revolutions at a 10% consistency. Subsequently the pulps were refined in a PFI (TMI, Amityville, NY, USA) mill for 20,000 revolutions.

After PFI refining, microgrinding was done using a SMC (SuperMassColloider, MKZA6-2, Masuko Sangyo Co. Ltd, Japan) at 1500 rpm. The SMC consists of two stone

discs grinding pulp between them, with a certain gap in between which can be adjusted based on degree of fibrillation required. The discs were set at a gap of -100μm which represents a negative setting; however, the constant presence of pulp ensures no direct contact between the discs and a high degree of fibrillation of the pulp. Pulp was fed continuously through the SMC and samples were removed periodically for analysis.

5.2.6 Fabrication of Films from Pulp

The pulps produced from the four different stages, disintegration, PFI refining, 20 passes through SMC, and 60 passes through SMC were used to fabricate films. All slurries were diluted to 1% to fabricate films via an ultrafiltration process. Millipore polyvinylidene difluoride (PVDF) membranes of a 142mm diameter and a pore size of 0.22μm were used. After the slurries were dewatered with the ultrafiltration apparatus they were placed between smooth metal caul plates and then between three sheets of blotter paper and compressed at a load of 60psi to remove any excess water. Subsequently the films were dried in a flatbed dryer under approximately 20psi load and 50°C for 24 hours. Multiple films were made for each type of pulp.

5.2.7 Characterization of Films

After fabrication the films were characterized for physical dimensions, contact angle, mechanical properties, thermal analysis and SEM imaging of the fracture surface of mechanically tested films to ascertain the morphology of fibers and nature of the boding between fibers.

Firstly, films were cut into discs of 47mm in diameter. Three discs were cut and weighed, and for every disc, five measurements of thickness were made to ascertain film grammage. For mechanical testing, a standard ASTM dogbone D-1708 was used and 4

samples for each type of film were tested in an Instron Bluehill II machine for measuring the mechanical strength of films.

To measure contact angle, films were taped onto glass slides to create a flat surface then a 5µl drop of water was carefully placed on top of the films surface for 5 minutes. Five measurements were made for each type of film sample. Contact angle was measured using a First Ten Angstrom goniometer, and the results were analyzed using FTA32 image processing software.

UV Vis measurements were performed in the range 300-800nm with an Agilent UV-Vis instrument.

Morphology of the fibers and fracture surface was analyzed by SEM (LEO 1530 SEM, Carl Zeiss) at 5kV. The fracture surface samples were mounted vertically on SEM stages, whereas the fiber samples were prepared by air drying a drop of fiber suspension on an SEM stage and gold sputtering (Quorum 150ES) for 60 seconds. Thermal analysis was performed in a Perkin Elmer TGA from 25°C – 500°C at a rate of 10°C/min under a nitrogen atmosphere.

5.3. Results and Discussion

5.3.1 α – Cellulose Quantification

Table 7: α - Cellulose Content of Native and Mercerized Pulp

Sample	Cellulose-I	Cellulose-II
α - Cellulose Content (g/g dry sample)	0.84±0.02	0.96±0.03

α - Cellulose content can help quantify the purity of both cellulose I and II. By using the method described, almost all the hemicelluloses can be removed from the cellulose samples. This gives insight into the pure cellulose and hemicelluloses contents

of the samples. By comparing this for the pure samples, we can indirectly gain insight into the removal of hemicelluloses during the initial mercerization process. Table (**1**) shows the α-cellulose content of the native and mercerized cellulose. The α - cellulose content of the native cellulose and the mercerized cellulose were about 84% and 95% respectively. The residue is mainly thought to be hemicelluloses which are removed due to the high alkali concentration. The mercerized cellulose showed a much higher α - cellulose content since they had already been through the mercerization process, during which most of the hemicelluloses were removed.

5.3.2 SEM: Fiber Morphology

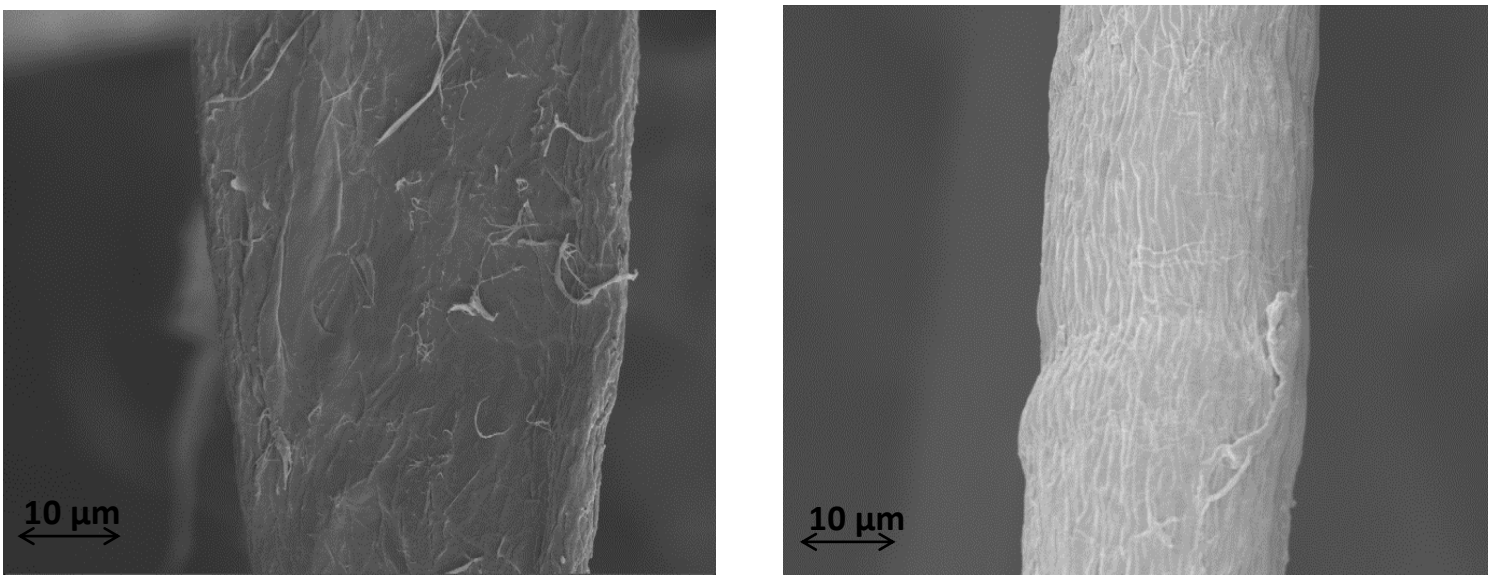

Figure 5.1: Cellulose-I Fiber (left), Mercerized Cellulose Fiber (left)

SEM images of individual fiber surface before and after mercerization are shown in figure (**1**). Cellulose-I fibers before mercerization show a flat morphology with some small fibrils visible on the surface. Cellulose-II fibers on the other hand have a smoother, cylindrical morphology and show aggregation of surface fibrils on the surface of the

fibers. This aggregation of fibrils is due to the formation of stronger bonds between fibrils during the mercerization process [23, 82, 83].

5.3.3 XRD Analysis

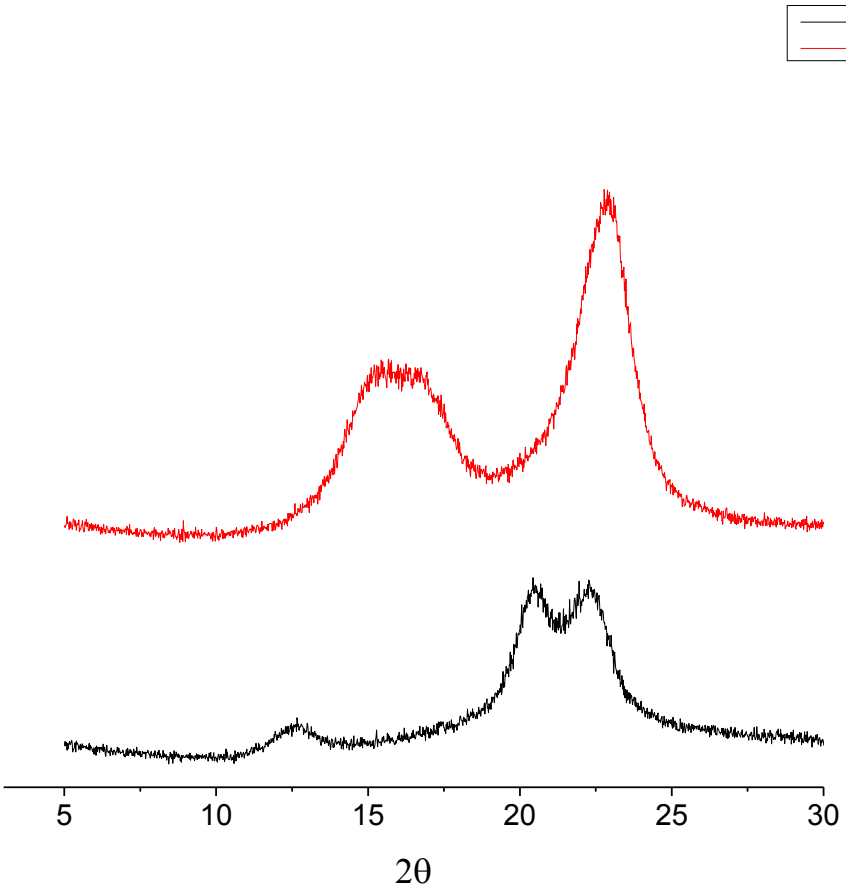

Figure 5.2: XRD Analysis: Cellulose and Mercerized Cellulose

The mercerization of the cellulose-I fibers was also confirmed via XRD analysis shown in figure (**2**). Both materials showed a high degree of purity indicated by absence of any extraneous peaks. Cellulose-I fibers showed characteristic peaks at approximately 16° and 23°, which are typical for cellulose-I. Mercerized cellulose-I fibers showed characteristic peaks at approximately 12.6°, and a doublet of peaks at 20.2° and 22°. The conversion of the singlet peak to the doublet are characteristic of mercerization of cellulose-I [23, 82, 83]. Wang et al also studied the mercerization of cellulose-I for the

purpose of conversion to cellulose-II nano fibers and obtained similar characteristics of XRD patterns of the mercerized cellulose. Yue et al studied the properties of freeze dried cellulose nano crystals (CNCs) CNC-I and CNC-II and found that the change of singlet to doublet peak signifies the change of crystallites from the 200 plane in CNC-I to 110 and 200 planes.

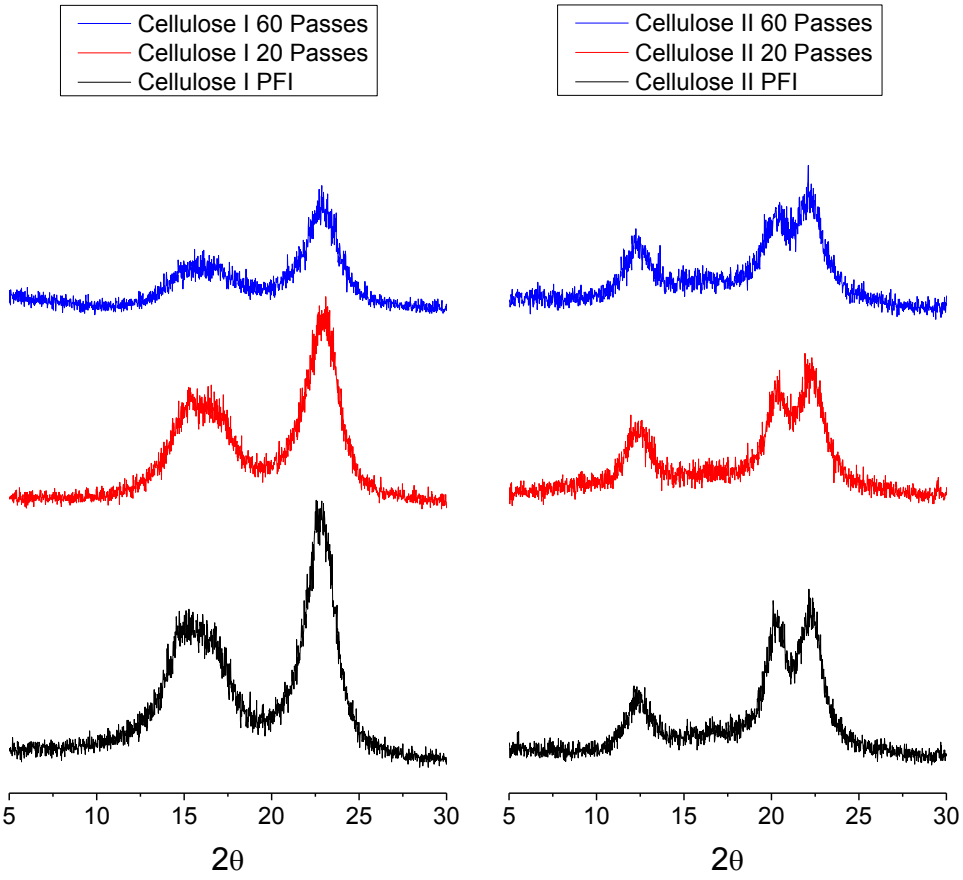

Figure 5.3: XRD Analysis of films

Figure (**3**) shows the typical XRD patterns obtained for films made from cellulose-I and the mercerized fibers at different stages of fibrillation. The patterns acquired are very similar to the staring materials shown in figure (**2**) indicating that the micro grinding process does not significantly change the crystalline structure of the

materials in either case. However, some reduction in crystallinity index are expected due to the constant shear in the micro grinder. For a more detailed treatment of the changes in crystallinity due to fibrillation the reader is referred to Nair et al.

5.3.4 Physical Properties of Films

Table 8: Physical Properties of Films

	Sample	Disintegrated	PFI	20 Passes	60 Passes
Film Grammage	**Cellulose-I (g/m^2)**	34.2±1.2	38.3±1.5	37.6±0.3	34.1±0.6
	Cellulose-II(g/m^2)	37.8±1.3	39.5±0.7	36.5±0.8	39.1±1.4
Film Density	**Cellulose-I (g/m^3)**	181.9±6.3	376.9±14.7	447.9±7.8	455.5±3.6
	Cellulose-II(g/m^3)	95.4±3.2	311±5.5	312.3±6.8	384.8±13.7
Contact Angle	**Cellulose-I (°)**	14.4±0.3	58.17±0.6	63.1±0.6	64.2±0.5
	Cellulose-II (°)	Water wetting is too fast and the contact angle could not be measured	Water wetting is too fast and the contact angle could not be measured	Water wetting is too fast and the contact angle could not be measured	57.7±0.4

Films grammage, density, and contact angle measurements are shown in table (**2**). Film grammage was measured to make sure that the films were of similar dimensions and were comparable in nature. Film grammage showed to be highly consistent for both celluloses of materials and across the different degrees of fibrillation. Consistent grammage was obtained by the fabrication process used where the mat formation, compression, and compressed drying processes are highly uniform[35, 80] . The target for grammage was $40 g/m^2$, while the films are close to the target grammage, some variability is observed. This is clearly due to some fiber losses during the film formation process. Generally speaking, density also increased at every stage, except for cellulose-I fibrils at

the last stage. This is most likely due to a larger degree of fibril loss than earlier stages since the fibrils at this stage, as will be observed from the SEM images subsequently, have been fibrillated to a diameter in the 10 - 100nm scale and are lost easily during the filtration process.

Contact angles were measured to provide an estimate of the wettability of the films made from different fiber celluloses. Generally speaking, with increased refining and fibrillation of cellulose fibers, films become increasingly dense and lose porosity. This is due to stronger hydrogen bonding between fibrils which agglomerate to fill the interstitial pore space in the fiber network. This phenomenon leads to an increase in the surface contact angle. Contact angle for films made from the two materials evolved very differently for the two materials with increasing fibrillation stages. Cellulose-I fiber films show some contact angle from the first stage, whereas cellulose-II fiber films show that the water wetting is too fast so the contact angle could not be measured until 60 passes in the SMC.

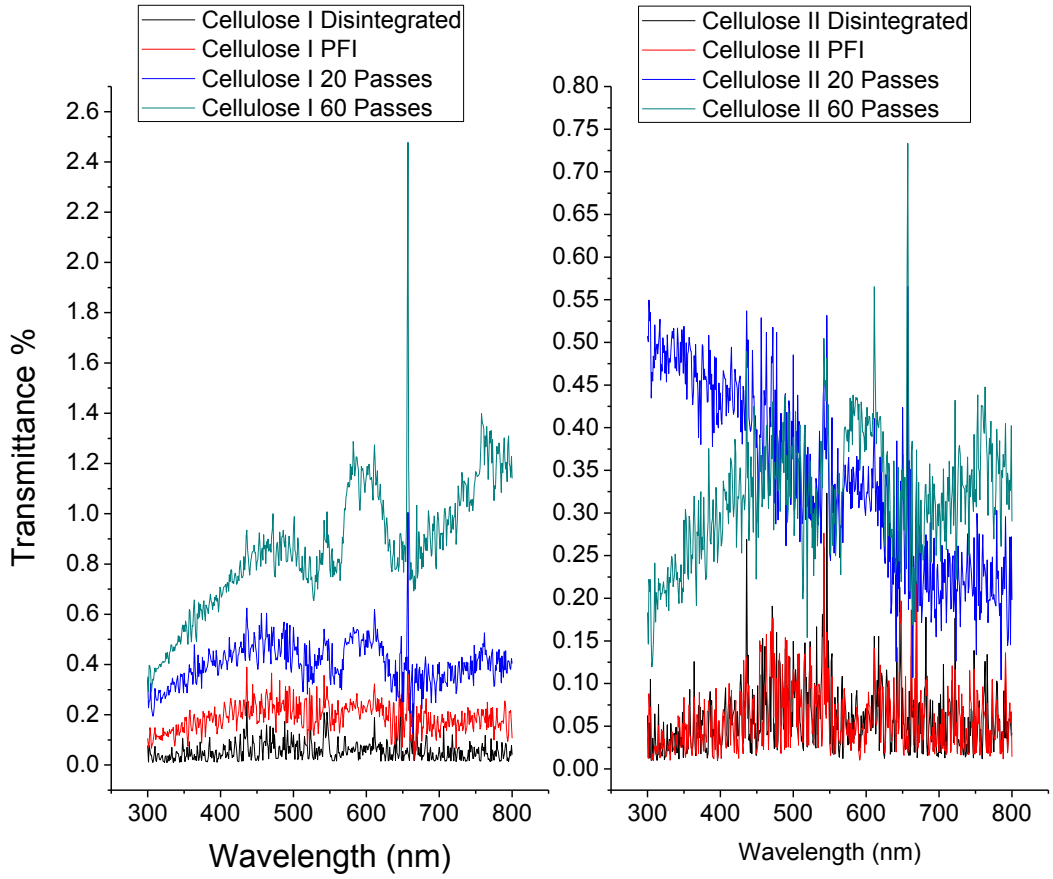

Figure 5.4: UV Vis Spectra

To observe the optical properties UV Vis measurements in the visible range were performed for all films. The spectra are shown in figure (**4**). The films were quite thick, in the order of 75 – 100µm and therefore the spectra obtained were quite noisy. However, in both cases of cellulose I and II films the spectra show a clear reduction of absorbance with increasing degree of fibrillation. In the case of cellulose-I there is a clear reduction in the absorbance with every stage. On the other hand, in the case of cellulose-II the disintegrated fiber and the PFI fiber films show a great degree of overlap in their spectrum. A reduction in absorbance is observed after 20 passes, and there is still some

overlap observed in the 20 passes and 60 passes films. By observing the physical images and the SEM images of the surface of the films, these results become much clearer.

In the case of cellulose-I fibers, every stage induced an increasing degree of fibrillation. Whereas for cellulose-II fibers the fibrillation was limited until the very last stage due to initial agglomeration of fibrils resulting in poor bonding between fibrils and porosity for films. Due to the ease of fibrillation of cellulose-I fibers as observed in SEM images in figures (**5**), at every stage the films formed were structurally denser and showed an increase in contact angle whereas cellulose-II fibers did not. However, in the case of cellulose-II fibers due to initial agglomeration of fibrils on the surface of fibers, fibrillation was limited at every stage. Due to the difficulty of fibrillation, cellulose-II films were porous until 60 passes in SMC as observed in the cross section SEM images, and therefore the water wetted the film too fast so the contact angle for the films could not be measured until 60 passes in SMC [42, 90].

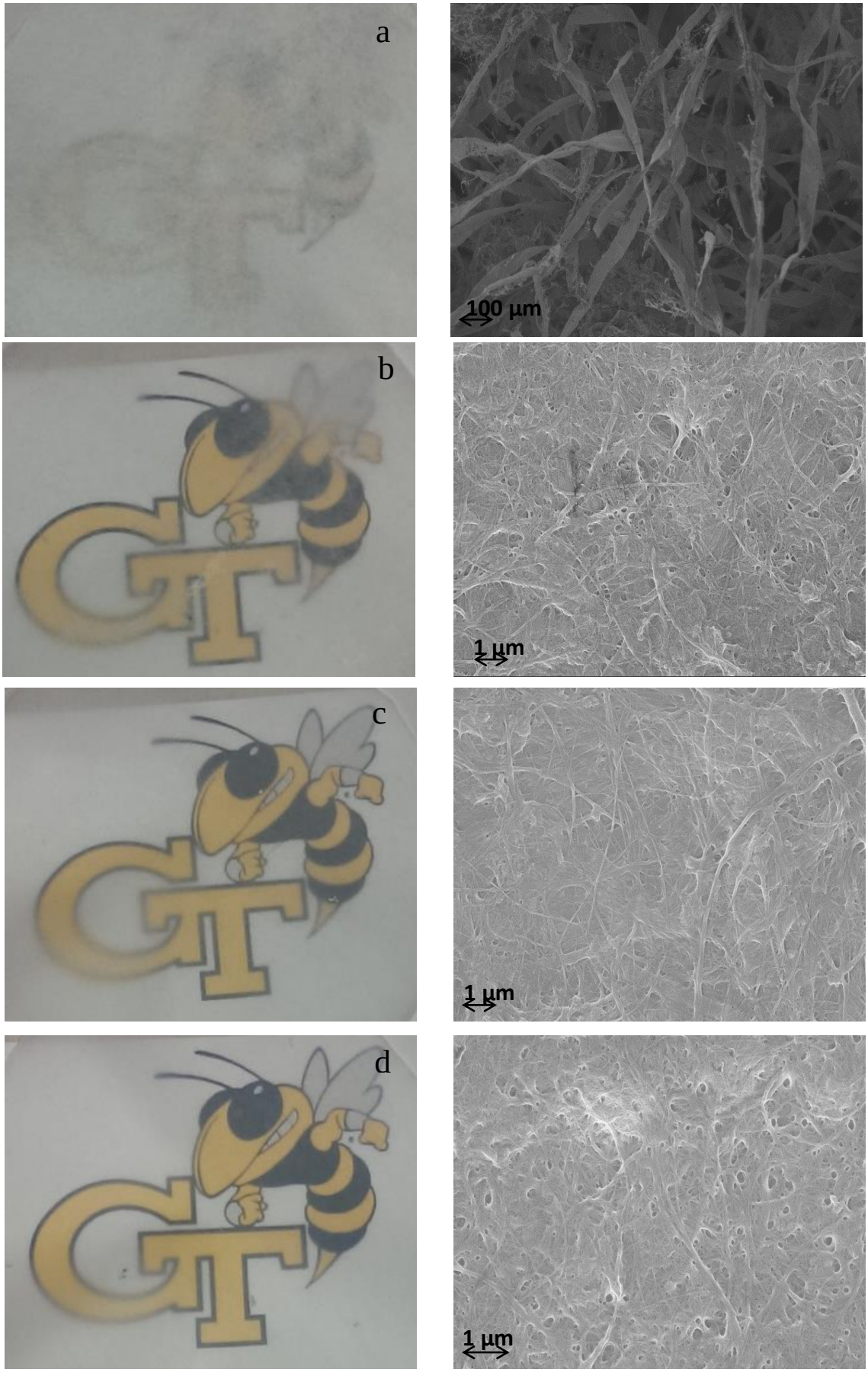

Figure 5.5: Cellulose-I Films and Fiber SEMs (a. Disintegrated, b.PFI, c.20 Passes in SMC, d.60 Passes in SMC)

Figure (**5**) shows images of films made from cellulose-I fibers and SEM images of corresponding fibers at different degrees of fibrillation. Cellulose-I fiber films show a simple progression of decreased opacity at every fibrillation stage, due to ease of fibrillation and reduction in fiber size. Films made from fibers after PFI refining films are significantly more translucent than just disintegrated fiber films. Figures **(5 (a, b))** correspondingly show the reduction of fiber size. In figure (**5a**), large fibers with cross section of tens of microns are visible and after PFI refining (figure (**5b)**), fibers show a significant reduction in size and submicron sized fibers are visible. After 20 passes in the SMC (figure (**5c**)), fibers with diameters of the order of hundreds of nanometers are visible. Finally, after 60 passes in SMC, fibers with diameters of a few nanometers are visible (figure (**5d**)). The SEM images in figures (**5 (a, b, c, d**)) shows a decreasing fiber size at every stage of fibrillation which correlates well with the decreasing opacity of films [91].

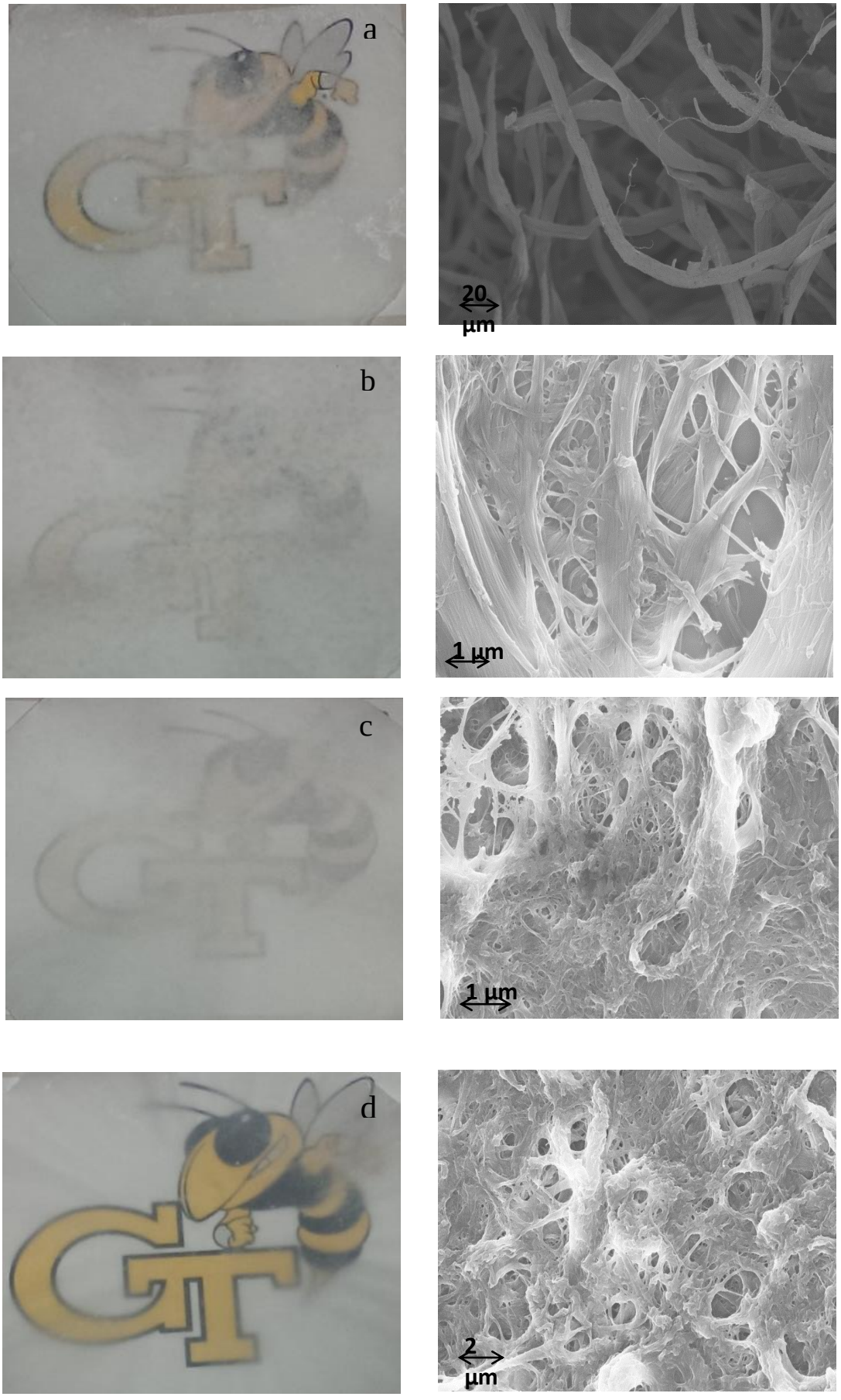

Figure 5.6: Cellulose-II Films and Fiber SEMs (a. Disintegrated, b.PFI, c.20 Passes in SMC, d.60 Passes in SMC)

Figure (**6**) shows images of films made from cellulose-II fibers and SEM images of corresponding fibers at different degrees of fibrillation. Cellulose-II fiber films showed a much different progression than cellulose-I fiber films. They initially displayed some translucence but this is because there is significant porosity in the film structure due to poor bonding between fibers. The SEM image in figure (**6a**) shows the structure of disintegrated cellulose-II fibers, which are smooth and display no surface fibrillation. This lack of surface fibrillation would cause porosity in the films due to lack of inter fiber bonding. After PFI refining (figure (**6b**)), the fibers showed some increase in fibrillation but no decrease in fiber size, causing only the inter fiber bonding to slightly improve. This resulted in the films being more opaque than the last stage, even though some porosity in the films is observable. After microgrinding for 20 passes, the films still showed limited reduction in opacity to the PFI refined fiber films due to no limited reduction in fiber size. In the SEM images, fibers of cross section revealed few microns and submicron sized fibers that were visible. Only after microgrinding for 60 passes did the films show a significant decrease in opacity as compared to the previous stages. SEM image in figures (**6d)** shows that finally after 60 passes in SMC there is significant reduction in size of fibers down to the submicron level and films show a reduction in opacity [91].

5.3.5 Mechanical Properties of Films

We attempted to obtain similar grammage for the films, and as shown earlier, the grammage was maintained to be as consistent as experimentally possible. However, it was also observed that the density of the films amplified with increasing degree of fibrillation. This is expected because as the fibers become smaller, they form a better

packed structure, which is higher in density. Increased density will in turn translate to better mechanical performance due to better entanglement of fibers and higher specific bonding between the fibers.

Table 9: Mechanical Properties of Films

		Disintegrated	PFI	20 Passes	60 Passes
Cellulose-I	**Strain at Break (mm/mm)**	-	0.0021	0.0024	0.0045
	UTS (MPa)	-	75.7	96.7	134.5
Cellulose-II	**Strain at Break (mm/mm)**	-	-	0.0015	0.0016
	UTS (MPa)	-	-	41	75.1

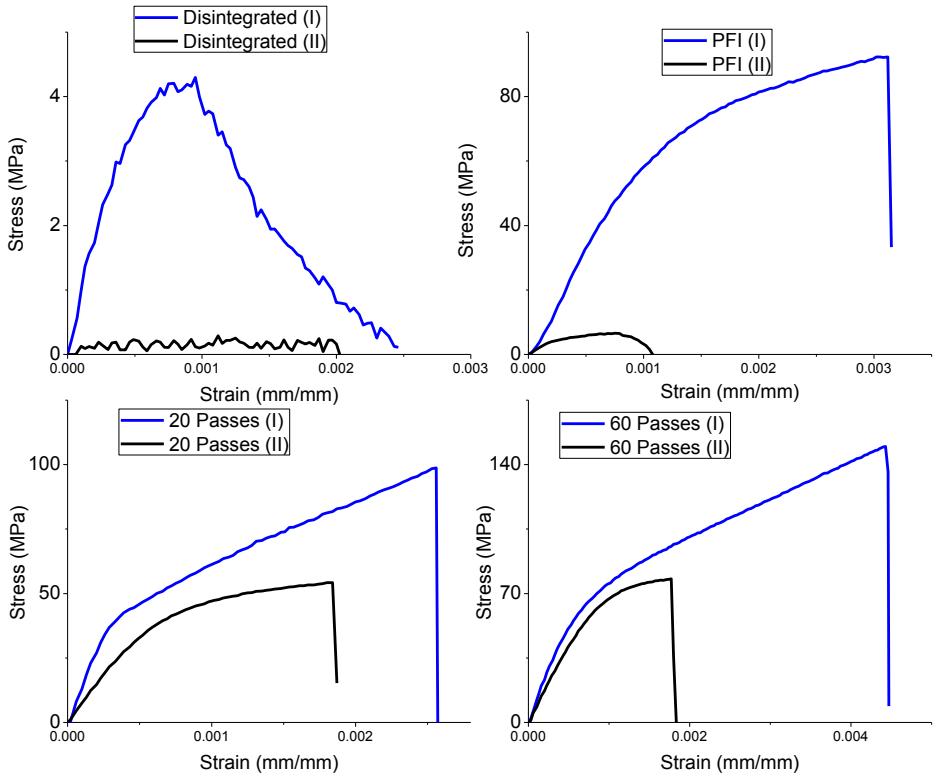

Figure 5.7: Typical Stress-Strain curves

Figure (**7**) displays typical stress-strain curves obtained for cellulose I and II fiber films made at different degrees of fibrillation. Table (**3**) shows the mean of 4

observations. The fracture cross section of the mechanically tested films was analyzed by SEM imaging, shown in figures (**8-11**). This gave us the opportunity to observe the cross section of the films, the breaking mechanism, fiber size, and degree of fibrillation at different stages. Generally speaking, a greater degree of fibrillation leads to increased mechanical strength [4, 17, 92]. This increase is directly related to the increase in exposed surface area of micro fibrils on the surface of fibers, which leads in turn to increased bonding strength per until area [17]. The break at ultimate tensile stress in highly bonded films is observed because these bonds act in unison under strain until failure is reached [17, 23].

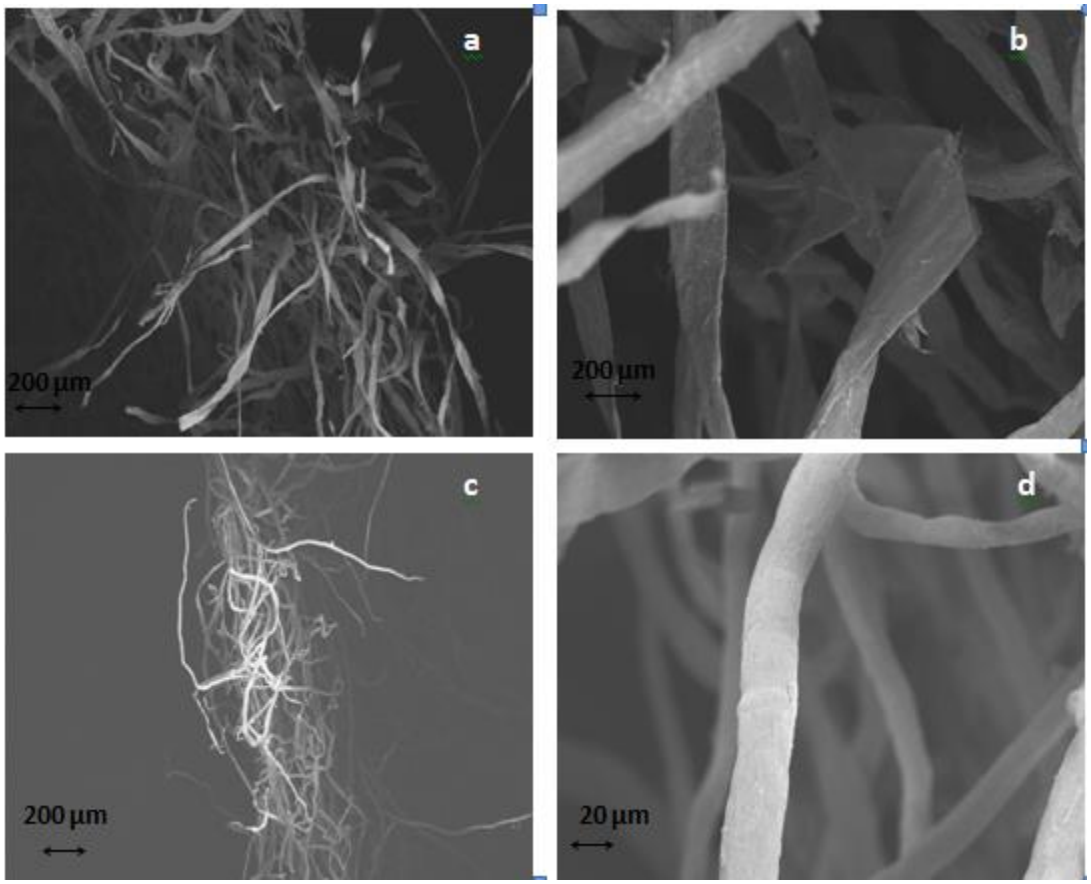

Figure 5.8: (a, b): Cellulose-I Disintegrated Fibers, (c ,d): Cellulose-II Disintegrated Fibers

In figure (**8**), the SEM images of the cross sections of films made from disintegrated fibers show long and large diameter fibers in the orders of tens of microns. The two types of fibers show very different morphology as well. Cellulose-I fibers have a flat cross section with some fibrillation on the surface visible, whereas cellulose-II fibers show a smoother, more cylindrical cross section [4, 17, 23, 82]. No break in the fiber morphology is observed in these images and long entangled fibers can be clearly seen, implying that the fibers are merely entangled with each other and there is no significant inter-fiber bonding. This results in the films displaying a tear behavior rather than a break behavior under strain.

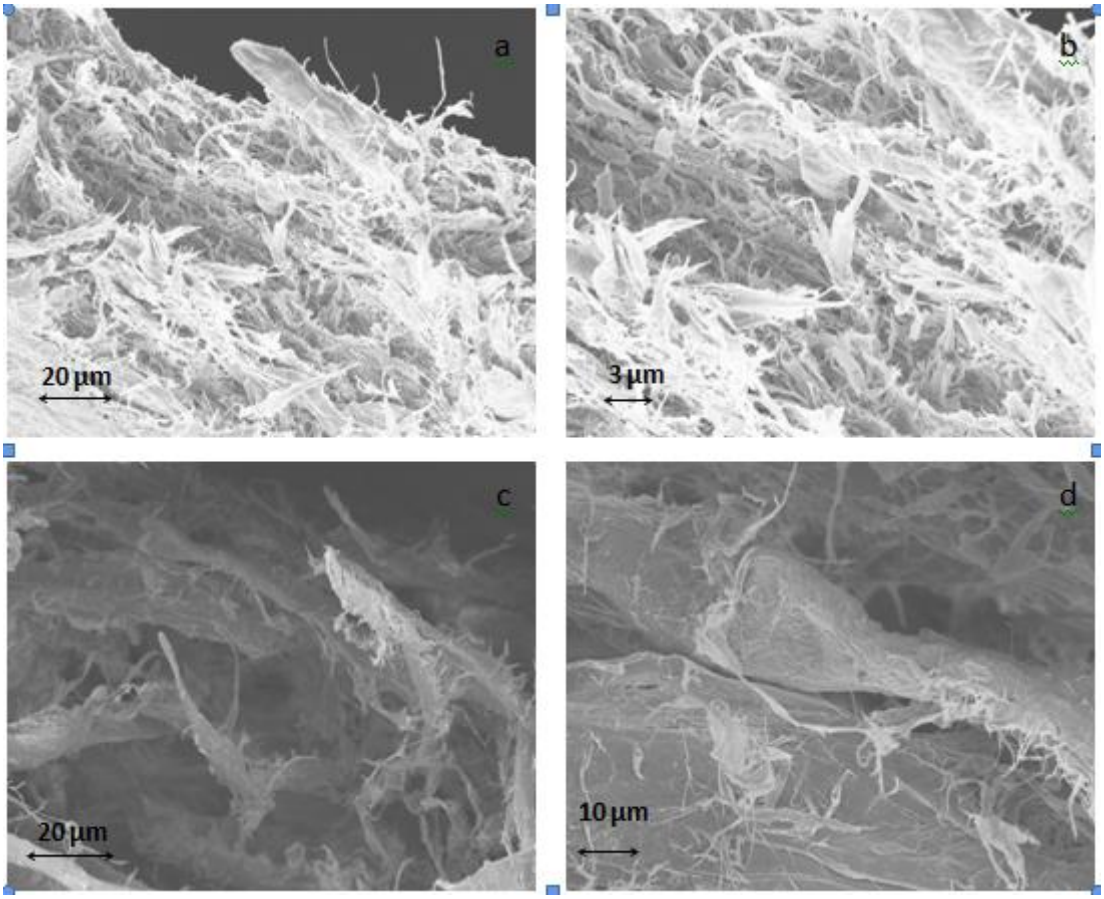

Figure 5.9: (a, b): Cellulose-I PFI Fibers, (c ,d): Cellulose-II PFI Fibers

Figure (**9**) shows the morphology of the cross section of films made from PFI refined fibers. After being refined in the PFI, both types of fibers show some changes in morphology. The cellulose-I fibers show a significant degree of fibrillation, and a heterogeneous morphology is observed. A large number of micron and submicron sized fibrils are now visible alongside much larger fibers [4, 78]. In the case of cellulose-II the larger fibers show change in shape from a cylindrical form to a more flat fiber structure with some surface fibrillation. This is typical when fibrillation is only limited to the fiber surface and shearing forces flatten the surface [78].

Under strain, cellulose-I fiber films showed significant increase in mechanical strength, while cellulose-II fiber films still showed tear behavior. This can be attributed to

the physical changes observed in the fiber morphology. The smaller fibrils visible in cellulose-I fibers allude to an increase in inter fiber bonding. Additionally, there was significant improvement in the density of the films' packing structure. Whereas cellulose-II fibers only showed minor fibrillation and still displayed tear behavior indicating that inter fiber bonding was limited and the main film forming mechanism was still an entanglement of fibers [17, 78].

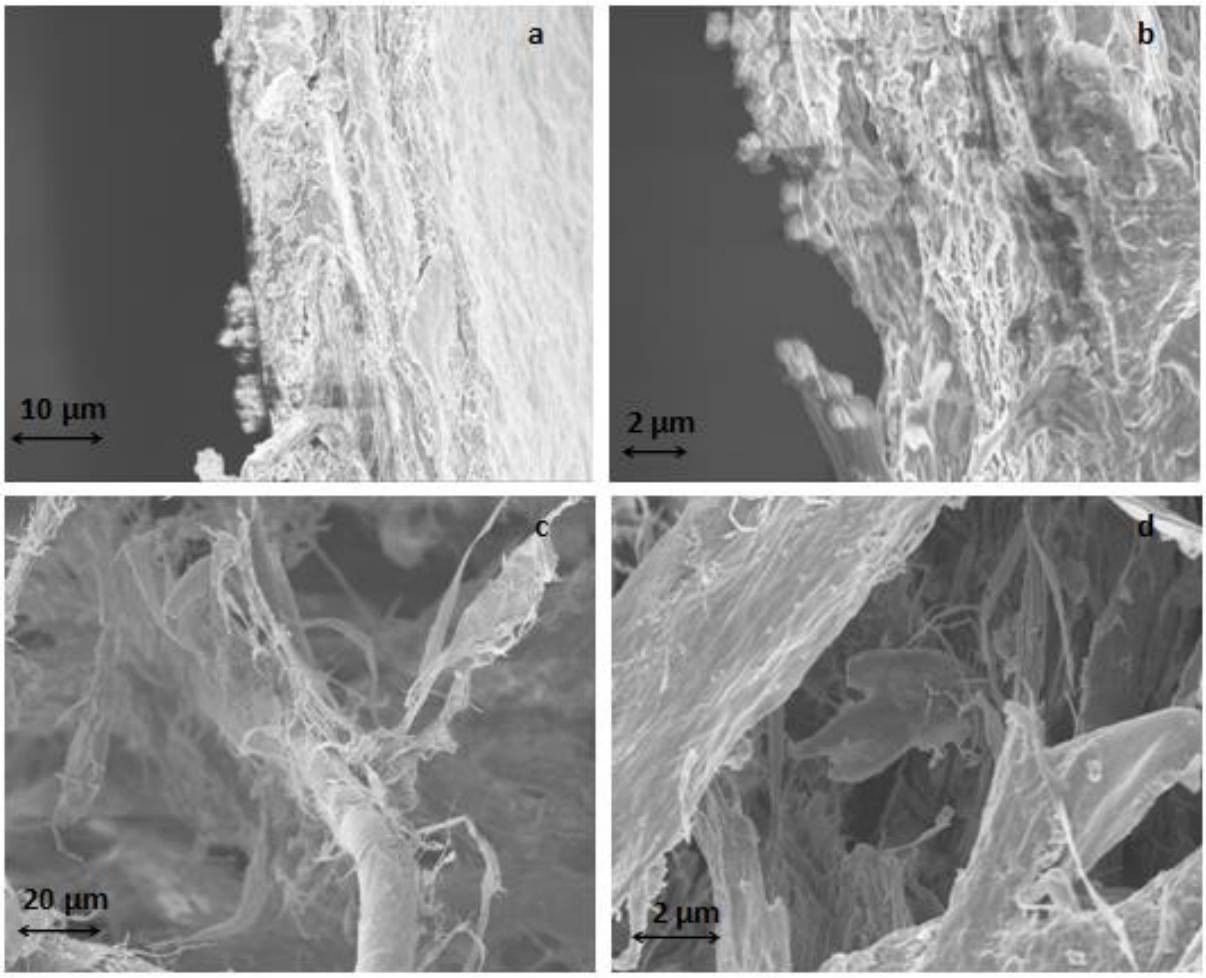

Figure 5.10: (a, b): Cellulose-I 20 Passes in SMC Fibers, (c ,d): Cellulose-II 20 Passes in SMC Fibers

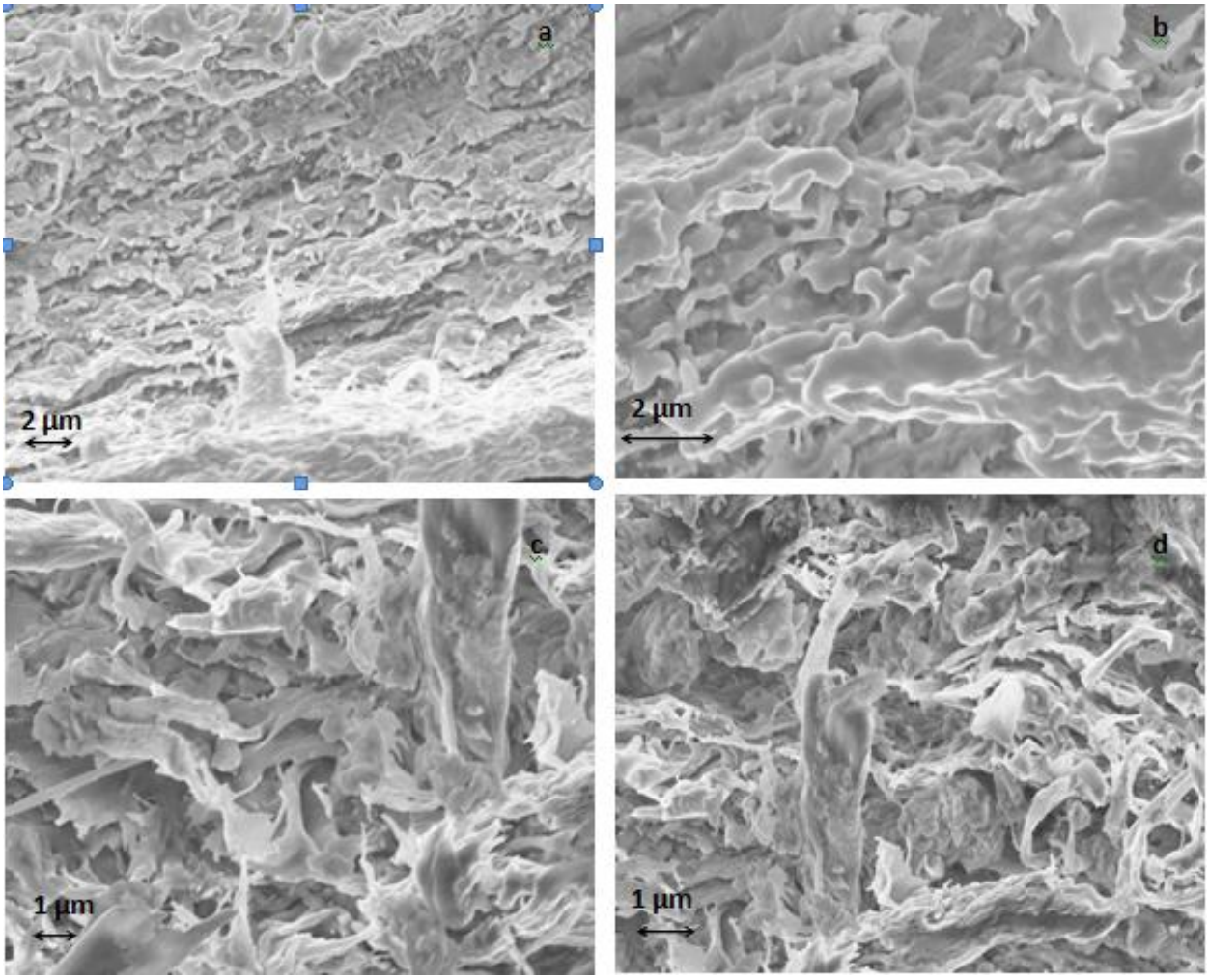

Figure 5.11:(a, b): Cellulose-I 60 Passes in SMC Fibers, (c ,d): Cellulose-II 60 Passes in SMC Fibers

Figure (**10**) shows the morphology of films made from fibers after 20 passes in SMC. In this instance, both types of fibers show a significant increase of mechanical strength. It is expected for the cellulose-I fiber films to show some increment due to the ease of fibrillation. Cellulose-II fiber films after this stage of fibrillation have evolved from a tear behavior to displaying a break at a defined tensile strain, rather than tearing apart while being strained. Cellulose-I fibers displayed a significant shift in fiber size, no large fibers are visible, and the structure is more homogeneous. Microgrinding has previously been shown to be very effective in converting cellulose-I fibers to micro fibrillated cellulose. This phenomena is observed here as well[93]. For cellulose-II fibers, microgrinding has limited effect on the degree of fibrillation as indicated by the morphology of fibers. Fibrillation still seems to be hampered due to the initial aggregation of fibrils during the mercerization process[23]. However, these films were observed while under strain to show break at a defined stress. This indicates that 20 passes in SMC has caused enough fibrillation to increase strength of the films by enhancing bonding between exposed fibrils[17].

Figure (**11**) shows the morphology of films made from fibers after 60 passes in SMC, in which both celluloses of fibers showed a micro fibrillated structure. This also translated into significantly better mechanical properties for both celluloses of materials. Cellulose-I fibers do not display microfiber like morphology, but an almost amorphous polymer like structure, where individual fibrils cannot be observed even at the high magnification shown here. The films made from cellulose-I fibers show an extremely well packed dense structure. In the case of cellulose-II fibers, micro fibrils can now be observed and the films show a very well packed dense structure as well. However, these

fibers are still very different in morphology from cellulose-I fibers. Cellulose-II fiber films now showed an average ultimate tensile stress of 75MPa, whereas cellulose-I showed an ultimate tensile stress of 135MPa.

3.6 Thermal Analysis

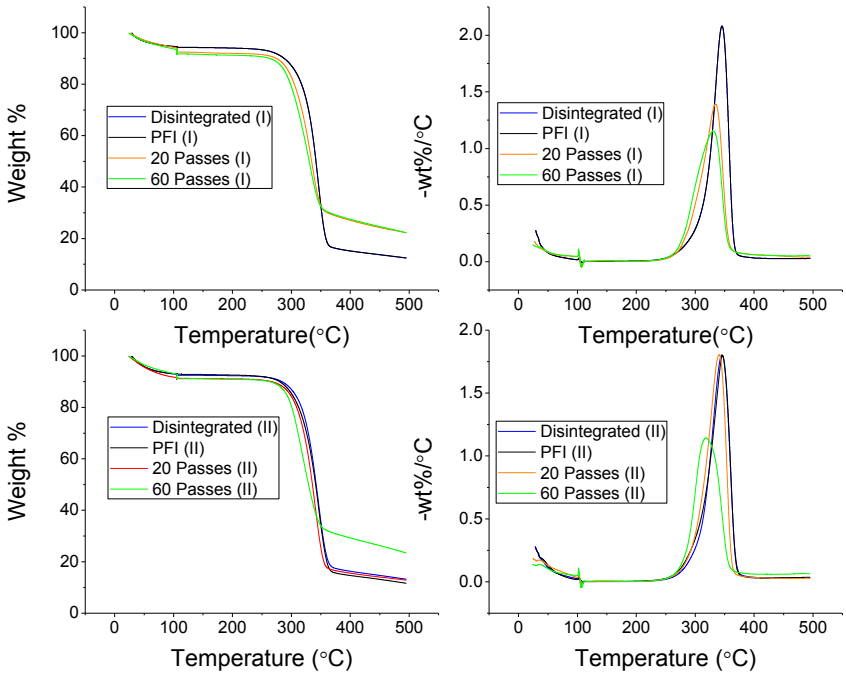

Figure 5.12: TGA / DTG Analysis

Thermogravimetric and derivative thermogravimetric analysis were performed to compare the differences in thermal degradation of films made from cellulose I and II fibers at different levels of fibrillation. TGA and DTGA curves are shown in figure (**12**), maximum degradation temperatures and maximum rate of degradation are shown in table (**4**). Generally speaking, the degradation process for celluloses and hemicelluloses begins above 200°C, at which point any linked water also starts evaporating, causing loss of mass. While the temperature is less than 200°C, there is some mass loss and limited degradation. The onset for degradation was observed in all the different fiber celluloses in

approximately 300°C region. With increasing degree of fibrillation an increase in surface area occurs, therefore thermal degradation is easier and a drop in maximum degradation temperature is expected.

Table 10: Thermal Properties

		Disintegrated	PFI	20 Passes	60 Passes
Cellulose-I	**Max Thermal Degradation (°C)**	347	347	335	329
	Max Rate of Degradation (-wt% / °C)	2.04	2	1.39	1.15
Cellulose-II	**Max Thermal Degradation (°C)**	346	345	340	316
	Max Rate of Degradation (-wt% / °C)	1.81	1.8	1.8	1.14

For both cellulose I and II fibers, the behavior of disintegrated and PFI stage fibers is almost identical, with cellulose-II fibers displaying a lower maximum rate of degradation as compared to cellulose-I fibers. After 20 passes in the SMC the thermal behavior of the two cellulose types begins to differ markedly. Cellulose-I fibers show a significant drop in both maximum degradation temperature and the maximum rate of degradation from previous stages, whereas cellulose-II fibers show a minor shift from the previous stages. This is due to the differing degrees of fibrillation of the two celluloses. Cellulose-I fibers show a significant decrease in fiber size at this stage, where submicron sized fibrils are visible, whereas cellulose-II still shows large micron sized fibers. This difference clearly alludes to the fact that there is a large difference in the specific surface area of the two fibers at this stage. After 60 passes, cellulose-I fibers show further reduction in maximum degradation temperature, which is expected since an increased degree of fibrillation is observed in the fibers. Cellulose-II fibers on the other hand, show

a large decrease from the previous stage. Cellulose-II displays this large difference because after 60 passes in SMC, a high degree of fibrillation has been induced as observed in the SEM images and film structure. This causes the maximum degradation temperature to drop, indicating an increase in surface area of the fibers [4, 93].

5.4. Conclusions

Cellulose-I pulp was converted to cellulose-II by mercerization with a 20% NaOH solution. The successful conversion of cellulose-I to cellulose-II via mercerization was confirmed by α – cellulose content, XRD, and SEM analysis. α – cellulose content changed from 84% to 96% upon mercerization, indicating loss of almost all hemicelluloses during mercerization. XRD analysis confirmed the change in arrangement of crystalline domains to an antiparallel arrangement typical of cellulose-II. SEM analysis of individual fibers shows a difference in the arrangement of surface fibrils. Cellulose-I fibers were initially flat and had some micro fibrils visible on the surface, whereas cellulose-II fibers showed a smooth cylindrical morphology indicating aggregation of surface fibrils. Both types of fibers were subjected to increasing stages of fibrillation in the following order: disintegration, PFI refining, microgrinding by 20 passes in SMC, and 60 passes in SMC. Films were made via ultrafiltration followed by the hot press method and were characterized from fibers of the different stages of fibrillation. The films obtained were found to be uniform in terms of grammage and thickness owing to the ultrafiltration, hot press method. However, density displayed significant growth with the increasing degree of fibrillation. This is expected due to better packing efficiency and bonding between a smaller, higher surface area of fibrils.

The grammage of the films was approximately 35g/m^2. The target grammage was 40g/m^2, and the slightly lower grammage indicated some fiber loss during the fabrication process. The density of the films enlarged with increasing degree of fibrillation from about 180g/m^3 to 455g/m^3 for cellulose-I and 95g/m^3 to 385g/m^3 for cellulose-II. Cellulose-I films showed some contact angle to begin with which increased at every stage (14° - 64°), whereas cellulose-II films did not display a contact angle until the final stage of fibrillation. The films also showed increasing strength and an evolution of tensile strength from initially displaying a tear behavior indicating poor bonding to typical micro fibrillated cellulose films behavior as the fibers became increasingly fibrillated. The ultimate tensile strength for cellulose changed from tear behavior with no defined break to 134.5MPa. While on the other hand, the same change for cellulose-II was a maximum of 75.1MPa from tear behavior.

It was observed that cellulose-I fibers were significantly easier to fibrillate compared to cellulose-II fibers. SEM images showed that cellulose-I fibers followed a pattern of increasing fibrillation and decreasing fiber size at every stage. While for cellulose-II fibers, disintegration and PFI refining produced almost no fibrillation. After 20 passes some fibrillation was observed and only after 60 passes were nanofibers observed. For cellulose-I fibers the fibrillation stages directly correlated with an increase in mechanical strength and the films cross section density at every stage due to increased bonding strength between small fibrils with large surface area. For cellulose-II fibers, significant fibrillation was observed only after 20 passes in the SMC, and film properties showed improvement thereafter.

CHAPTER 6

CONCLUSIONS AND FUTURE WORK

Conclusions

In this dissertation the application of cellulose nano fibers (CNFs) as barrier materials for oxygen and water vapor was studied. This topic is of extreme importance for industrial application as the need for renewable, sustainable materials to replace petroleum derived polymers becomes ever more important due to rising environmental concerns. The extraordinary properties of CNFs make them an ideal candidate for this application. The high aspect ratio of the CNF physical structure gives them extraordinary physical, mechanical, and barrier properties. CNFs are a biodegradable, sustainable, renewable, recyclable source for the production of barrier materials and have been the subject of research for quite some time. The reason widespread application of CNFs as a barrier material has not yet been observed is due to the loss of both mechanical and barrier properties in humid environments – which is naturally expected given the hydrophilic nature of cellulose. In this particular context the improvement of membranes made from CNFs was the main focus of this dissertation. Three main strategies to enhance the properties of the membranes were used as detailed below. Additionally, the possibility of using CNFs derived from cellulose II, and the different stages of fibrillation was also studied in great detail.

Films made from CNFs were subjected to heating at different temperatures to purposefully induce hornification in the films. The increase in crystallinity, loss of inter fibril porosity, and the hydrogen bonding between free –OH groups on the CNF, and therefore loss of hydrophilicity of the films, were all desired to improve the barrier

properties. Films were fabricated by evaporation casting, after drying were heated at different temperatures, and subsequently conditioned before characterization. Films were found to be increasingly hydrophobic with growing temperature. Both the oxygen and water vapor permeability both reduced significantly with heating. However, with increasing temperature there was significant reduction in the strength and toughness of the films as well. In the best case, the films showed a 25 fold decrease (from 0.17 to 0.007 cc.μm/m^2.kPa.day) in oxygen permeability whereas a twofold reduction of water vapor permeability (57,500 to 27,500 g.μm/m^2.kPa.day) was also observed. These are significant improvements in barrier properties produced by a simple heating treatment. However, the films also underwent a reduction in mechanical properties and became increasingly brittle with increasing treatment temperature.

CNF films were fabricated with PAE resin for cross linking. PAE resin based wet strength enhancing agents are commonly used in the paper industry. Previously significant study has elucidated the mechanism of PAE cross linking with cellulose by heat curing the resin. Other studies have also shown significantly better retention of PAE resins in NCF materials as compared to native cellulose fibers. Here we investigated the properties of CNF films cross linked with PAE based cross linker Kymene™. We observed that the CNF film surface transitions from hydrophilic to hydrophobic after the cross linking process displaying a contact angle increase from 50° to 110°. Additionally, the water retention value also displayed about a 25% decrease implying an increase in bulk hydrophobicity of the material. As was expected, the wet strength of the cross linked material showed significant enhancement. The pure CNF film showed a simple *tear* behavior as expected to be displayed by wet and swollen CNFs; while on the other hand

the cross linked films showed a single elastic region, ending in an eventual failure at a similar stress level as dry CNF film. It was found that crosslinking for the intended purpose of wet strength enhancement was very effective, with the wet strength to dry strength ratio of the crosslinked CNF films to the films without crosslinker proving greater than 90%. Surprisingly it was also found that crosslinking significantly changed the stress-strain behavior of the dry films as well. The behavior of dry crosslinked films was quite complex with multiple different regions implying different load bearing mechanisms at different stress levels. It was found that crosslinking is effective due to bonding between the PAE and carboxyl groups of the CNFs, and also formation of PAE networks during the extended curing period. The complex behavior was attributed to the formation of new bonds by PAE crosslinking. It was also found that the water retention of the films decreased by about 25% after crosslinking, which is expected due to the heating introducing some hornification in the films and the crosslinker also occupying some of the water interaction sites.

After the previous study showed great promise in the use of PAE cross linker for improving the behavior of CNF films under wet and humid conditions, CNF films were made with high aspect ratio filler materials and crosslinked with the same PAE resin. The aim was to exploit the benefits of using the high aspect ratio materials to increase the tortuosity of the diffusion path and crosslinking to stop degradation in wet environments as previously observed. It was found that the mechanical properties showed some increasing complexity after forming a composite, which was studied in some detail. The pure CNF films showed an Oxygen Permeability and Water Vapor permeability of 0.6ml.μm/m^2.Pa.day and 0.6ml.μm/m^2.Pa.day 2100.6ml.μm/m^2.Pa.day respectively.

First, the benefit of using high aspect ratio filler material as barrier enhancer was studied, and it was found that using 1% filler by fiber weight had a reduction of 47%, and 65% of oxygen permeability and 60% and 67% for the clay and graphene composites without crosslinker. Whereas when the films were crosslinked, a further reduction of 50% and 85% in the water vapor permeability was further obtained for clay and graphene films respectively. Additionally, the filler materials also showed some reinforcement behavior to improve the mechanical properties of the films, and UTS increased from 35MPa for pure film to 57MPa, and 75MPa in the cases of clay and graphene composites respectively. Upon cross linking all the materials showed similar behavior as the cross linked pure films, as observed in the previous stud. The benefit of the composite films was an increase of about 5% in the UTS of the films, and a slight delay in the onset of the secondary mechanism of loading as observed in the pure films.

The mechanical process to form nano cellulose fibers from native cellulose and mercerized cellulose pulp was studied, and films made from the different stages of fibrillation were characterized in detail. The films were categorized for mechanical, optical properties, wettability, and water retention. A detailed study of the films and fiber morphology, as well as the crystal structure of the fibers was also completed. Mercerized cellulose was studied in particular because it has an inherently different crystal structure and has become the subject of recent curiosity in the literature for producing CNFs. First, the mercerization was confirmed via XRD, SEM, and α – cellulose content characterization. Both cellulose I and II showed characteristic patterns and showed high purity, α – cellulose content showed an increase in content from 84% to 97% after mercerization, indicating removal of most hemicelluloses during mercerization. The SEM

images of native cellulose fibers showed typical flat fiber morphology, whereas the mercerized cellulose showed a cylindrical and smooth morphology. This indicates the aggregation of fibrils on top of the mercerized cellulose which is expected to occur during mercerization. After that the pulp was subjected to the following subsequent order of fibrillation: disintegration, PFI refining, 20 Passes in SMC, and finally 60 passes in SMC. Films were made from fibers collected at each stage and characterized. It was found that the native cellulose was much easier to fibrillate, whereas the mercerized cellulose, due to initial fibril aggregation, was much more difficult to fibrillate. Transition of physical, mechanical, and optical properties was observed at each stage for cellulose-I fibers, whereas for cellulose-II a transition in mechanical properties was observed only after 20 passes in SMC.

Overall, CNFs were further established to be effective barrier materials against oxygen under dry conditions, and upon some improvement also for water vapor. Even though CNFs suffer from a high degree of hydrophilicity due to an abundance of –OH surface groups, easy thermal treatment and mild chemical treatment can easily modify that behavior to obtain performance even under wet or humid conditions. Even though in this dissertation strategies for combating the degradation under wet or humid conditions have been provided and studied in detail, some further steps are needed to ensure practical operation. These mainly include thorough testing under operation under wet and humid conditions, where the permeability and strength are tested under long term exposure to humidity. Additionally, in this dissertation the possibility of using CNFs derived from cellulose II was also explored. From a theoretical perspective CNFs from cellulose II seem to offer better properties, however obtaining CNFs from cellulose II is

challenging with current strategies and better methods need to be developed to be able to exploit the properties of cellulose II CNFs.

Recommendations for Future Work

Studies on film behavior in humid environments; In this dissertation barriers made from CNFs were studied in the context of barrier properties for gases and water vapor. In context of both barrier and mechanical properties the materials were studied in perfectly ideal, dry environments after being conditioned. From an experimental perspective this works to make comparisons between materials made in a similar fashion. However, while in application the environment would be humid and of varying humidity. Therefore, both mechanical and barrier properties of the materials should be studied in detail in humid environments. Previously other authors have shown the severe degradation of barrier and mechanical properties in humid environments for pure CNF films. However, in the studies presented here various strategies to enhance both barrier and mechanical properties in wet environments have been developed and tested, and these must be evaluated in humid environments as well.

A study on the formation of barrier films by different methods of formation and standardization: What is common in this study as well as the literature is a difficulty in obtaining consistent behavior of films due to different fabrication methods. In this study, the first test was done by fabrication of films via casting evaporation, while the next two studies were done by forming films by ultrafiltration and compressed drying. Again, the second and third studies were done with a flatbed dryer, which was compressed by

placing weights on top. These factors can introduce some variability in the formation of films. Therefore, a study in detail to evaluate these differences and how to remove them is necessary so that highly consistent films can be obtained for all future studies. Moreover, it causes the additional burden of finding studies that formed films close to the method used, since the literature is highly inconsistent in this aspect as well.

Study of other crosslinkers: PAE or epicholorohydrin – polyamide based crosslinkers have been used commonly in the paper industry for a long period of time as an effective wet strength enhancing agent. Even though studies were performed with this material in this dissertation as well and some interesting properties were discovered, it should be noted that it is an extremely toxic material and is not suitable for packing material, which is subject to severe federal restrictions, especially in the context of food packaging. Therefore, with application in mind there exists a host of other more environmentally friendly crosslinkers that must be studied. A comparative study also needs to be completed to evaluate their efficacy in the context of wet strength, water interaction modification, and barrier properties for CNF films.

Formation of lignin / CNF composites by blending instead of grafting. Lignin, also a biopolymer derived from the same source as CNFs, could have a significant impact on the wet properties and possibly reduce the cost of usage of CNF based membranes as barriers. Lignin is very hydrophobic and has been the focus of some studies to graft lignin onto CNFs to improve compatibility. However, the grafting of lignin ends up adding another step to the process and actually deteriorates the properties of the resulting CNF

membranes. In the last study, graphene and CNF composite films were made even though they are highly incompatible – this was made possible due to high shear mixing and rapid dewatering of the mixed slurry followed by compressed drying. This process removes the opportunity for segregation between the two phases. This could be a highly effective process for incorporating lignin in to CNF films to form highly effective humidity resistant barrier films.

REFERENCES

1. D. Klemm, B. Heublein, H.-P. Fink and A. Bohn, *Angewandte Chemie International Edition*, 2005, **44**, 3358-3393.
2. X. Xu, F. Liu, L. Jiang, J. Y. Zhu, D. Haagenson and D. P. Wiesenborn, *ACS Applied Materials & Interfaces*, 2013, **5**, 2999-3009.
3. D. Topgaard and O. Söderman, *Cellulose*, 2002, **9**, 139-147.
4. S. Nair, J. Y. Zhu, Y. Deng and A. Ragauskas, *Journal of Nanoparticle Research*, 2014, **16**, 1-10.
5. E. Kontturi, M. Suchy, P. Penttilä, B. Jean, K. Pirkkalainen, M. Torkkeli and R. Serimaa, *Biomacromolecules*, 2011, **12**, 770-777.
6. P. Zugenmaier, *Progress in Polymer Science*, 2001, **26**, 1341-1417.
7. R. C. Weatherwax, *Journal of Colloid and Interface Science*, 1977, **62**, 432-446.
8. M. G. A. Vieira and S. C. S. Rocha, *Chemical Engineering and Processing: Process Intensification*, 2007, **46**, 955-963.
9. X. Samain, V. Langlois, E. Renard and G. Lorang, *Journal of Applied Polymer Science*, 2011, **121**, 1183-1192.
10. D. Roy, M. Semsarilar, J. T. Guthrie and S. Perrier, *Chemical Society Reviews*, 2009, **38**, 2046-2064.
11. T. Zimmermann, E. Pöhler and T. Geiger, *Advanced Engineering Materials*, 2004, **6**, 754-761.
12. W. Zhang, Y. Zhang, C. Lu and Y. Deng, *Journal of Materials Chemistry*, 2012, **22**, 11642-11650.
13. K. Syverud and P. Stenius, *Cellulose*, 2009, **16**, 75-85.

14. I. Siró and D. Plackett, *Cellulose*, 2010, **17**, 459-494.

15. H. Sehaqui, Q. Zhou, O. Ikkala and L. A. Berglund, *Biomacromolecules*, 2011, **12**, 3638-3644.

16. K. Uetani and H. Yano, *Biomacromolecules*, 2010, **12**, 348-353.

17. W. Stelte and A. R. Sanadi, *Industrial & Engineering Chemistry Research*, 2009, **48**, 11211-11219.

18. G. Rodionova, Ø. Eriksen and Ø. Gregersen, *Cellulose*, 2012, **19**, 1115-1123.

19. A. Isogai, T. Saito and H. Fukuzumi, *Nanoscale*, 2011, **3**, 71-85.

20. M. Henriksson, L. A. Berglund, P. Isaksson, T. Lindström and T. Nishino, *Biomacromolecules*, 2008, **9**, 1579-1585.

21. F. Ansari, S. Galland, M. Johansson, C. J. G. Plummer and L. A. Berglund, *Composites Part A: Applied Science and Manufacturing*, 2014, **63**, 35-44.

22. J. Wu and Q. Yuan, *Journal of Membrane Science*, 2002, **204**, 185-194.

23. H. Wang, D. Li, H. Yano and K. Abe, *Cellulose*, 2014, **21**, 1505-1515.

24. G. Rodionova, M. Lenes, Ø. Eriksen and Ø. Gregersen, *Cellulose*, 2011, **18**, 127-134.

25. Q. Yang, T. Saito and A. Isogai, *Cellulose*, 2012, **19**, 1913-1921.

26. L. C. Tomé, C. M. B. Gonçalves, M. Boaventura, L. Brandão, A. M. Mendes, A. J. D. Silvestre, C. P. Neto, A. Gandini, C. S. R. Freire and I. M. Marrucho, *Carbohydrate Polymers*, 2011, **83**, 836-842.

27. K. L. Spence, R. A. Venditti, O. J. Rojas, J. J. Pawlak and M. A. Hubbe, *BioResources*, 2011, **6**, 4370-4388.

28. J.-W. Rhim, J.-H. Lee and S.-I. Hong, *Packaging Technology and Science*, 2007, **20**, 393-402.

29. H. J. Park and M. S. Chinnan, *Journal of Food Engineering*, 1995, **25**, 497-507.

30. S. A. Paralikar, J. Simonsen and J. Lombardi, *Journal of Membrane Science*, 2008, **320**, 248-258.

31. J. Lange and Y. Wyser, *Packaging Technology and Science*, 2003, **16**, 149-158.

32. V. Siracusa, I. Blanco, S. Romani, U. Tylewicz and M. Dalla Rosa, *Journal of Food Science*, 2012, **77**, E264-E272.

33. V. Siracusa, *International Journal of Polymer Science*, 2012, **2012**, 11.

34. A. B. Reis, C. M. P. Yoshida, A. P. C. Reis and T. T. Franco, *Polymer International*, 2011, **60**, 963-969.

35. M. Österberg, J. Vartiainen, J. Lucenius, U. Hippi, J. Seppälä, R. Serimaa and J. Laine, *ACS Applied Materials & Interfaces*, 2013.

36. A. S. Michaels and H. J. Bixler, *Journal of Polymer Science*, 1961, **50**, 393-412.

37. N. K. Lape, E. E. Nuxoll and E. L. Cussler, *Journal of Membrane Science*, 2004, **236**, 29-37.

38. E. L. Cussler, S. E. Hughes, W. J. Ward Iii and R. Aris, *Journal of Membrane Science*, 1988, **38**, 161-174.

39. A. Al-Jabareen, H. Al-Bustami, H. Harel and G. Marom, *Journal of Applied Polymer Science*, 2013, **128**, 1534-1539.

40. I. S. Bayer, D. Fragouli, A. Attanasio, B. Sorce, G. Bertoni, R. Brescia, R. Di Corato, T. Pellegrino, M. Kalyva, S. Sabella, P. P. Pompa, R. Cingolani and A. Athanassiou, *ACS Appl Mater Interfaces*, 2011, **3**, 4024-4031.

41. G. Findenig, S. Leimgruber, R. Kargl, S. Spirk, K. Stana-Kleinschek and V. Ribitsch, *ACS Applied Materials & Interfaces*, 2012, **4**, 3199-3206.

42. L. Li, V. Breedveld and D. W. Hess, *ACS Applied Materials & Interfaces*, 2013, **5**, 5381-5386.

43. M. I. Vázquez, C. Milano, R. de Lara, O. Guerrero, C. Herrera and J. Benavente, *Desalination*, 2006, **200**, 15-17.

44. Y. Kamiya and F. Takahashi, *Journal of Applied Polymer Science*, 1977, **21**, 1945-1954.

45. W. L. Hyden, *Industrial & Engineering Chemistry*, 1929, **21**, 405-410.

46. C.-N. Wu, T. Saito, S. Fujisawa, H. Fukuzumi and A. Isogai, *Biomacromolecules*, 2012, **13**, 1927-1932.

47. N. D. Luong, N. Pahimanolis, U. Hippi, J. T. Korhonen, J. Ruokolainen, L.-S. Johansson, J.-D. Nam and J. Seppala, *Journal of Materials Chemistry*, 2011, **21**, 13991-13998.

48. S. Belbekhouche, J. Bras, G. Siqueira, C. Chappey, L. Lebrun, B. Khelifi, S. Marais and A. Dufresne, *Carbohydrate Polymers*, 2011, **83**, 1740-1748.

49. M. Minelli, M. G. Baschetti, F. Doghieri, M. Ankerfors, T. Lindström, I. Siró and D. Plackett, *Journal of Membrane Science*, 2010, **358**, 67-75.

50. C. Aulin, M. Gällstedt and T. Lindström, *Cellulose*, 2010, **17**, 559-574.

51. D. Stanssens, H. Van den Abbeele, L. Vonck, G. Schoukens, M. Deconinck and P. Samyn, *Materials Letters*, 2011, **65**, 1781-1784.

52. S. Cao, D. Song, Y. Deng and A. Ragauskas, *Industrial & Engineering Chemistry Research*, 2011, **50**, 5628-5633.

53. V. Bhardwaj, A. Macintosh, I. D. Sharpe, S. A. Gordeyev and S. J. Shilton, *Annals of the New York Academy of Sciences*, 2003, **984**, 318-328.

54. G. W. Jeon, J.-E. An and Y. G. Jeong, *Composites Part B: Engineering*, 2012, **43**, 3412-3418.

55. H. Kim, Y. Miura and C. W. Macosko, *Chemistry of Materials*, 2010, **22**, 3441-3450.

56. Y.-m. Chen, J.-q. Wan, M.-z. Huang, Y.-w. Ma, Y. Wang, H.-l. Lv and J. Yang, *Carbohydrate Polymers*, 2011, **85**, 759-764.

57. Y. Chen, Y. Wang, J. Wan and Y. Ma, *Cellulose*, 2010, **17**, 329-338.

58. Y. Liu, D. Thibodeaux, G. Gamble, P. Bauer and D. VanDerveer, *Applied Spectroscopy*, 2012, **66**, 983-986.

59. Å. Östlund, T. Köhnke, L. Nordstierna and M. Nydén, *Cellulose*, 2010, **17**, 321-328.

60. A. Brancato, F. L. Walsh, R. Sabo and S. Banerjee, *Industrial & Engineering Chemistry Research*, 2007, **46**, 9103-9106.

61. S. Park, R. A. Venditti, H. Jameel and J. J. Pawlak, *Carbohydrate Polymers*, 2006, **66**, 97-103.

62. N. M. L. Hansen and D. Plackett, *Biomacromolecules*, 2008, **9**, 1493-1505.

63. F. Hussain, M. Hojjati, M. Okamoto and R. E. Gorga, *Journal of Composite Materials*, 2006, **40**, 1511-1575.

64. J. Su, Mosse, W. K. J., Sharman, S., Batchelor, W., and Garnier, G., *Bioresource Technology*, 2012, **7**, 913-924.

65. S. Ahola, M. Österberg and J. Laine, *Cellulose*, 2008, **15**, 303-314.

66. T. Obokata and A. Isogai, *Colloids and Surfaces A: Physicochemical and Engineering Aspects*, 2007, **302**, 525-531.

67. T. Obokata, M. Yanagisawa and A. Isogai, *Journal of Applied Polymer Science*, 2005, **97**, 2249-2255.

68. Y. Geng, K. Li and J. Simonsen, *Journal of Applied Polymer Science*, 2006, **99**, 712-718.

69. S. Sharma, X. Zhang, S. S. Nair, A. Ragauskas, J. Zhu and Y. Deng, *RSC Advances*, 2014, **4**, 45136-45142.

70. H. Cai, S. Sharma, W. Liu, W. Mu, W. Liu, X. Zhang and Y. Deng, *Biomacromolecules*, 2014, **15**, 2540-2547.

71. X. Luo and J. Y. Zhu, *Enzyme and Microbial Technology*, 2011, **48**, 92-99.

72. S. Singh and A. K. Mohanty, *Composites Science and Technology*, 2007, **67**, 1753-1763.

73. H. Sehaqui, S. Morimune, T. Nishino and L. A. Berglund, *Biomacromolecules*, 2012, **13**, 3661-3667.

74. H. Sehaqui, A. Liu, Q. Zhou and L. A. Berglund, *Biomacromolecules*, 2010, **11**, 2195-2198.

75. H. Sehaqui, M. Allais, Q. Zhou and L. A. Berglund, *Composites Science and Technology*, 2011, **71**, 382-387.

76. M. Haggkvist, D. Solberg, L. Wagberg and L. Odberg, *NORDIC PULP & PAPER RESEARCH JOURNAL*, 1998, **13**, 292-298.

77. X. Zhang, Z. Lin, B. Chen, W. Zhang, S. Sharma, W. Gu and Y. Deng, *Journal of Power Sources*, 2014, **246**, 283-289.

78. S. S. Nair, S. Sharma, Y. Pu, Q. Sun, S. Pan, J. Y. Zhu, Y. Deng and A. J. Ragauskas, *ChemSusChem*, 2014, **7**, 3513-3520.

79. X. Zhang, Z. Lin, B. Chen, S. Sharma, C.-p. Wong, W. Zhang and Y. Deng, *Journal of Materials Chemistry A*, 2013, **1**, 5835-5839.

80. H.-D. Huang, C.-Y. Liu, D. Li, Y.-H. Chen, G.-J. Zhong and Z.-M. Li, *Journal of Materials Chemistry A*, 2014, **2**, 15853-15863.

81. Y. Yue, C. Zhou, A. French, G. Xia, G. Han, Q. Wang and Q. Wu, *Cellulose*, 2012, **19**, 1173-1187.

82. A. Sarko and R. Muggli, *Macromolecules*, 1974, **7**, 486-494.

83. E. Dinand, M. Vignon, H. Chanzy and L. Heux, *Cellulose*, 2002, **9**, 7-18.

84. H. Shibazaki, S. Kuga and T. Okano, *Cellulose*, 1997, **4**, 75-87.

85. L. A. Ramos, D. L. Morgado, F. Gessner, E. Frollini and O. A. El Seoud, *ARKIVOC: Online Journal of Organic Chemistry*, 2011, 416-425.

86. B. S. Kaith, A. S. Singha, S. Kumar and S. Kalia, *International Journal of Polymeric Materials*, 2008, **57**, 54-72.

87. T. Isogai, M. Yanagisawa and A. Isogai, *Cellulose*, 2008, **15**, 815-823.

88. M. Floros, L. Hojabri, E. Abraham, J. Jose, S. Thomas, L. Pothan, A. L. Leao and S. Narine, *Polymer Degradation and Stability*, 2012, **97**, 1970-1978.

89. J. Zhu, X.-T. Dong, X.-L. Wang and Y.-Z. Wang, *Carbohydrate Polymers*, 2010, **80**, 350-359.

90. B. Balu, V. Breedveld and D. W. Hess, *Langmuir*, 2008, **24**, 4785-4790.

91. I. Siró, D. Plackett, M. Hedenqvist, M. Ankerfors and T. Lindström, *Journal of Applied Polymer Science*, 2011, **119**, 2652-2660.

92. A. N. Nakagaito and H. Yano, *Appl Phys A*, 2005, **80**, 155-159.

93. K. Abe, S. Iwamoto and H. Yano, *Biomacromolecules*, 2007, **8**, 3276-3278.